Electro-Spark Deposition Machine Design, Physical Controls and Parameter Effects

by

Stephen Peterkin

A thesis

presented to the University of Waterloo

in fulfilment of the

thesis requirement for the degree of

Master of Applied Science

in

Mechanical and Mechatronics Engineering

Waterloo, Ontario, Canada, 2016

Authors Declaration

I hereby declare that I am the sole author of this thesis. This is a true copy of the thesis, including any required final revisions, as accepted by my examiners.

I understand that my thesis may be made electronically available to the public.

Abstract

Electro-spark deposition (ESD) is a micro welding process characterized by short duration high current pulses, often generated by capacitors, arcing between a conductive electrode and substrate. The high intensity, low net power process results in metallurgical bonded coatings or alloyed layers with practically no heat affected zone. The unique characteristics of this process facilitate the bonding of high ceramic content cermet materials, as well as heat sensitive high value materials. The process is used to repair components where low heat input, low distortion depositions are required, as well as apply coatings for the improvement of corrosion resistance, tribological properties and local alloy content.

The objective of this study was to evaluate the effects of ESD power supply designs on the control of ESD process parameters. Electrical power supply parameters such as voltage, capacitance and voltage were examined, along with physical parameters including; application force, movement speed, movement pattern and shielding gas were explored.

Three different custom power supplies were developed to encompass performance improvements reported in previous studies and compare advanced circuit and parameter behavior against the traditional ESD machine. This was done by analyzing the possible voltage and current signals recorded from the power supply with a data acquisition system. The electrical signals were used to compare advances in voltage, capacitance, frequency and pulse sequence control.

Key parameters were identified and implemented in a universal power supply as a simplified user interface. A wider range of electrical parameters were tested in order to meet the needs of a wider variety of material pairings. The new universal ESD power supply was tested to determine the parameter effects on the coating quality of titanium carbide nickel sintered electrodes deposited on copper substrates. Pulse voltage and frequency were identified as having the most significant effect on the coating thickness and defect formation.

The deposition experiments for relating the electrical parameters to coating quality revealed errors in the coating measurements caused by variations in the ESD physical parameters. A computer numerical controlled machine was developed with a force feedback system to control the physical parameters. Using this system the effect of controlled deposition patterns, movement speed, application force, and argon shielding gas was tested against the effects of the ESD voltage and frequency.

The experimental data concluded that the physical controls paired with the management of electrical parameters improved the coating thickness, and lack of defects. Implementation of a physical control system including movement and force control would be beneficial for future experiments and for some industrial applications. The combined electrical power effects of varying the voltage, frequency with the use of shielding gas resulted in improved coating thickness and quality. This demonstrated that testing to determine the effective parameter ranges for new applications and material pairings is integral to the deposition of thicker coatings with reductions in the typical pore, crack and oxidation defects.

Acknowledgments

Table of Contents

List of Figures

xvi

List of Tables

List of Equations

List of Abbreviations

ESD: Electro-spark deposition   Micro-welding process utilizing short duration high powered electrical pulses to deposit conductive materials on conductive substrates

CNC: Computer numerical controls   Computer controlled physical location driven marching

IGBT: Insulated-gate bipolar transistor   Solid state switching device

DCEP: Direct current electrode positive   An electrical polarity of welding processes

AC: Alternating current   Municipal power, typically 120VAC, 60Hz, 15A

DC: Direct current   Transformed municipal power for use in charging the ESD capacitors

RSW: Resistance spot welding   Electrical resistance welding process using high currents and typically copper electrodes

G-Code: RS-274 generic programming code   Typical programming language used for the communication with CNC machines

VISA   Virtual Instrument Software Architecture   LabView serial – digital port emulator and control

Chapter 1.0: Introduction

Electro-spark deposition (ESD) is a micro welding process in which short duration; high current electrical discharges are used to deposit conductive material from an electrode to the substrate surface. Relative motion is required between the electrode and the substrate to prevent sticking and deposit continuous coatings.

This process has been historically used for the repair of high valued components where there is a requirement for minimal distortion and heat affected zones. ESD benefits from the metallurgical bonding of the deposited material while the short duration pulses result in low net heat input, reducing the heat affected zone. Other applications include electro-spark alloying to treat the surfaces of metallic products with alloying elements to change the hardness, wear, corrosion and surface properties. Notably ESD has been used to deposit high melting temperature cermet electrodes onto softer metallic substrates to drastically change the surface properties of the products.

1.1   Problem Statement

Different material pairings and end use applications for coatings and alloying operations achieved through the use of ESD require the selection of optimized parameters out of a wide range of possible variables. There is a need for the design of a power supply which can meet the needs of various applications while maintaining control of the key parameters. Understanding the interactions between the ESD electrical and physical parameters is necessary for the effective use of the ESD process for new applications.

1.2   Objective

Study is needed into the development of advanced ESD power supplies capable of meeting the various parameter needs of different applications and realizing improvements presented in past research. Selection of the significant electrical parameters and understanding the effects on coating quality will help in the development of a procedure for determining the process range for future applications.

The ESD process can be powered by a wide variety of power supplies with a wide range of potential electrical parameters and settings. Applicators typically provide the required relative motion by rotating or vibrating the treating electrode. Physical considerations as to the motion pattern, movement speed and

application force can have a significant effect on the quality of the coatings. Figure 1 outlines some of the different parameters which are relevant to the ESD process, [1].
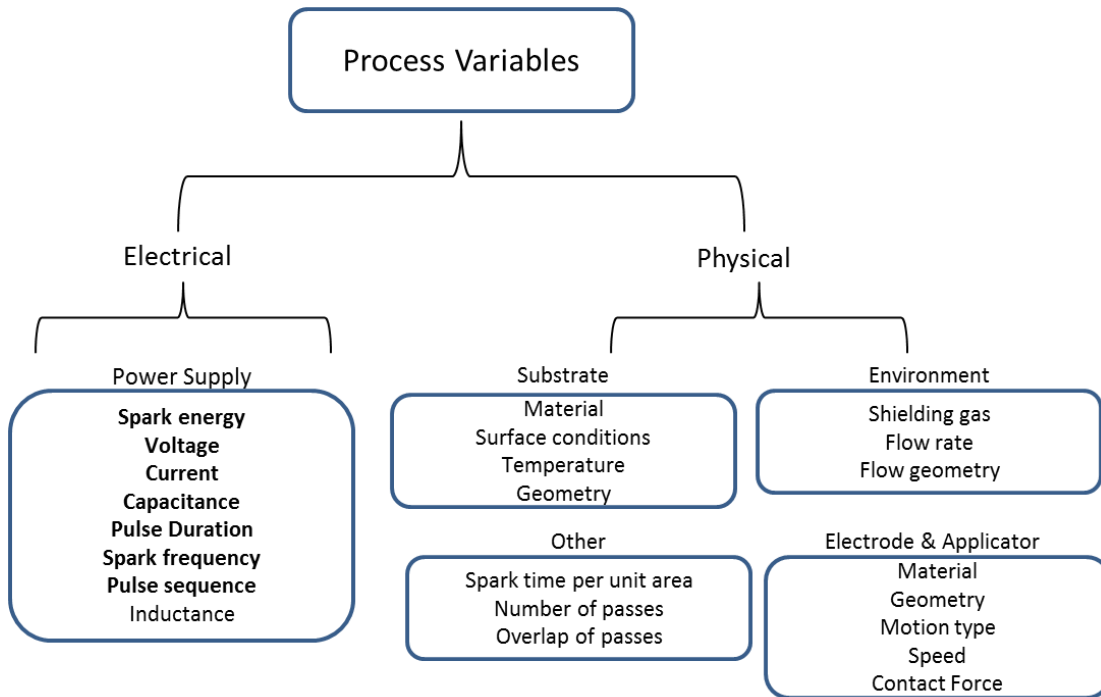
Figure 1: ESD Parameter chart [1]

The various ESD process parameters have varying effects on the quality of coatings and depositions. There is a need to understand and relate the relevant parameters in order to effectively apply the ESD process to emerging applications.

1.3 Outline

This study evaluates the performance and contributes to improvements of advanced ESD power supplies. Design changes are evaluated with a focus on increasing the possible material pairings possible with ESD and presenting a procedure and results for the effect of electrical parameter on the quality of ESD coatings and effects on mass transfer mechanisms.

The effects of the ESD voltage, pulse frequency, shielding gas and physical controls are examined versus the performance of more traditional ESD power supplies and application methods.

Chapter 2 presents the background and literature review related to the ESD process. The studies focus on the design of ESD power supplies, the effects of ESD parameters and the mechanism of mass transfer. The theory relating to the controls system developed in Chapter 5 is presented.

Chapter 3 exhibits the analysis and characterization tools and methods used to quantify the performance of experiments.

Chapter 4 follows the development of advanced ESD power supplies, applying improvements similar to previous studies from Chapter 2, in order to develop a machine which meets the needs of a wide variety of material pairings and applications, while demonstrating the accuracy to reduce defects and increase productivity.

Chapter 5 presents the need for a physical control system for the ESD process. A preliminary computer numerical controls (CNC) machine and force feedback system is developed to demonstrate the effect on characterizing electrical parameters to coating quality, while also exploring the effects of force, movement speed and deposition patterns on the process.

Chapter 2.0: Background

2.1 ESD Process

ESD is a direct current electrode positive (DCEP) micro-arc welding process; see Figure 2, process where high current, short duration pulses facilitate the flow of electrons from the substrate to the electrode. The flow of electrons interacts with gaseous ions in the intermediate distance forming a plasma arc. The short duration high current causes local arcing and joule heating promoting the formation the ESD characteristic arc, [2-8].

Treating electrodes and substrates require electrical conductivity and are often metal and ceramic alloys. Material is deposited as molten material from the electrode, impinging on the substrate forming a metallurgical bond. The material is deposited via a moving applicator and ground, which transfers the electrical signals and facilitates relative motion through the use of rotation, linear motion or vibration to prevent the electrode sticking to the surface. See Figure 3 for a schematic of the ESD process, [2-8].
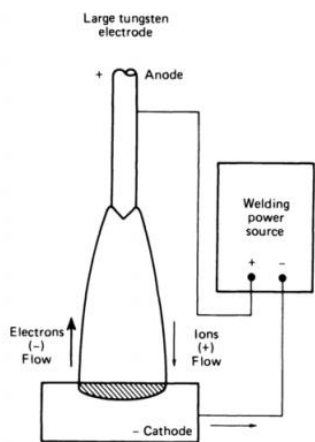
Figure 2: DCEP welding process [4]
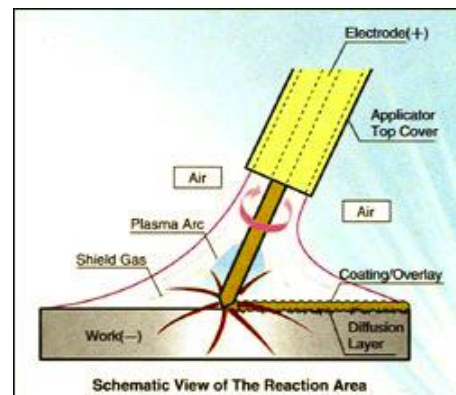
Figure 3: ESD process schematic [5]

2.2 ESD Electrical Components

ESD power supplies are typically powered by the principles of capacitors. The electrical component is used to generate the high current electrical pulses or a power supply with pulses driven by transistors. Other universal electrical components include transformers, and different rectifier types. More advanced

ESD power supplies use solid state microcontroller managed switching devices to vary the pulse behavior.

Different types of rectifiers, such as diode bridge rectifiers, single and full wave rectifiers as well as the transformer used in the generation of the direct current (DC) power required for charging capacitors can have a significant effect on the performance of the power supply. See Appendix A: Electrical component descriptions for a detailed description of the rectifier process, [9] [10] [11].
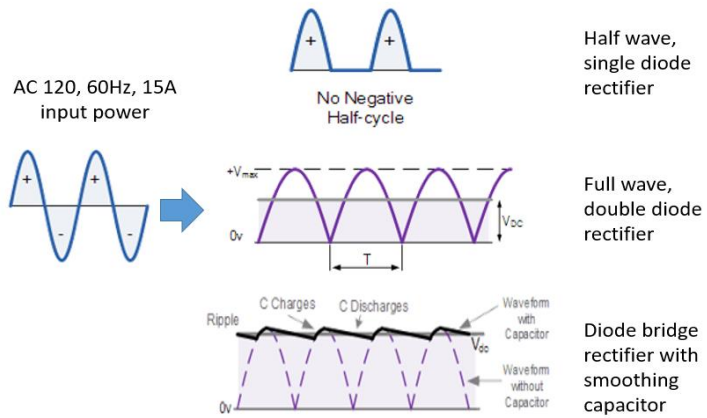
Figure 4: Rectified voltage outputs for different diode configurations [10] [11]

2.2.1   Capacitors

Capacitors are an integral part of many ESD power supply circuits. The ability to store and quickly discharge high currents is ideal for the high intensity spark generation that characterizes the ESD process. The capacitors are characterized by the quantity of electrical charge which can be stored relative to the change in electrical potential. The capacitance, measured in farads (F) is the ratio of the charge q in coulombs on the capacitor electrode and the potential difference in volts between the electrodes. Equation 1 represents the mathematical relation between the variables, [12].

Equation 1: Capacitance

$$C = \frac{q}{V}$$

The energy stored and discharged by the capacitor is characterized by the work performed by the power supply, or battery to create the electrical potential difference between the electrodes. The charging potential of the capacitor is related to the surface area of the electrodes, the spacing between them the dielectric solution between the electrodes and the applied charging voltage. Equation 2 relates the

electrical energy stored or discharged in joules from a capacitor to the capacitance in farads and charging potential in volts, [12] [13].

Equation 2: Capacitor energy

$$E = \frac{1}{2}CV^2 \ (J)$$

Electrolyte capacitors are used due to high capacitance relative to the device size. These capacitors function with an electrolyte solution which acts as the cathode and a thin oxide layer, often from aluminum or tantalum, which acts as the dielectric, [12]. Equation 2 relates the properties of capacitors which allows for the high powered, short duration discharges which define ESD processes. The equation notes that relatively low charging voltages will store and discharge large quantities of electrical energy.

2.2.2   Switching Devices

In order to design and develop advanced ESD power supplies, switching components need to be used along with microcontroller logic, to manage the charging and discharging of the circuit or capacitors. Thyristors and insulated gate bipolar transistors (IGBT) are components used to rapidly control and switch the current flow during different stages of the ESD signal generation. The use of these components can alter the pulse frequency, sequence and pauses in order to influence the results of the ESD process. See Appendix A: Electrical component descriptions for a detailed description of the IGBT and thyristor switching devices, [14] [15].

2.3   ESD Mass transfer

Several different mass transfer methods have been proposed for the ESD process. The methods include solid, liquid and gaseous transfer across the gap between the electrode and the substrate, the transfer of the molten material accelerated by plasma formed by the arc, and direct contact between the electrode and substrate molten material. Due to the localized and rapid mass transfer, and degeneration of the arc it is difficult to characterize the exact mass transfer method, [6].

The process for liquid mass transfer was divided into several process steps. Contact between the electrode and substrate and the discharge of the electrical circuit causes significant localized joule heating. The joule heating melts the contact point for the substrate and electrode. Rapid relative motion of the electrode results in the localized area moving before the electric circuit is completely discharged. The resultant gap results in thermionic emission forming a plasma arc between the electrode and substrate. The arc melts a

small section of the electrode which is accelerated by the plasma arc to adhere to the substrate. Figure 5 shows high speed images detailing the arc and droplet formation during ESD. This transfer mode has mechanics similar to the short circuit transfer mode in GMAW, [6] [16] [7] [17].
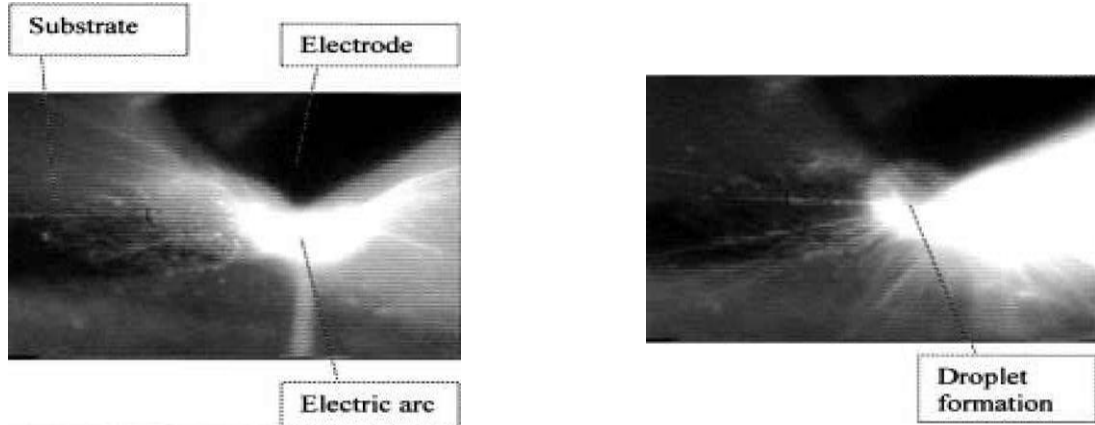
Figure 5: High speed images of arc ignition and droplet formation during ESD [6]

Research into the appearance and properties of single deposition spots using ESD with a rotating electrode characterized a splashing of the molten metal when testing certain material pairings. High pressure interactions with the arc, expanding gases and expulsed solid electrode materials serve to form the splash morphology in the depositions. The proposed steps for deposition formation, illustrating the spark initiation, high pressure zone, splashed and transferred material and solidification is seen in Figure 6. A set of different materials were tested to see if different formations would occur, all of the tested material pairings resulted in the splashed deposition seen in Figure 7, [18].
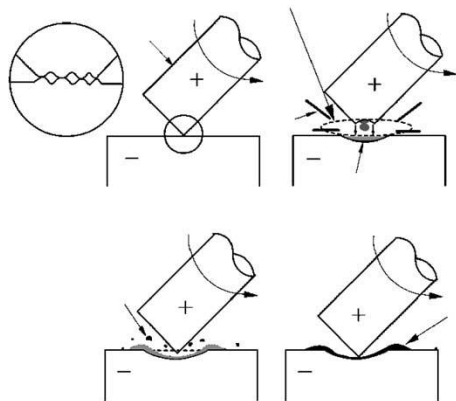
Figure 6: Formation of single pulse deposition spot [18]
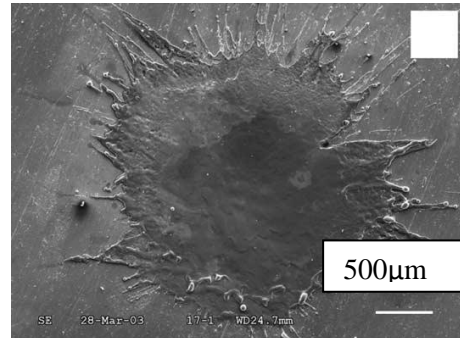
Figure 7: Single pulse rotating ESD; Inconel 182 on titanium [18]

Similarly researchers have proposed that the mass transfer occurs as the electrode locally bonds to the substrate, then the relative motion mechanically breaks the weak bond. In this method the joule heating

7

between the locally heated electrode and substrate forms a bond similar to a micro stud welding process. Then it is the relative motion which breaks the bond and leaves a deposition, [17].

A study was done to determine the effect of the electrode position relative to the substrate and the resulting mass transfer method. The study examined a static deposition mode and a dynamic deposition mode, relating to the relative motion of the electrode. Figure 8 and Figure 9 detail the stages of the ESD process for the different control modes. Depositions were made with the pairing of a titanium carbide nickel ceramic metal composite sintered electrode and a copper substrate, [7] [17].
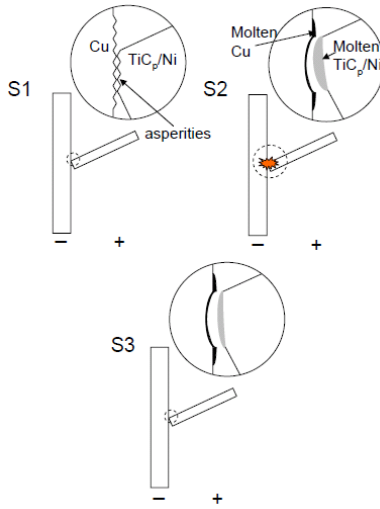
Figure 8: Static deposition mode ESD stages [7]   **Figure 9: Dynamic deposition mode ESD stages [7]**
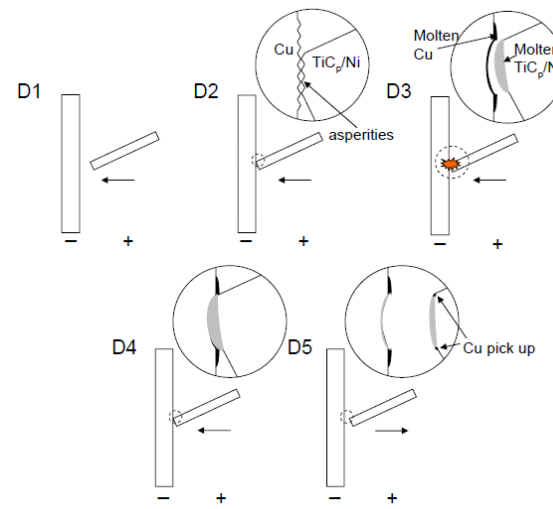
The static mode depositions resulted in the formation of an elliptical crater in the substrate showing signs of the splashed liquid substrate material caused by the arc. Figure 10 shows the surface of the ESD crater from the static control mode discharge, highlighting the splashed substrate material. Figure 11 highlights the substrate material, molten Cu, which transferred to the composite electrode. Localized melting was observed on the electrode, however no significant amount of the electrode material was transferred to the substrate. Figure 12 and Figure 13 quantify that there was little material transfer from the electrode to the substrate, and rather a somewhat localized contamination of the substrate surface with small concentrations of Ti and Ni, [7].

Figure 10: Crater from static ESD [7]
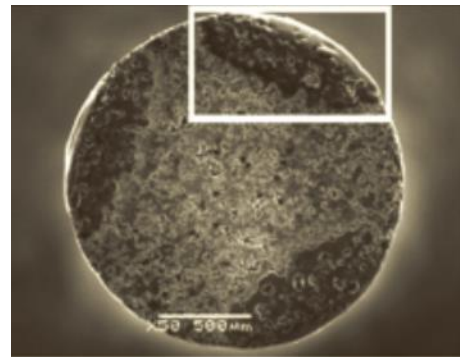
Figure 11: Cu substrate material transfer to TiC/Ni electrode after ESD [7]
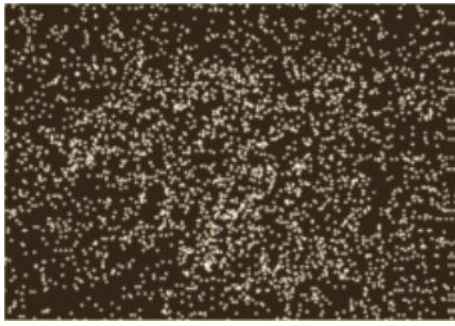
Figure 12: Ti element map of static ESD crater. Small scattered particles of Ti [7]
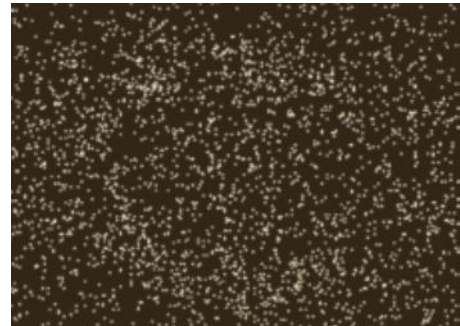
Figure 13: Ni elemental map of static ESD crater small scattered particles of Ni [7]

The dynamic mode depositions, where the electrode was allowed to continue to move forward after initial contact resulted in significant depositions. This experiment supported that the majority of mass transfer occurred when there was physical molten metal to molten metal contact between the electrode and the substrate.

The mass transfer rate was again increased when an additional discharge was permitted, so that there were two nearly instantaneous capacitor discharges. The initial discharge followed the static model, and then the electrode moved into the substrate crater discharges again increasing the volume of molten metal transferred to the substrate. The data graphed in Figure 14 clearly shows how the capacitor discharges twice, related to the movement of the electrode following the initial discharge. Figure 15 highlights the difference to the static mode, as there is now a visually significant amount of deposited electrode material on the substrate surface, [7].

9
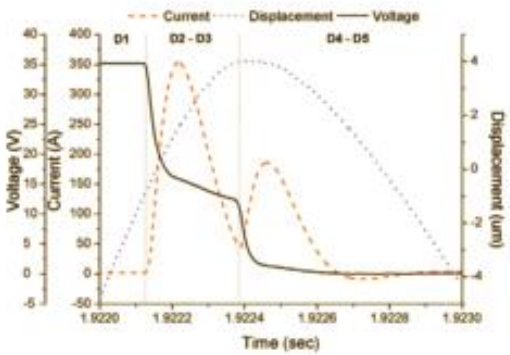
Figure 14: Dynamic deposition current and voltage data [7]

Figure 15: Surface of ESD crater using dynamic control mode [7]

The difference between the element maps for the static and dynamic mode depositions highlights that the dynamic mode significantly increased the molten metal to molten metal interactions and locally transferred more electrode materials to the substrate. Figure 16 and Figure 17 show the concentration of Ti and Ni respectively when compared to the elemental maps for the static mode depositions, [7].
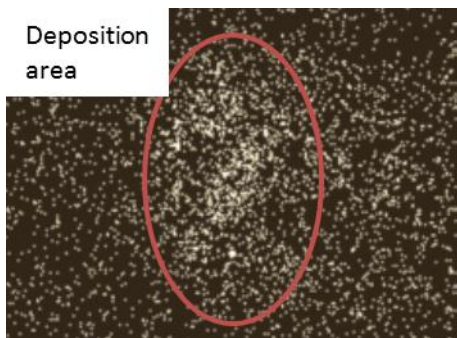
Figure 16: Ti element map of the dynamic ESD crater [7]
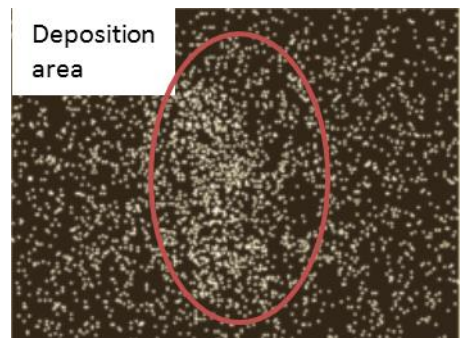
Figure 17: Ni element map of the dynamic ESD crater [7]

Consensus is that the majority of the mass transfer for ESD is achieved through molten metal to molten metal interactions, be it through the detachment of a molten droplet from the electrode to impinge on the substrate surface, or the mechanical transfer of molten metal from the surface of the electrode to the molten pool on the substrate. The method of liquid transfer would depend on the material pairing, atmospheric interactions and ESD parameters. Using multiple pulses can increase the mass transfer efficiency, [6] [7] [16] [17].

2.3.1 Erosion losses

It has been established that the liquid erosion from the ESD process accounts for the effective mass transfer. Concurrently changes in the substrate and electrode material, as well as ESD parameters will affect the negative losses from the solid, liquid and gaseous discharge from the process, [16].

Notably certain materials which have high levels of interactions with atmospheric elements, or lack a stable liquid phase will have difficulties with the ESD process. Materials such as graphite have difficulties being deposited using ESD, as well as the metallic materials bismuth telluride and chromium silicide have seen little success due to excessive losses during deposition. [19].

Erosion losses are defined by the phase in which they escape the electrode or substrate. Vapor components typically are lost to the atmosphere, a small amount of vaporized substrate material may condense on the adjacent electrode, however the majority of mass lost to vapor is not recovered. Particles eroded during the physical stress of the spark typically do not adhere to the surface of the substrate and are thus not considered in the substrate mass gain. Liquid material which splashes from the electrode or substrate during the spark will likely not properly adhere to the substrate due to surface oxides and contaminants. Only those materials which interact with the cathodic etching action of the spark, and the molten substrate material are considered to effectively form the metallurgical bond which characterizes effective ESD processes, [7] [16].

Increasing the ESD electrical parameters serves to increase the erosion rate of all phases. Tuning of the ESD parameters is key to achieving high mass transfer rates as well as reducing erosion losses. Figure 18 reports data showing the limitations of increasing the ESD electrical energy on the process efficiency of the mass transfer. A threshold of pulse energy results in a plateau of the process mass transfer, [6].
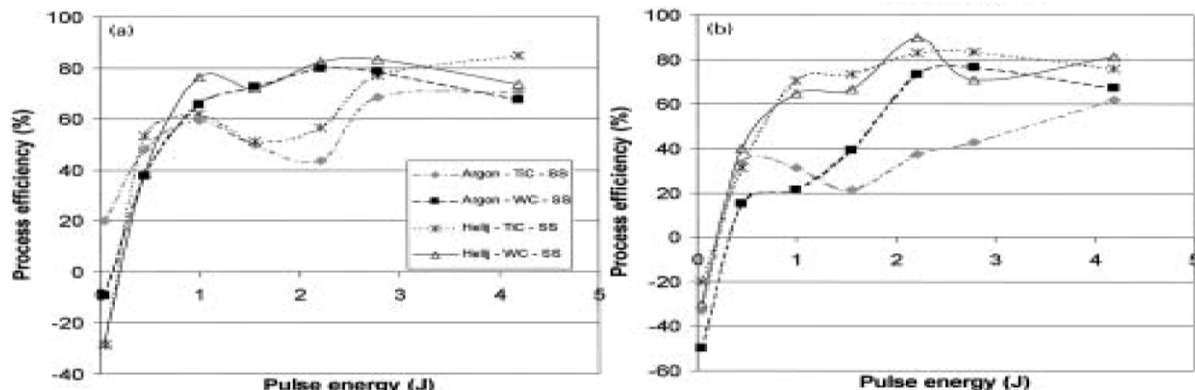
Figure 18: Process efficiency for increasing ESD power for WC and TiC respectively with different shielding gas [6]

11

Additional depositions on previously deposited layers are often desirable to increase coating thickness. However it is widely accepted that many tested materials have a limit for maximum consecutive coating thicknesses, often for high ceramic content coatings where the substrate resistance increases due to the deposition of highly ceramic electrode materials. Figure 19 compared to Figure 20 demonstrates the difference in the electrode erosion and the substrate mass gain when increasing the number of consecutive depositions with the TiC/Ni electrode. The electrode erosion remains higher than the weight gain of the substrate due to erosion of the substrate, and losses in the gaseous and solid phase. Additional depositions past 80 did not increase the mass of the substrate, [7].
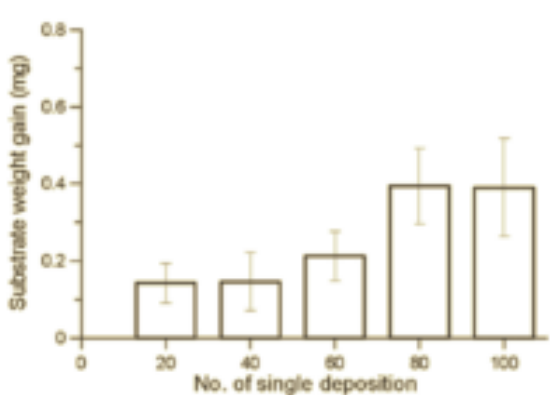
Figure 19: Weight gain by the Cu substrate during consecutive dynamic depositions [7]
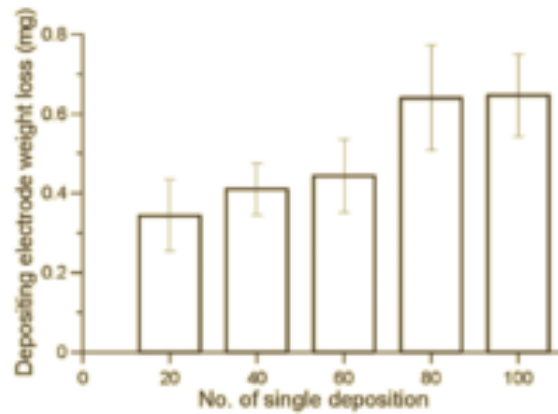
Figure 20: Weight loss by the TiC/Ni electrode during consecutive dynamic depositions [7]

2.4 ESD Machine considerations

ESD power supplies are characterized by high current short duration pulses, different methods of creating the electrical signals have been explored. Different methods have been tested to improve the electrical parameter control of the systems as well as use different pulse shapes and sequences to improve the deposition quality and mass transfer rates.

2.4.1 Improved ESD power supply

Initial designs for ESD machines often employed electrically simple transformer, rectifier charging circuits which supplied the discharging capacitors. With this power supply the discharge frequency is controlled by the intermittent contact determined by the vibrating or rotating electrode. The diagram in Figure 21 illustrates the simplicity of this design.
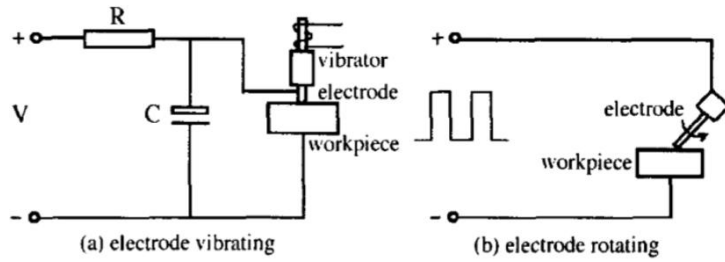
Figure 21: Conventional ESD power supply [8]

While electrically simple and easy to apply this setup has several drawbacks. The process frequency of the ESD process is entirely charged by the oscillation frequency of a vibrational applicator or the breaks in contact from a rotating applicator. In the case of a rotating electrode or high frequency vibrations there may be instances of constant discharging where the power supply discharged faster than charging. This results in much lower than expected output voltages and potentially insufficient electrical energy to deposit material, [8].

This study proposed to improve the typical ESD circuit by adding IGBT controlled switches to ensure that the capacitor was fully charged to the desired voltage before discharging. In this way the process frequency is determined by the desired capacitor voltage level and the intermittent contact by the applicator. However in instances where there is constant contact the capacitors will still fully charge before discharging. A schematic of the proposed improved power supply is illustrated in Figure 22, [8].
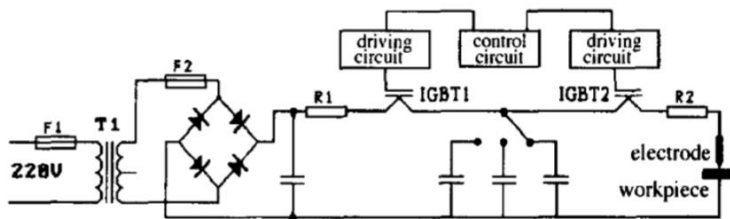
Figure 22: ESD Block diagram improved design [8]

Control of the capacitor discharge voltage with IGBT switches results in accelerated coating rates, near 3 to 4 times, related to the deposition of WC-8%Co tungsten carbide cobalt composites onto ASI 1045 Steel substrates. Table 1 details the electrical parameters for the two power supplies and the results of coating thickness, roughness and coating rate. It was noted that increasing the coating rate resulted in an increase in the surface roughness of the depositions, [8].

13

Table 1: Comparison between conventional D9130 ESD power supply and improved IGBT design [8]

	D9130	New
Power supply, V	220, single phase	220, single phase
Highest output voltage, V	40, 50	30-75
Operating current, A	1-3	<10
Maximum coating thickness, μm	50-60	100
Roughness, μm	1.6-6.3	2.6-6.3
Coating rate(a), mm^2/s	0.5-0.8	1.6-3.2

(a) For highest coating thickness

Experiments were done with varying electrical parameters to evaluate the effect on the coating thickness and the wear resistance. The pulse energy was varied in a measure of joules, the pulse frequency in kHz was varied and the total deposition time. Figure 23 and Figure 24 graph the results of the experiments for the coating thickness and wear resistance respectively. Notably there was an increase in the coating thickness with increases in the output energy and pulse frequency; however there was a decrease in the coating thickness after depositions longer than 3 minutes. This supports other research that for certain material pairings there is a limit to the number of beneficial sequential depositions. Increases in the parameters all resulted in increases in the wear resistance of the coatings.
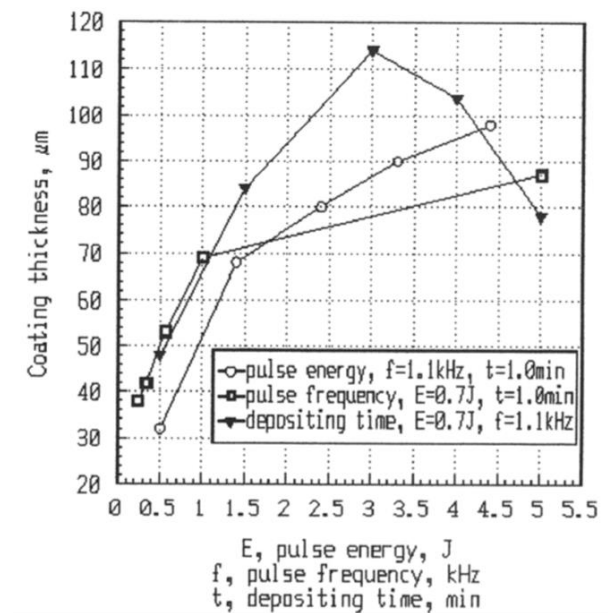
Figure 23: Effect of ESD parameters on coating thickness [8]
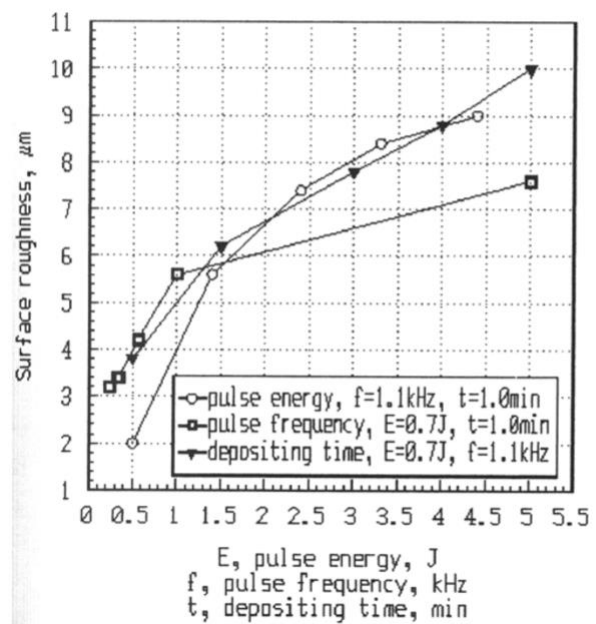
Figure 24: ESD parameters effect on surface roughness [8]

2.4.2   Pulse sequence

A different ESD power supply can employ a power transistor to control the duration of the current pulses out of the device. A study to determine the effect of pulse width and the pause between pulses, effectively the frequency ran experiments by treating steel 35 with a WC-8%Co electrode, [20].

Increasing the frequency is in an effort to increase the average current, such that the new heat transient process of the next pulse is affected by the previous pulse. Figure 25 demonstrates how pulse sequencing and the gap between pulses can drastically increase the heat input from the ESD process, [21].
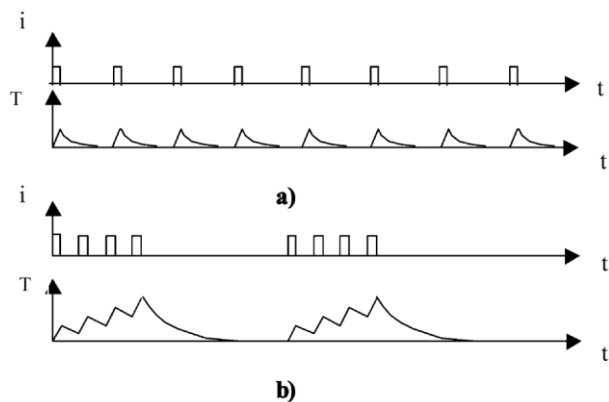
Figure 25: ESD heat buildup with pulse sequence; a) normally spaced pulses, b) grouped pulses [21]

Increasing the heat of the process simply by increasing the overall frequency would increase the heat input into the substrate and could reduce the beneficial effects of the ESD process. Figure 26 details the current buildup when a series of voltage pulses are sent in sequence. The aim of the experiment was to group different sets of current pulses so as to keep the overall energy level equal, but allow the heat transient effect to accumulate heat in the electrode so that the mass transfer rate would increase. Figure 27 details the different experimental conditions, where the pause between pulses is modulated, as well as the pulse duration and energy magnitude, [20].
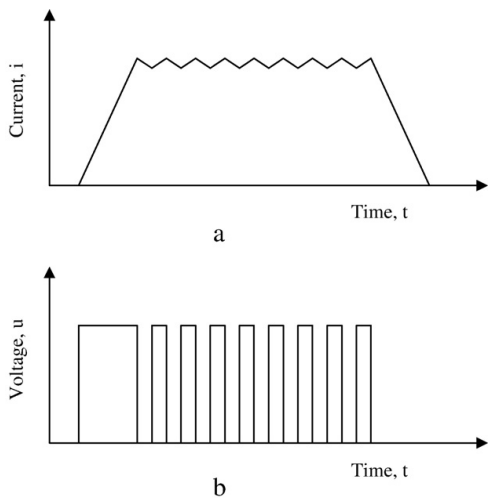
Figure 26: Current pulse formation for a voltage output from the power transistor [20]
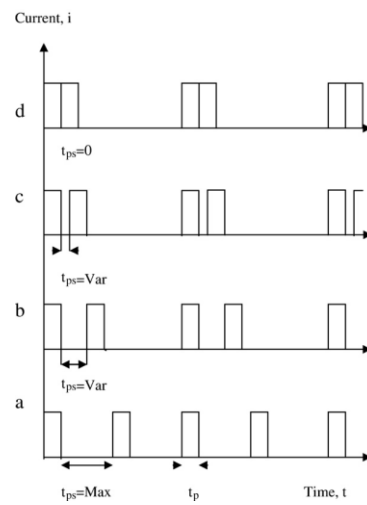
Figure 27: Schematic detailing pulse arrangements with varying pauses between pulses (t_ps) and pulse duration (t_p) [20]

Initial experiments tested square pulses with currents of 200A, durations of 100μs and pulse energy of 0.268J. Groups of 1, 2 4 and 8 pulses with the maximum pause in between were tested. Figure 28 shows the difference in the mass change between the different groups of pulses. Notably groups of two pulses resulted in the most mass gain by the substrate with the least electrode erosion and energy input for the majority of the pauses, [20].
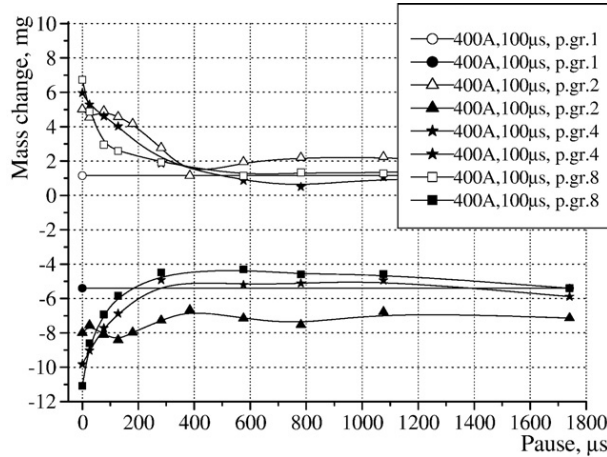
Figure 28: Mass change from the anode and cathode for groups of pulses [20]

The resultant best combination was determined to be a group of two pulses, where the first pulse had lower energy than the second. Experiments testing different energy values for the two pulses and pauses between the groups of pulses were done. Figure 29 details the experiment for one of the two pulse energy levels, where the first pulse is 0.443J and the second is 1.05J. The graph demonstrates that the maximum

gap and minimum gap are not the ideal levels for depositions, the variable gaps results in higher mass transfer rates. Table 2 reports the 7 experiments with different pulse energies for the first and second pulses and the resultant erosion loss from the electrode, [20].

Table 2: Pulse parameters and mass loss from the electrode [20]

No. of exp	No. of pulses in a pulse group	Pulse energy, J	Amplitude of pulse, A	Duration of pulse, µs	Frequency of pulse group, Hz	Mass loss, mg (base data)	Max mass loss, mg/time of pause
1.	First	0.268	200	100	41	9.06, t_{ps}=max	11.46/t_{ps}=30
	Second	0.982	200	300			
	Joined					10.88, t_{ps}=0	–
2.	First	0.268	200	100	109	6.12, t_{ps}=max	7.86/t_{ps}=285
	Second	0.443	400	100			
	Joined					6.18, t_{ps}=0	–
3.	First	0.982	200	300	15	10.16, t_{ps}=max	14.84/t_{ps}=75
	Second	2.5	400	400			
	Joined					12.02, t_{ps}=0	–
4.	First	0.982	200	300	13	9.56, t_{ps}=max	13.88/t_{ps}=180
	Second	3.02	500	400			
	Joined					12.28, t_{ps}=0	–
5.	First	0.443	400	100	24	6.02, t_{ps}=max	13.18/t_{ps}=180
	Second	1.82	400	300			
	Joined					11.16, t_{ps}=0	–
6.	First	0.443	400	100	34	7.5, t_{ps}=max	11.08/t_{ps}=375
	Second	1.07	500	170			
	Joined					9.54, t_{ps}=0	–
7.	First	1.82	400	300	10	12.16, t_{ps}=max	14.56/t_{ps}=180
	Second	3.12	400	500			
	Joined					14.52, t_{ps}=0	–
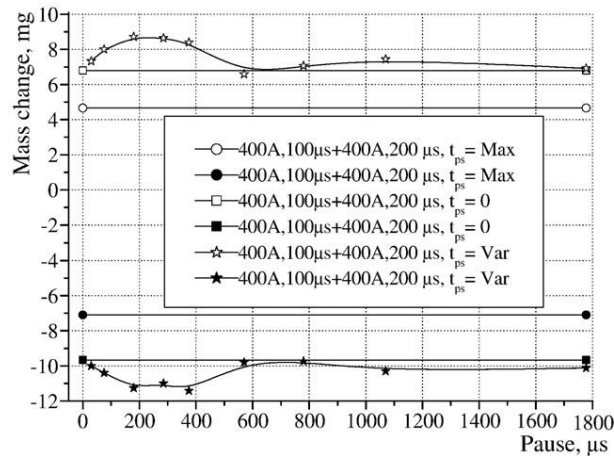
Figure 29: Mass change for the electrode in solid dots and mass gain for the substrate versus the pause between groups of pulses [20]

It was noted that for conventional ESD systems in order to achieve the same erosion rates without pairs of pulses significantly higher energy would be required. The paper concluded that through the use of different pulse durations, groups of pulses and pauses between groups of pulses the mass transfer rate of the typical ESD process can be improved. Pairs of pulses where the second pulse has higher energy than the first resulted in the highest mass transfer rates and significantly lower energy levels than those required from traditional ESD power supplies for the same erosion rates. However significant increase in the mass transfer rate resulted in vaporization of the electrode material forming significant defects. Figure

30 images show the porosity and defects caused by high energy with the pairs of pulses, inferring that subsequent high energy pulses vaporize some of the previously deposited material. Finally the paper concluded that a longer pause than this system allowed, near 1ms would allow for the deposited material and electrode to cool sufficiently that higher energy pairs of pulses could be used, [20].
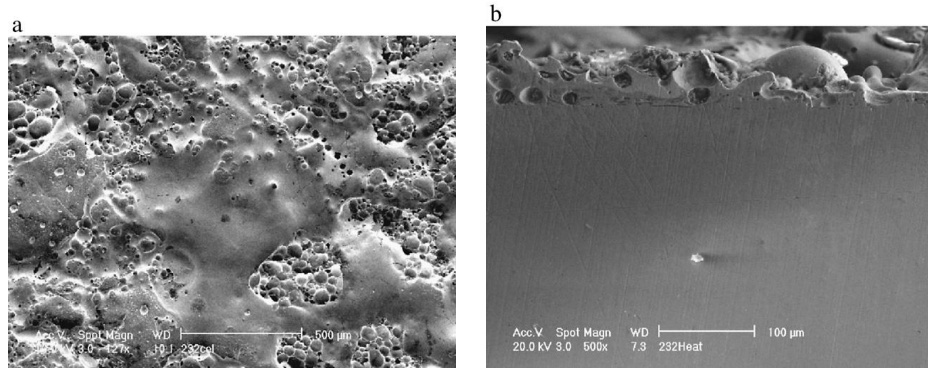
Figure 30: Morphology of ESD coating with the first pulse at 200A 300us and the second at 400A 300us and 75us pause between pulse groups [20]

2.4.3 Surface roughness

Previous research has shown, that due to the small scale and locality of depositions, increasing the deposition rate often accompanies an increase in the surface roughness, and often additional defects, [8][20]. A study aimed to join the effects of electro-spark machining with the traditional depositions, [22].

A base pulse was applied for to power the typical ESD process and erode the electrode material onto the substrate. Then a series of high current triangular pulses were applied, ideally with a short duration peak current to promote the grinding of the deposited material and the substrate rather than erode additional material from the electrode. Figure 31 details the plan for the base deposition pulses and the triangular grinding pulses, [22].
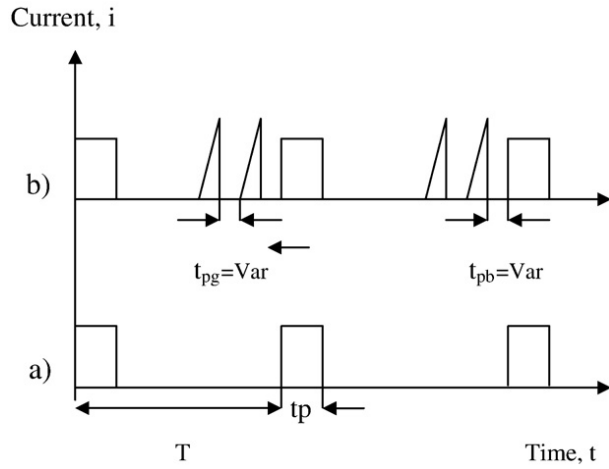
Figure 31: Scheme representing the proposed sequence of pulses with the triangular grinding pulses [22]

Table 3 details the parameters for the experiments, noting that the triangular pulses, while intended for the grinding of the depositions add significant amounts of additional electrical energy, [22].

Table 3: Grinding pulses experimental parameters [22]

Type of pulse	Shape	Ampl. of current, A	Durat., µs	Amount of electr., C	Energy, J	Number of grinding pulses	Additional amount of electr., %
Base pulse	Square	400	200	0,07	1,19	1	–
Grind. pulse	Triang.	500	60	0,0165	0,28	1	23
Grind. pulse	Triang.	500	60	0,0165	0,28	2	46
Grind. pulse	Triang.	400	48	0,0096	0,163	2	27,4
Grind. pulse	Triang.	400	48	0,0096	0,163	3	41,1
Grind. pulse	Triang..	300	35	0,0055	0,094	3	23,5
Grind. pulse	Triang.	300	35	0,0055	0,094	6	47
Grind. pulse	Triang.	200	22	0,00217	0,037	9	28

Figure 32 graphs the results from one of the experiments in the study. The Base 1 parameters were square wave pulses at regular intervals as the baseline for normal ESD mass transfer rates and surface roughness. Base 2 was a deposition with only the grinding triangular pulses, which still developed sufficient energy to form depositions. Combinations of the Base 1 and triangular pulses can be seen from the other charts, demonstrating that the combination of the square and triangular pulses both increased the deposition rate and decreased the surface roughness, in opposition to the previous studies, [22].
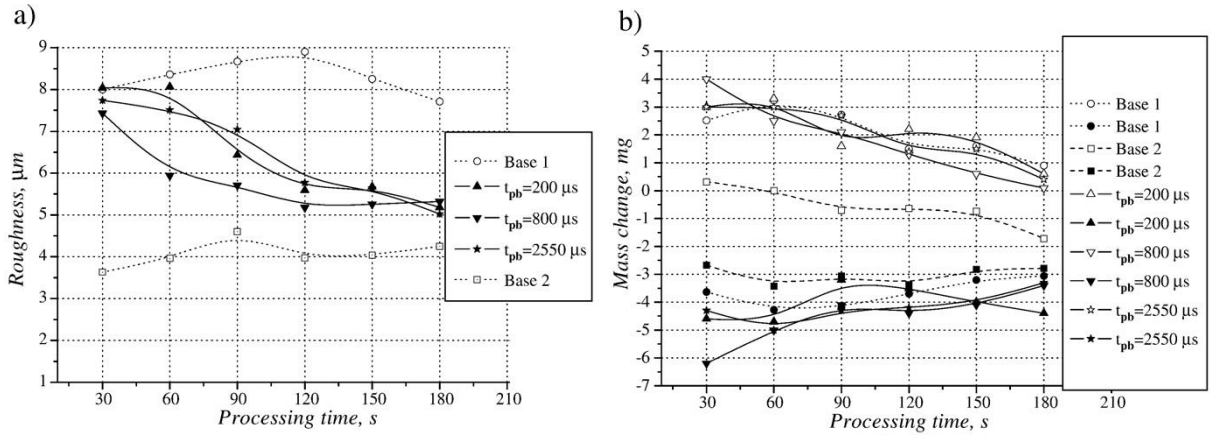
Figure 32: a) as deposited surface roughness; b) mass transfer values versus processing time [22]

The study concluded that there is a benefit to mixing the square pulses with the triangular grinding pulses. Issues arose when adding the triangular pulses resulted in overheating of the coatings or electrode and added defects to the coatings. Coatings comprising of more than 2 ESD layers resulted in little benefit from the grinding pulses. Such that a careful selection of parameters paired with the chosen material so as to not generate excessive heat would increase the mass transfer rate and reduce surface roughness, [22].

2.5 Controls Theory

Proportional-integral-derivate (PID) control is a mathematical control algorithm used for closed loop feedback response. The system operates by sensing a feedback from the active system, then calculating the appropriate output to the plant to achieve the desired output. The feedback is factored by calculating the proportional, integral and derivative response and adding the components to predict an output. The error between the last recorded data point and the desired input setting is used by the controller to determine the magnitude of the output response. Figure 33 shows a block diagram detailing the closed loop feedback system, [23] [24].
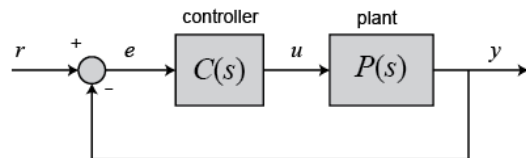
Figure 33: Generalized PID feedback system [23]

Tuning of the PID gain values serves to affect the efficacy of the controller, typically measured by comparing the effects on rise time; percent overshoot, settling time and steady state error. Figure 34 graphically details how a PID system controls the real response in red to the set point of 1, [23] [24].
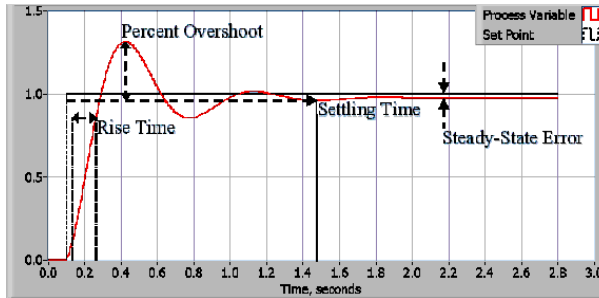
Figure 34: Graphical PID response [24]

Equation 3 states the generalized equation for a PID controller output. The variable e(t) is the real time error, representing the quantified difference between the set value r and the output value y. Kp, Ki and Kd represent the proportional, integral, and derivative gain values which modify the inputted error value in order to generate the control signal u.

$$u(t) = K_p e(t) + K_i \int e(t)dt + K_d \frac{de}{dt}$$

Equation 3: General PID output equation in the time domain

Depending on the complexity of the system to be controlled, additional variables such as dead time, where the system is not responding. This is often due to slow cycle times in the PID closed loop system or a relatively slow action to be performed by the plant. Fast cycle times and reduced, or accounted dead time is required for more complex plant systems where there is a smaller margin of error, [24].
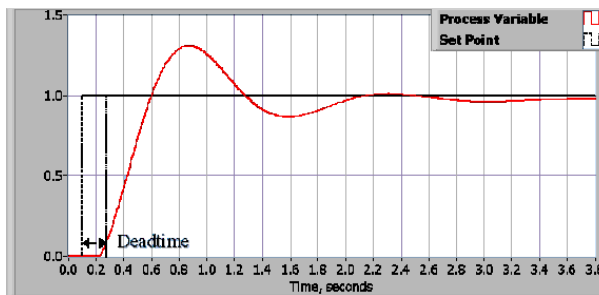
Figure 35: PID controller response dead time [24]

Each gain value of the PID controller contributes a different effect to the modified output. Different control situations call for a different combination, and varying magnitudes of each gain type. The PID algorithm detailed in Equation 3 is illustrated as a sequential block diagram for the closed loop control system in Figure 36, [24].

21
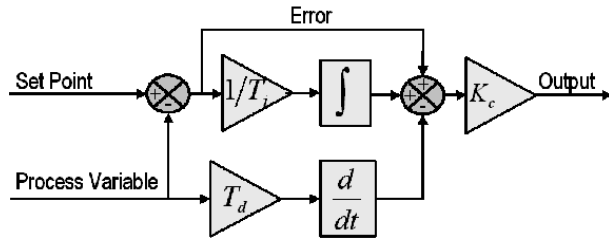
Figure 36: Block diagram of PID control algorithm [24]

2.5.1 Proportional gain

The proportional gain contribution to the control system is to factor the magnitude of the error, as a measurement between the set point and the process variable. The ratio between the output response and the error signal is determined by the proportional gain. Increasing the proportional gain will increase the reaction time of the system, thus reducing the rise time. Significant increases in the proportional gain will increase the steady state error and may cause the error to increase every cycle, [24].

2.5.2 Integral gain

The integral gain responds to the accumulated error over time, using the integral to add the area between the real response and the set point. This term will cause reactions even to small error values over time. This results in the integral gain serving to reduce the magnitude of the systems steady state error, [24].

2.5.3 Derivative gain

The derivative gain considers the rate of change in the process variable, in an effort to reduce the response if the increase is too extreme. Increasing the derivative term serves to modulate the output response based on the error, reacting more rapidly when the error signal is changing. Typically the derivative gain is set very low as the response is susceptible to noise, or if the loop cycle speed is too slow. Applying derivative control under these conditions can result in an unstable response, and a very slow reaction, as the derivative gain may dampen controller output with low cycle speed systems, [24].

2.6 ESD Control

Feedback control is relevant for controlling the application force and movement speed during the ESD application. Traditional ESD setups involve manual operation of the applicator where the skill of the operator directly affects the result of the coating. Creating complex coatings and patterns may also be advantageous when implementing ESD with a CNC system.

A study has linked the effect of ESD application force to the heat generated in the substrate. Additional force tends to reduce the heat generated in the substrate. At a local level the additional force closes gaps and reduces the distance between small protrusions. Reducing the gaps and resistance serves to more easily allow the passage of current and voltage, lowering the joule heating effect. Figure 37 relates the effects of the ESD force on the resulting substrate temperature for experiments in this study with ceramic coatings being deposited on steel substrates, [25].
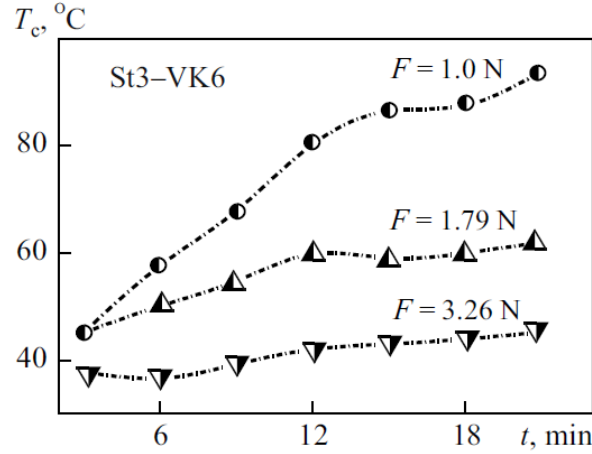
Figure 37: Temperature change in the substrate from ceramic depositions on steel relating pressing force [25]

A subsequent study used a typical capacitor ESD pulse generator and a CNC system with an optical feedback sensor to measure the force. A spring load was applied to a rotating applicator to maintain a constant application force and alter the force if needed. A scanning pattern was used to deposit an aluminum electrode onto stainless steel with a range of ESD electrical parameters and argon shielding gas. Experiments were done to determine the effect on the mass change from the anode to the cathode and the process efficiency when considering the contact force, traverse movement speed, pulse frequency, and number of raster scans, where results are graphed in Figure 38, Figure 39, Figure 40 and Figure 41 respectively, [26].

Increasing the contact force resulted in a continuous drop in process efficiency and the range of contact forces was already very small, between 0.25 and 0.8N. Increasing the traverse speed resulted in a decrease in process efficiency; with the same electrical parameter moving quickly will reduce the thermal input into a given area which will reduce the deposition rate. Increasing the pulse frequency increased the mass gained by the substrate, but more rapidly increased the erosion by the electrode, thus slightly reducing the process efficiency. Increasing the number of scans results in a slight increase and then plateau of the process efficiency, most likely due to the warming of the electrode and substrate to an optimal level, [26].
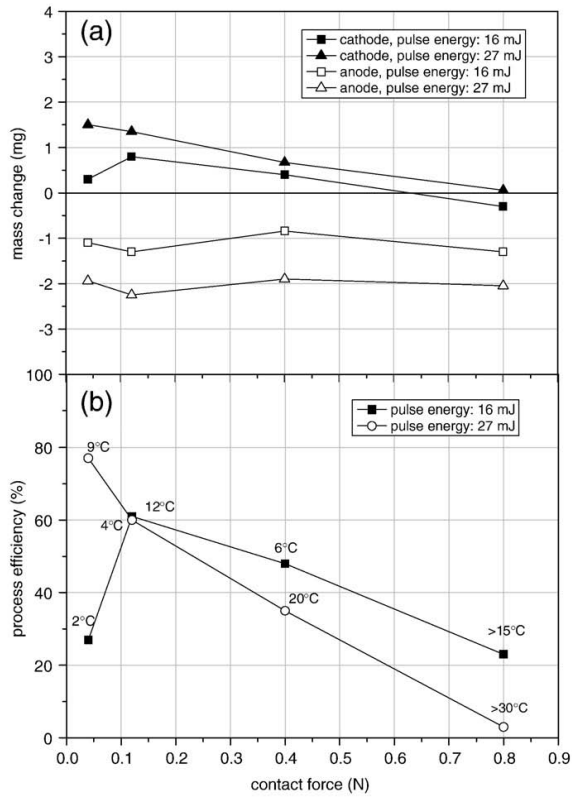
Figure 38: Effect of contact force with pulse frequency of 55Hz, traverse speed of 5mm/s and deposition time 200s [26]
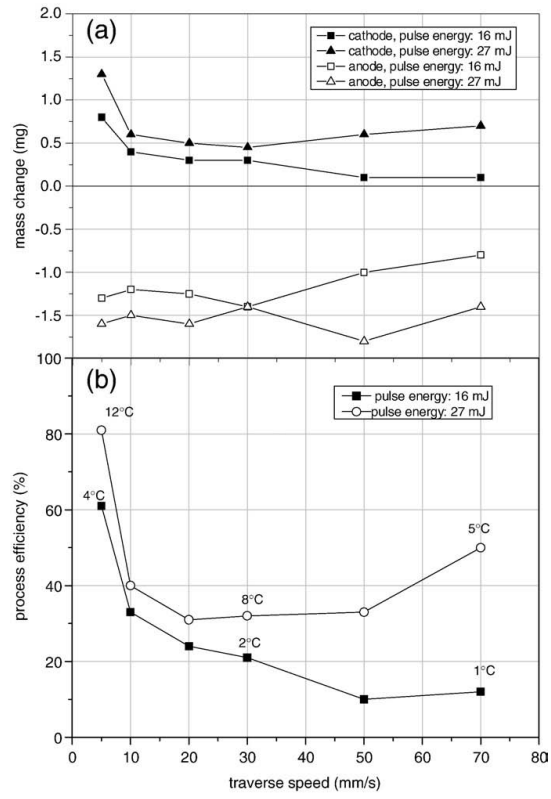
Figure 39: Effect of traverse speed with 0.12N contact force and 55Hz pulse frequency [26]
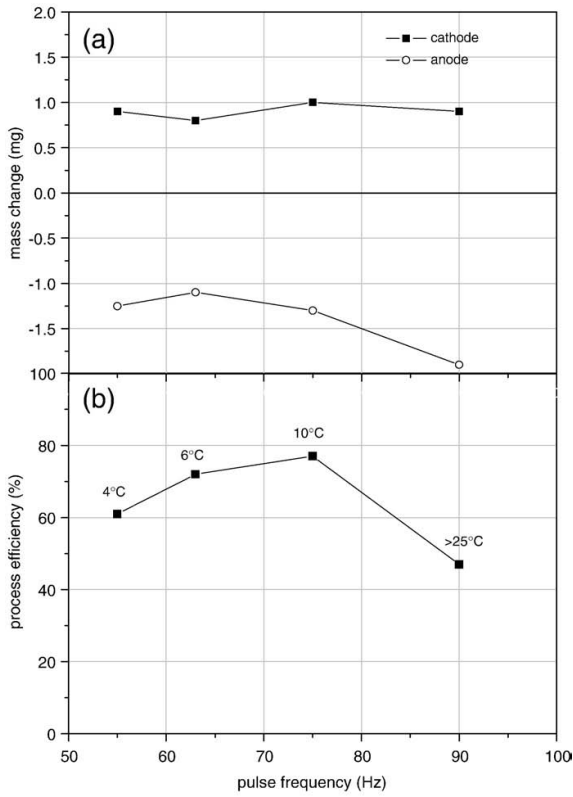
Figure 40: Effect of pulse frequency with 16mJ pulse energy, 0.12N contact force, 5mm/s traverse speed and 200s deposition time [26]
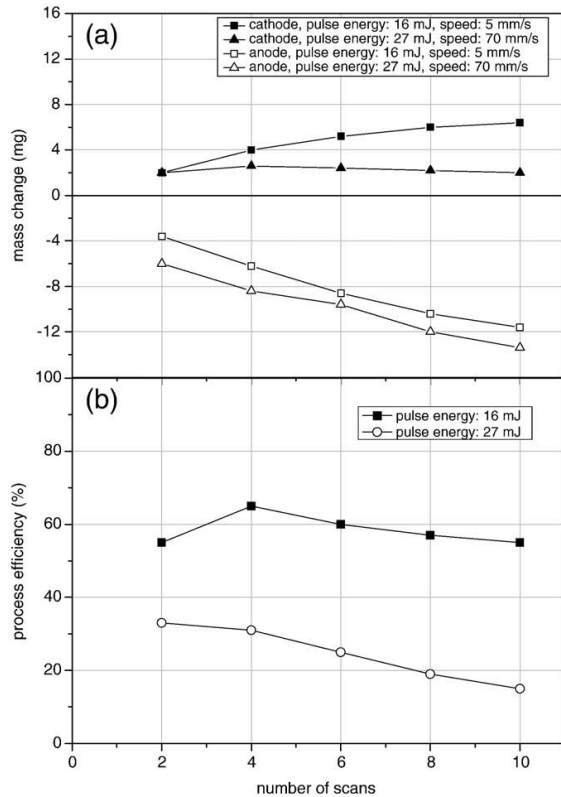
Figure 41: Effect of the number of raster scans with 55Hz pulse frequency, 0.12N contact force, 200s single scan deposition times 5mm/s; and 14s at 70mm/s [26]

The study concludes that the contact force is an integral parameter to the effective control of the ESD process. Low contact forces serve to increase the potential gaps and reduce the resistance of the protrusions, this is said to promote spark breakdown and promote lower substrate erosion and cratering. The lower forces also resulted in lower surface roughness, allowing for higher electrical energies to increase the coating thickness to be employed, [26].

Chapter 3.0: Experimental Setup

3.1   ESD Machines

3.1.1   ESD Machine #1

ESD Machine #1 is a traditionally designed power supply, similar to the design presented in section 2.4.1 Figure 21. The machine operates by transforming and rectifying the alternating current (AC) municipal power to directly charge a high powered fixed capacitor. Depositions are applied with an eccentrically vibrating electrode powered by a cam and electric motor. The fixed electrical parameters were designed specifically for the application of depositing high ceramic content coatings on metallic substrates.

3.1.2   ESD Machine #2: Pulse controlled machine

ESD Machine #2 controls two ESD circuits with 2000µF and 200µF fixed capacitance, a range of 20 to 40V with varying pulse sequencing control modes. The same vibrating applicator as ESD Machine #1 is used. See Figure 42 for an image of the ESD power supply.

Figure 42: ESD Machine #2

3.1.3   ESD Machine #3: Universal ESD Machine

The universal ESD machine power supply is managed by a microcontroller with the option to control the capacitance from 10-300µF, voltage from 10-135V, maximum frequency from 10-500Hz and charging speed from 10-95% of maximum capacitor charging speed. Figure 43 exhibits the front panel for the Universal ESD machine. The system uses a rotating applicator which maintains a more constant contact with the substrate.

Figure 43: Universal ESD machine #3

3.2 Material characterization

Cross sectioned samples were prepared with standard grinding and polishing techniques, with various etching procedures depending on the appropriate characterization method and material.

3.2.1 Optical microscopy

Optical microscopy used an Olympus BX51M System metallurgical microscope with magnification lenses for 5x to 100x magnifications. Integration with a digital camera allowed for the digital post analysis of microstructure images.

3.2.2 Elemental analysis

High magnification images and quantified analysis of elemental composition used a Scanning Electron Microscope (SEM) Jeol JSM 6460 with EDX analysis employing an Oxfords Instruments INCA-350.

3.2.3 Materials

Typical materials used in the following experiments often include, but not exclusive to the pairing of TiC/Ni sintered cermet electrodes with approximately 75% TiC to 25% Ni with Copper resistance spot welding (RSW) electrodes and pure copper substrates. As well as evaluating the buildup capabilities of DP-980 grade steel substrates with carbon steel electrodes.

3.3 Sensing devices

Recording data from the ESD process and electrical signals from the power supplies is necessary for characterizing the performance of the systems.

3.3.1 NI-DAQ

Collecting sensor data, and controlling the force feedback system was done using the National Instruments data acquisition system 6003 (NI-DAQ USB 6003), see Figure 44. This equipment integrated with the NI LabVIEW software via a USB serial connection to a laptop. The equipment has 8 analogue inputs with 16-bit resolution at 100,000 samples per second. 2 analogue outputs at 16-bit resolution and 5,000 samples per second per channel, 13 toggle control I/O lines, 1 32 bit counter and 5V output power supply from the USB computer interface. High sampling speeds allows for the recording of the ESD short duration current pulses and capacitor voltage degeneration, [27].

Figure 44: NI-DAQ USB 6003 [27]

3.3.1.1 *Voltage step-down*

Voltage measurements were recorded by the NI-DAQ by stepping down the voltage from the ESD power supply and directly connecting to an analogue input from on the NI-DAQ device.

3.3.1.2 *Hall Effect Sensor*

A Hall Effect sensor, seen in Figure 45, functioning based on the Hall principles of electromagnetic conversions, as detailed in section 0, was used to measure the real current output from the ESD power supplies. The Hall Effect sensors detected current flow ±10V, integrating with the NI-DAQ system. The Hall Effect sensor is a solid state device, whose sampling speed is related to the recording speed of the DAQ system. Typical data resolution is set at 30kHz, 50kHz and 100kHz for recording ESD power

supply current. Figure 46 illustrates the capability of the Hall Effect sensor setup to record over 15 data points for the often less than 5ms current pulses generated by the ESD process.
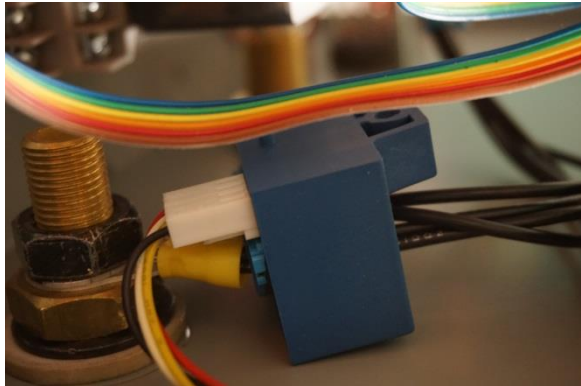
Figure 45: Hall effect sensor in ESD machine
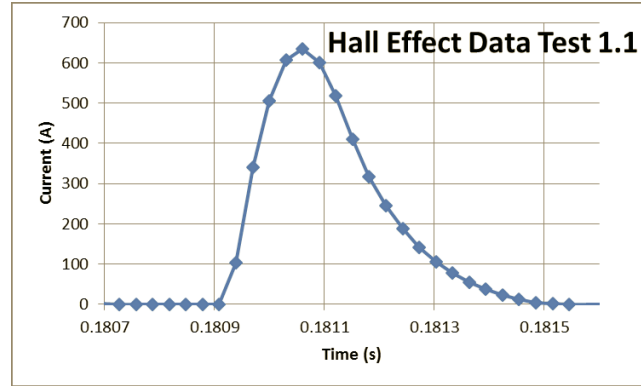
Figure 46: Single current pulse Hall Effect recorded data

3.3.1.3   Capacitive Force Sensor

Capacitive force sensors measure the electrical potential between two conductive plates a Single Tact 44N capacitive force sensor was used for integration with the NI-DAQ and force feedback system. The sensors, depending on the setup can be used to measure both the shear and normal forces. Arrays of electrodes are spatially separated by dielectric materials, when force is applied the potential between the two conductors registers as a change in the force, [28].
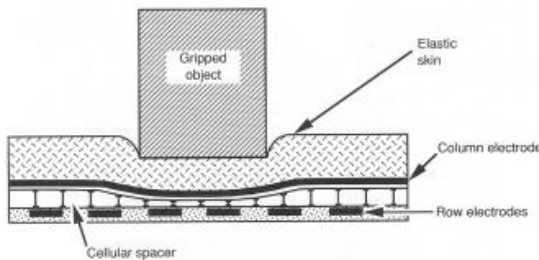
Figure 47: Capacitive force sensor illustration [29]

The single tact 45N capacitive force sensor with a calibrated analogue output board was used to measure the ESD process force. See Figure 48 for a reference image of the sensor and the calibration and analogue output board. [30] The range of 45N was ideal to manage higher than ideal force ratings, in order to achieve the low force values, below 5N, reported in literature, [25].

Figure 48: Single Tact Capacitive Sensor and analogue integration board [30]

The sensor operates from the USB NI-DAQ 6003 operating off the 5V output power and reading from an analogue input connection at ±10V DC. The sensor system outputs a range of 0 to 2V DC where the valid readings are between 0.5V and 1.5V, values under 0.5V can represent damage to the sensor or suction on the contact patch, values above 1.5V are invalid and represent over pressure of the sensor see Figure 49, [30].
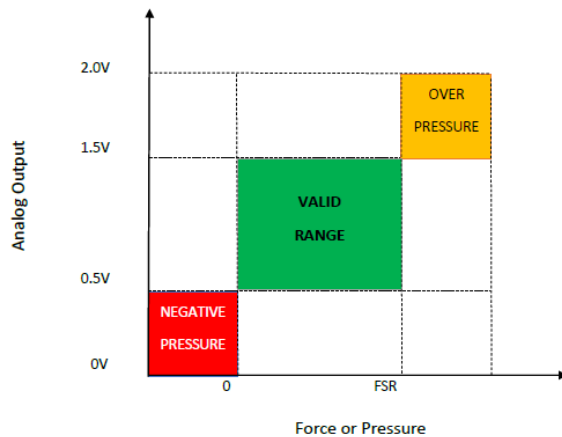
Figure 49: Valid data range for capacitive sensor [30]

3.4 High speed camera

High speed images were recorded using the FASTCAM Mini UX50 model, see Figure 50. The equipment has a maximum frame rate of 160,000 frames per second, and a 1.3 Megapixel CMOS sensor which relates to an example resolution of 1280x1024 pixels at 2000fps. The system detects ISO 10,000 in monochrome and 5,000 in colour. Suitable with filters for recording low wavelength radiation from welding applications, [31].

Figure 50: FASTCAM Mini UX50 [31]

3.5 CNC

The CNC is comprised of three controlled stepper motors each powering one of the CNC physical axis, see Figure 51. The applicator interface on the z-axis uses a spring suspension system to reduce the application force during the ESD process, see Figure 52.
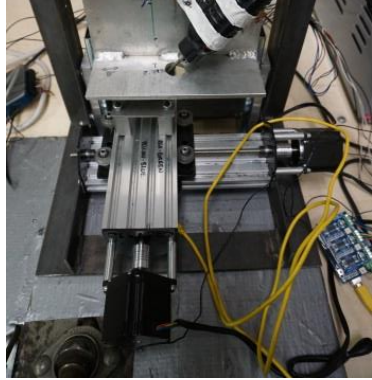
Figure 51: CNC machine

Figure 52: CNC machine z-axis mount and suspension

3.5.1 Arduino Uno

The CNC interface with the laptop was facilitated through the use of the Arduino Uno microcontroller device, see Figure 53. The device employs an ATmega328P microcontroller chip, with an operating voltage drawing 5V, 6 PWM out I/O pins, 6 PWM in I/O pins, 20mA DC limit for I/O pins and 50mA limit current for 2 3.3V pins. The system has an internal clock speed of 16MHz, and internal memory of 32kB. See Appendix B: Arduino Uno Schematic Figure 135 for the schematic diagram for the Arduino Uno device, [32].

Figure 53: Arduino Uno microcontroller device [32]

3.5.2 Driver shield

Integration from the Arduino Uno microcontroller to the CNC machine is facilitated through the use of the Synthetos gShield V5, see Figure 54. The gShield is designed for integration with the Arduino Uno, and allows for the interpretation of rs274/ngc gcode standards also employed by the popular Linux CNC software. The shield manages the control of 3 axis, x, y and z with support for arc motion, acceleration and deceleration management as well as predictive actions.

The system outputs 8x micro stepping bi-polar stepper motor pulses, with 2.5A per winding 12V-30V DC power input powering TI DRV8818 stepper drivers, and importantly independent current chopper controllers per axis.

Figure 54: Synthetos gShield V5 [33]

3.5.3 GRBL Software

GRBL V0.9 is the open source software used for integrating the computer and G-Code to the CNC machine. The controller is written in C and compatible with the Arduino Uno Atmega 328 microcontroller chip. The software allows for management of a CNC system through the simulated parallel port connection created by the Arduino Uno. The software is compatible with standard gcode

32

conventions supporting arcs, circles and helical motions. The software includes acceleration management with predictive planning up to 18 commands in the future to allow for jerk reduced direction changes, [34].

3.5.3.1   Universal G-Code Sender

Rather than employ the Arduino Uno IDE interface with a serial monitor function an open source graphical user interface (GUI) was used, called the Universal G-Code Sender. The software is a Java based interface with the GRBL software using the Arduino serial USB connection. The software provides a 3D gcode visualizer with real time tool positioning feedback, along with metrics and macro functions for the CNC operation. See Figure 55 for an example of one of the interface pages from the GUI of the Universal Gcode Sender, [35].
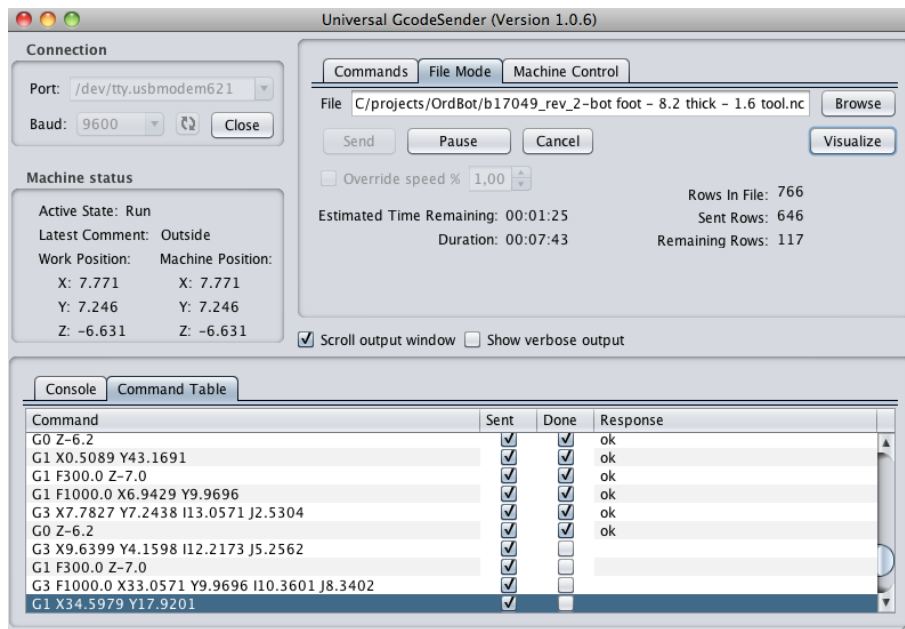
Figure 55: Universal G-Code Sender software [35]

Chapter 4.0: ESD Machine design and coating experiments

All the ESD power supplies presented function off the principle of the spark energy generated by a discharging capacitor. Depending on the electrical parameters and pulse control systems in general the capacitor is charged, and then when the electrode contacts the substrate there is a rapid discharge resulting in a current spike. Figure 56 illustrates the voltage reading at the capacitor, characterizing the rapid charging and discharging. Figure 57 presents the capacitor voltage drop from 140V, causing a 600A current pulse, over a time frame of less than 0.2ms. The period of pulses with these settings was approximately 18ms, which can be altered with the electrical power supply parameters.
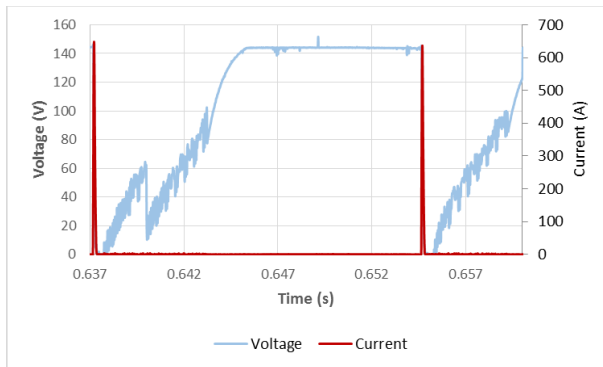
Figure 56: Capacitor charging and discharging behavior
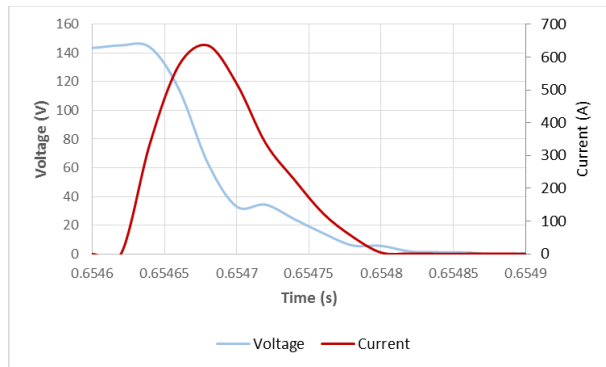
Figure 57: Capacitor discharge pulse behavior

Study into the effects of different ESD power supply configurations aims to improve the range of potential applications while improving the coating quality and efficiency. Application of the improvements presented in background sections 2.2, 2.3 and 2.4 provides the basis for improvements to traditional ESD power supplies.

4.1   Machine #1

Machine #1 is the first generation of the ESD machines with a similar performance to the traditional power supply design presented in section 2.4.1. This was the simplest power supply with only a positive and negative port for the integration of the ground clamp and applicator. The machine used a vibrating applicator which utilized a rapidly spinning cam to create the vibrating motion.

Figure 58 illustrates a flow detailing the initial ESD power supply. With this system the AC power from the typical 120V 15A power supply is transformed and half wave rectified to the desired maximum

discharge voltage. A high powered constant capacitance is charged and discharges based on the contact frequency developed by the vibrating applicator.

Figure 58: ESD Machine #1 electrical components block diagram [36]

Due to the fixed electrical parameters this power supply is not effective at working with different material pairings, as there is no control of the electrical parameters. In Figure 59 the output current from the power supply changes significantly with every subsequent pulse, as well as the discharge voltage. With this setup the ESD sparking is also contingent on the frequency of the applicator vibrations as there is no microcontroller or switching functions. Operation of this power supply would regularly see different voltages and currents if contact is at a higher frequency than the full charging of the capacitors, this is similar to the issues detailed in the typical ESD power supplies in section 2.4.1.
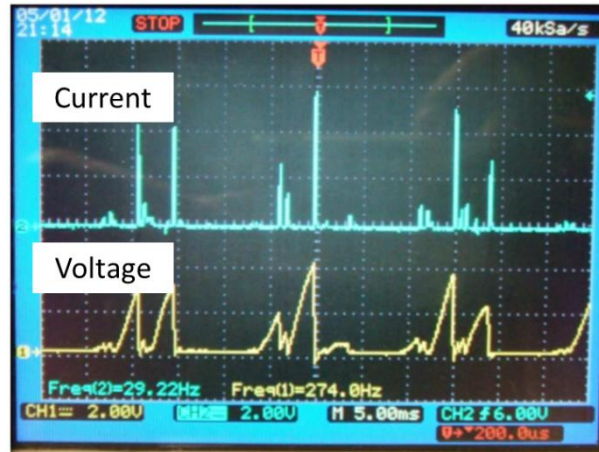
Figure 59: ESD Machine #1 electrical signals: Current and voltage [36]

The fixed electrical parameters may not be effective for other material pairings and coating conditions. Uncertainty in the output power of the machine, and the discharge conditions depending on the contact with the vibrating electrode makes the performance of the power supply difficult to predict, and renders the machine unsuitable for ESD research into the coatings of a wide array of materials and applications. [36]

4.2 Machine #2

ESD Machine #2 was developed as a culmination of many of the different beneficial effects from the research into ESD power supplied summarized in section 2.4.

35

The first improvement to the ESD circuit is to control the charging power, and when the circuit discharges. This was achieved with the implementation of a microcontroller which allowed for the tuning of the charging voltage, and discharge frequency.

Notably this system employed solid state switching devices, IGBTs in a manner similar to the research presented in section 2.4.1. The integration of the IGBTs and microcontroller allowed for the full charging of the capacitors and controlled discharges allowing for voltage, and frequency control for different ESD applications. Further electrical performance was realized through the use of a diode bridge rectifier with smoothing capacitor, to maintain constant charging current to the capacitors. See Appendix A: Electrical component descriptions for comparisons between different rectifier types.

Multiple concurrent discharges were realized with the addition of a secondary parallel ESD circuit with lower capacitance and voltage. Figure 60 details the final block diagram for the final iteration of the ESD Machine #2 power supply.
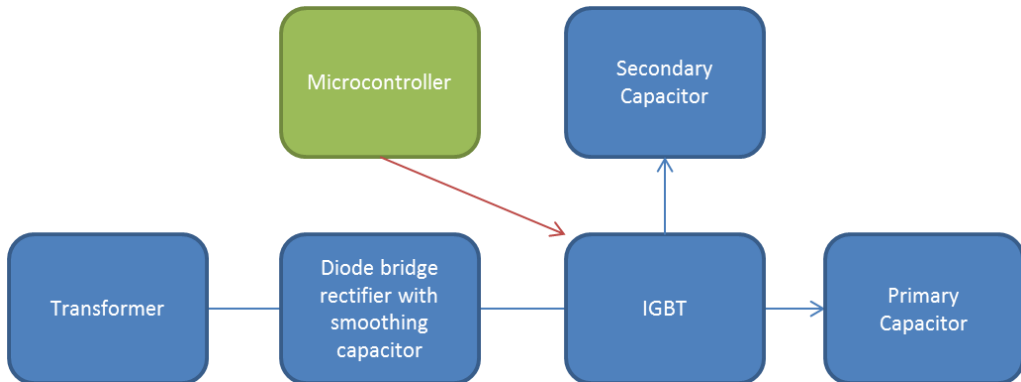
Figure 60: Improved ESD Machine #2 power supply block diagram [37]

Using IGBTs to manage the discharge and charging of the capacitor the discharge can now be maintained at a constant controlled energy level versus the random performance supplied by the ESD Machine #1. Management of the pulse discharge voltage and frequency allows for the relation of performance to the electrical parameters. The consistent electrical signals seen in Figure 61 are in contrast to the performance of Machine #1 demonstrated in Figure 59 above.
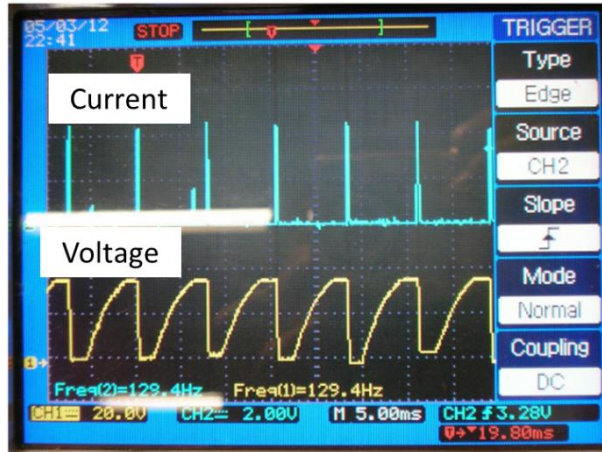
Figure 61: ESD Machine #2 electrical signals: Current and voltage [36]

4.2.1 ESD Parameters

Control of the discharging circuit allowed for sophisticated control of the ESD pulsing behavior. Beyond the typical control of the ESD spark energy through varying the voltage and current the advanced pulsing behavior can realize fine adjustments in the heat input, mass transfer rates and cooling behavior of the process. The addition of multiple pulse arrangements, as well as potential changes in the pulse energy supports the need for characterization of the effect of pulse sequences and metallurgical effects on coatings.

Table 4 summarizes the range of parameters, pulse sequences and circuits available in the ESD Machine #2. The main circuit controlled the pulse sequence through the use of a high and low powered pulses with the parameter range detailed in Table 4. A secondary circuit or arc circuit was parallel to the main circuit and allowed two simultaneous capacitor discharges, where the higher voltage of the main circuit would pulse first followed by the secondary circuit. These pulse sequences were in an effort to harness the improvements to the traditional ESD pulses detailed in section 2.4.

Table 4: ESD Machine #2 electrical parameter ranges

ESD Circuit	Discharge Control	Voltage (V)	Capacitance (µF)	Charging Speed (%)	Recharge Delay (#)
Main Circuit	High	25-45	2000	0-45	0-5
	Low	10-45	2000	0-45	0-5
Secondary Circuit	Arc	5-20	200	0-95	0-5

37

Management of the different possible pulse sequences and circuit discharges was managed through the use of a control mode parameter in the ESD Machine #2 microcontroller. The different possible control mode combinations are detailed in Table 5. An experiment recording the voltages for the two circuits was performed to test the real performance of the control modes, the results are summarized in

Appendix C: ESD Machine #2 Control Modes Experiment, Table 20 and Figure 136 to Figure 146.

Table 5: ESD Machine #2 control modes

Mode #	V_High	V_Low	V_ARC	Comment
0	1	1	0	Pulses are discharged sequentially
1	1	0	1	Pulses are discharged sequentially
2	1	0	0	Low Pulses are not discharged, this leaves a space between high pulses
3	1	0	0	Only High pulses are discharged sequentially
4	0	1	0	Only Low pulses are discharged sequentially
5	0	0	1	Only Arc pulses are discharged sequentially
6	1	1	1	High and Low pulses discharge sequentially. Arc pulses discharge at the same time as those on the ESD circuit
7	1	1	1	High and Low pulses discharge sequentially. Arc pulses discharge on the High pulses
8	1	0	1	Low Pulses are not discharged, this leaves a space between High pulses. Arc pulses are added to the High pulses
9	1	0	1	High pulses discharge sequentially, Arc pulses are added to the High pulses

Selection and setting of the different parameters was effected through interface with the display panel and control board. Interface with the machine and selection of parameters is achieved through the interface with the ESD Machine #2 control panel seen in the Experimental Setup section Figure 42.

4.2.2 Frequency

The pulse frequency output from the ESD power supply Machine #2 is dependent on the interaction between several other parameters, and is not controllable as an independent variable. The frequency is altered through the relation between the capacitance level, set voltage, charging speed as a percentage, holding time and recharge delay. Previous studies into the effect of ESD parameters explored in section 2.4 demonstrated that control of the ESD pulse frequency is necessary to the proper management of heat generation and effective coatings. The voltage data, representing the pulse frequency is detailed in Figure 62.
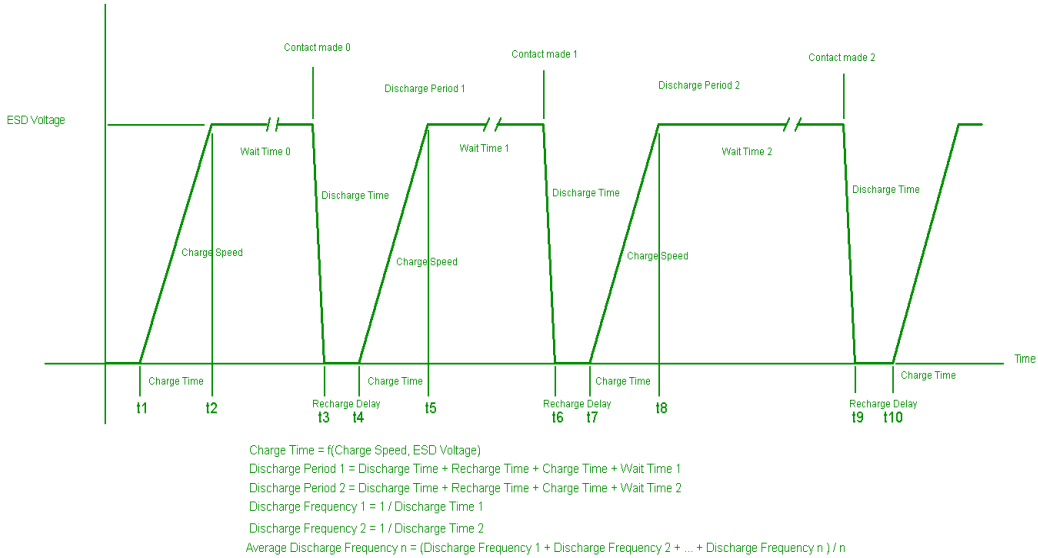
Figure 62: ESD voltage behavior and frequency response [36]

The charging speed related to a percentage of the maximum voltage slope for the capacitor to reach maximum charge. Depending on the set voltage level and the charging rate there will be a different maximum potential frequency. A hardcoded minimum holding time referred to as the discharge delay also affects the maximum possible frequency. Figure 63 demonstrates the real electrical signals representing the time response of the capacitor voltage and corresponding current spike from the capacitor discharge. In order to experimentally quantify the pulse frequency the DAQ setup was used to record the voltage and current signals, then the number of current pulses, or voltage degeneration was measured in the time scale.
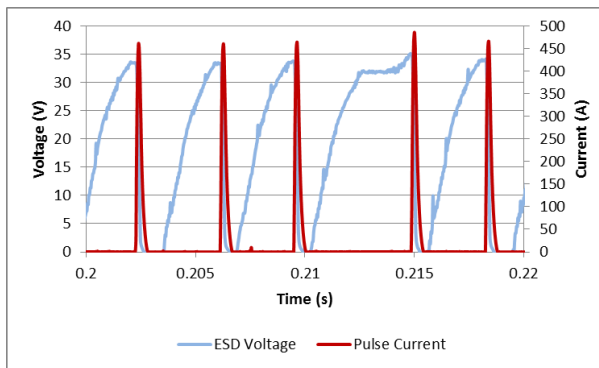
Figure 63: Voltage and current response from ESD Machine #2

40

4.2.2.1 Recharge delay

The recharge delay was intended to be a parameter related to a set pause between ESD pulses. Experiments to determine the effect of this parameter resulted in a contrary conclusion. The control of this parameter is varied by the selection of a numerical value between 0 and 5. An experiment was designed to measure the effect of the recharge delay on the real output frequency of the ESD power supply, in order to effectively characterize the effective parameters for depositing materials. The general parameters for the experiment are stated in Table 6.

Table 6: Machine #2 ESD parameters for Recharge delay experiment

Data Frequency (Hz)	Capacitance (µF)	ESD Voltage (V)	ARC Voltage (V)	ESD Charge
33,000	2,000	45	30	45
ARC Charge	ESD 1 Pulses	ESD 2 Pulses	Control Mode	EXT Control
35	1	0	9	0

Six tests were performed with varying recharge delay settings to monitor the effect on the gap between the pulses. Several experiments were done at every setting while attempting to short circuit the applicator and electrode to determine the maximum electrical output. The results are summarized as averages and errors in Table 7 and graphed in Figure 64. The average time values in ms are reported for each recharge delay setting, along with the associated values along a linearized average of the experimental values.

Table 7: Machine #2 recharge delay experiment

Test #	1	2	3	4	5	6
Recharge DLY	0	1	2	3	4	5
Frequency (Hz)	134.1	136.8	356.0	140.5	140.1	129.6
Recharge Delay (ms)	**0.357**	**0.791**	**1.010**	**2.075**	**1.975**	**2.480**
StDev (ms)	0.053	0.242	0.227	0.399	0.729	0.747
Error (%StDev)	15.0%	30.6%	22.5%	19.2%	36.9%	30.1%
Maximum (ms)	0.433	0.980	1.309	2.798	3.017	3.756
Minimum (ms)	0.296	0.447	0.696	1.575	1.012	1.625
Linear Value (ms)	0.360	0.795	1.230	1.666	2.101	2.536
Linear Error (ms)	0.78%	0.55%	21.86%	-19.75%	6.39%	2.25%
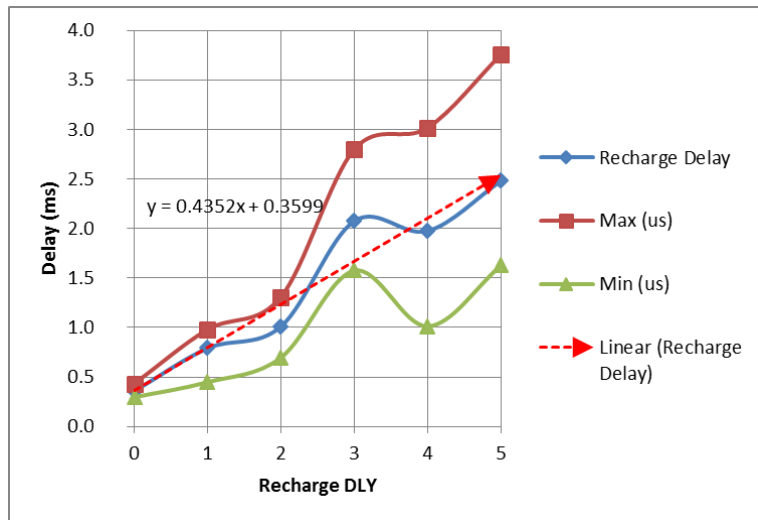
Figure 64: Machine #2 recharge delay millisecond response

The recharge delay experiment resulted in a semi linear behavior; the deviation from the linear trend for test number 3 could be affected by a change in the electrode contact. Test 3 was found to be aberrant when the voltage and current levels were evaluated. Table 8 denotes the change in the average voltage and current values for test number 3.

Table 8: Recharge delay experiment voltage and current data

Test #	1	2	3	4	5	6
ESD Voltage (V)	45.48	46.22	28.44	46.09	45.47	45.56
Current (A)	653.57	670.44	378.09	658.03	649.68	641.74

Figure 64 clearly shows the increase in the delay time between pulses, however there is a significant increase in the error, as the recharge delay setting increases. This increase in the variability of the recharge delay contributes to uncertainty in a predicted frequency value with different recharge delay settings. Furthermore this experiment does not conclusively determine the time value related to each recharge delay setting due to the non-linearity of the results and the increasing error.

4.2.3   Secondary Capacitance Circuit

Pulse control was managed through the selection of one, of the 8 possible control modes comprising different high and low voltage pulses varied with the secondary circuit pulses. The high and low settings were sequential pulses from the main ESD 2000μF capacitance circuit with independent charging speed settings. The secondary circuit was a parallel circuit with 200μF with independent charging speeds. The secondary circuit, depending on the selected control mode, was designed to discharge at the same time as

42

the main circuit, the lower secondary voltage and capacitance results in a second capacitor discharge from the electrode, practically simultaneous with the main pulse. Figure 65 illustrates the high speed discharge and interactions between the two circuits. The primary circuit voltage rapidly degenerates indicating the discharging of the 2000μF capacitor. There is a corresponding high current pulse near 450A, followed by a smaller <50A pulse caused by the subsequent and immediate, within 2ms of the initial pulse, discharge of the secondary circuit.
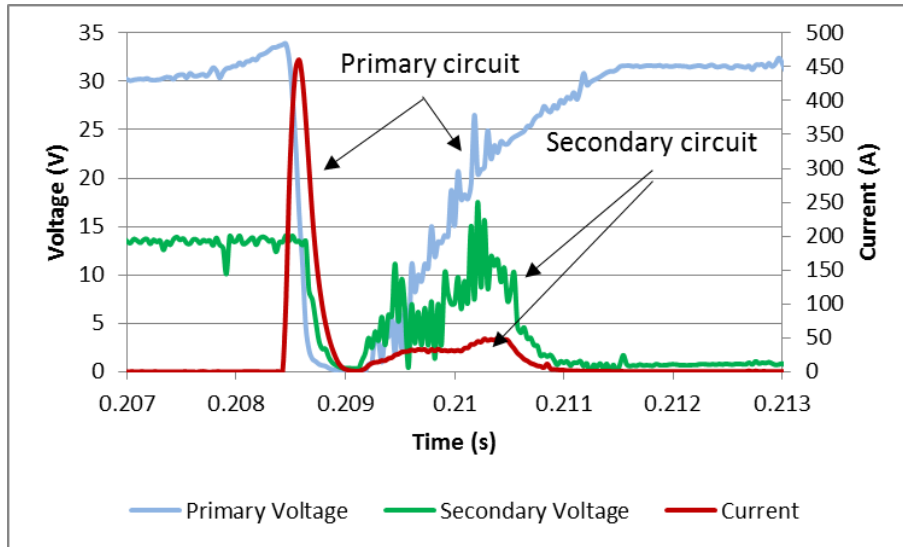
Figure 65: ESD Machine #2 control mode 6 secondary circuit discharge

4.2.4   Parameter experiments

In order to relate the electrical output of the main parameters an experiment was designed to relate the effect of changing the voltage, charging speed and recharge delay to the measured pulse frequency. Table 9 summarizes the range of parameters tested for the design of experiment. The resulting electrical signals were processed to evaluate the maximum current levels from the ESD pulses and the frequency of the pulses, cross referencing the electrical parameters with the Taguchi method. In order to ensure the electrical signals represented the power supply output the applicator was short circuited to the substrate without using the vibration function or relative motion.

Table 9: ESD Machine #2 parameter interactions experiment variables

Variables	Low	Medium	High
ESD Voltage (V)	25	35	45
Charging Speed (%)	10	30	45
Recharge DLY	0	3	5
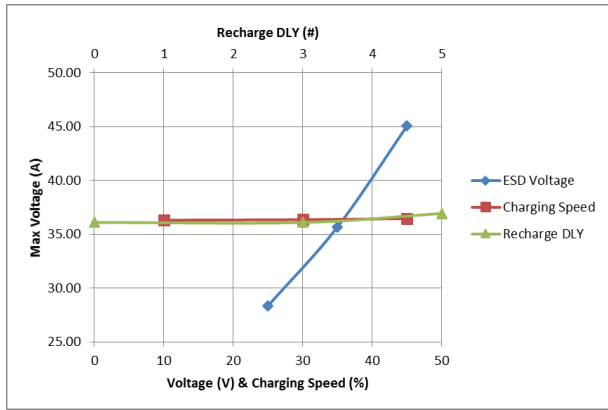
Figure 66: ESD Machine #2 voltage response
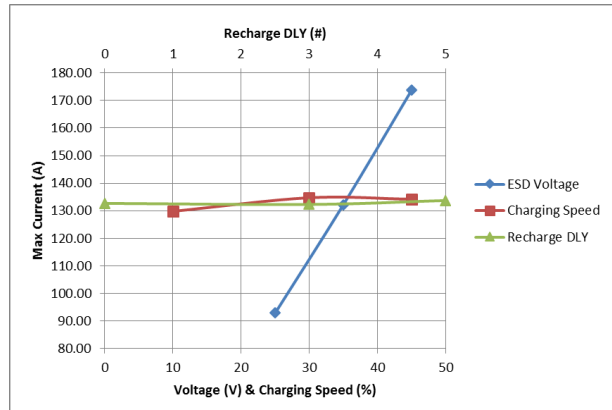
Figure 67: ESD Machine #2 current response
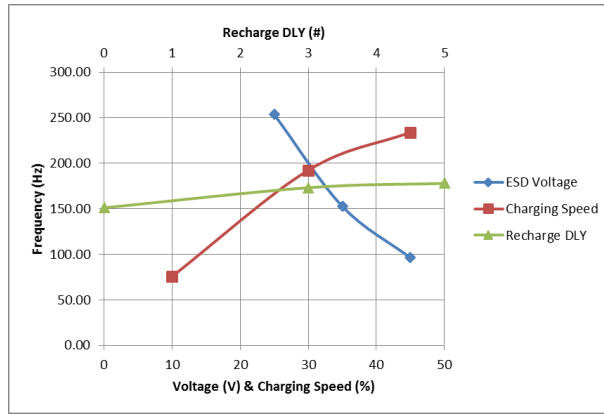
Figure 68: ESD Machine #2 frequency response

The results summarized in the charts displayed in Figure 66, Figure 67 and Figure 68 demonstrate that altering the charging speed and recharge delay did not affect the output voltage or the peak current of the ESD process. All three variables had a varying effect on the pulse frequency, thus the ESD energy per pulse is known but not the power output of the machine. Calculating the frequency without recording the electrical data would require knowledge of the interactions between all parameters. The effect of the recharge delay parameter demonstrated an increase in frequency, contrary to the increase in the delay between the pulses. The increase can be attributed to the increase in the error due to increasing recharge delay represented in   Figure 64. As a result of the interactions seen from this experiment and the increasing error conclusions presented in section 4.2.2.1 the recharge delay parameter will be removed as a user operated parameter and will remain effectively at the 0 setting for future experiments to reduce the effect of the increasing error.

The use of the vibrating electrode adds further uncertainty and error to managing the pulse frequency of the ESD process. Regardless of the ability of the power supply to manage pulse frequencies, the circuit is only available to discharge at the vibrational frequency of the applicator if a moderate force is applied. This results in difficulties predicting the ESD power without knowledge of the frequency interactions from the power supply with the contact frequency generated by the applicator vibrations.

The energy range of the machine calculated from the parameters detailed in Table 4 fed through Equation 2 results in the energy levels reported in Table 10. The capacitance is limited to a fixed 2000 μF for the primary circuit and energy is varied through the selection of different voltages. This high energy level is typically associated with the deposition of high ceramic content materials. The arc circuit does not provide sufficient energy to effectively deposit ESD coatings.

Table 10: ESD Machine #2 output energy

	Pulse setting	Minimum Output (J)	Maximum output (J)
Main circuit	High Pulse	0.625	2.025
	Low Pulse	0.1	2.025
Secondary circuit	Arc Pulse	0.0025	0.04

4.2.4.1   TiC/Ni on Cu experiment

Several experiments with the power supply Machine #2 were performed. The variability in the control modes proved difficult to characterize with a single experiment. The relation between the different control modes and the pulse power parameters were not accurately quantified. The improved power supply was shown to be able to manage the electrical parameters and provide advanced pulse sequences. A deposition experiment testing the performance of the power supply by depositing TiC/Ni cermet material on Cu-Cr-Zr RSW electrodes was performed.

The potential for the deposition of high ceramic content coatings on metallic substrates is demonstrated in an experiment. A sample of the microstructure images of ESD coatings made using the Machine #2 power supply are presented in Figure 69 to Figure 72.
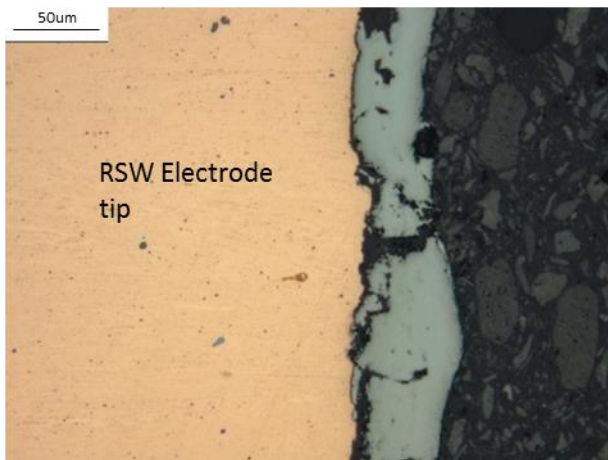
Figure 69: TiC/Ni on Cu RSW electrode tip optical image
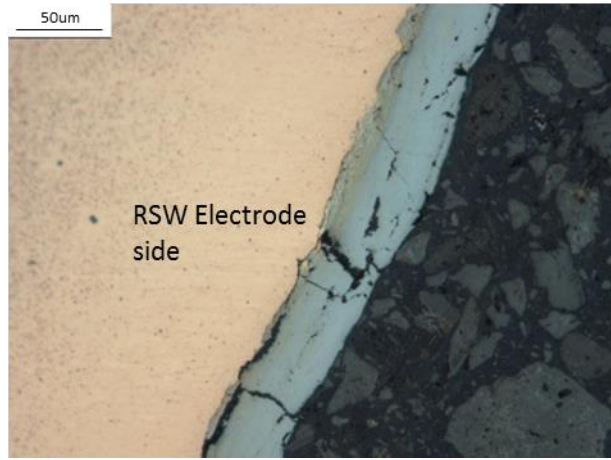
Figure 70: TiC/Ni on Cu RSW electrode side optical image
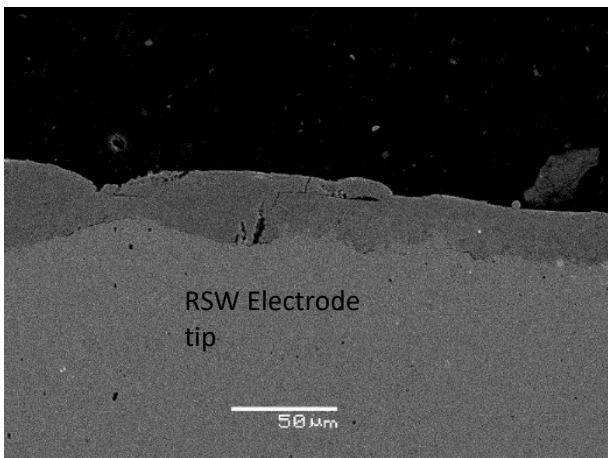
Figure 71: TiC/Ni on Cu RSW electrode tip SEM image
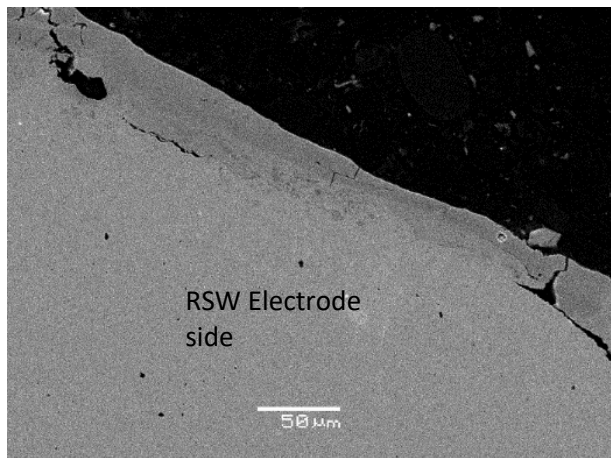
Figure 72: TiC/Ni on Cu RSW electrode side SEM image

The resulting microstructure images proved that effective ESD parameters can be used to improve the coating quality of TiC/Ni on Cu depositions. However the quantitative analysis of ESD parameter effects proved difficult due to the erratic contact nature of the vibrating electrode and the undefined relationship between the various possible control modes, charging speeds, and voltages. Additional difficulties with the geometry effects of the RSW cap resulted in differences in the coating quality of the tip and edge of the electrodes. This is highlighted in the resulting interfacial cracks between the TiC/Ni and Cu in Figure 69 and Figure 71 compared to Figure 70 and Figure 72.

4.2.5   ESD Machine #2 summary

Experiments examining the interaction between the ESD parameters which effectively determine the pulse frequency excluded the recharge delay parameter as a useful variable with the ESD power supplies. Increases in error resulted in unpredictability in the effects on the pulse frequency. The pulse frequency is mainly determined by the voltage and charging speed settings.

Tests show that the pulse energy and frequency is well controlled with the use of the various control modes. The use of the vibrating electrode is detrimental to the power supply controlled frequency.

4.3   Universal ESD power supply Machine #3

Lessons learned from the characterization of the Machine #2 parameters and an effort to meet the various electrical needs for a variety of material pairings. The universal ESD power supply was developed with a wider variety of parameters including a microcontroller bank of capacitors. Microcontroller memory limits, as well as the added complexity demonstrated from some ESD Machine #2 parameters saw the removal of the High and Low pulses, recharge delay and secondary circuit parameters. Initial experiments did not demonstrate significant increases in coating quality with the implementation of the additional parameters.

The Universal ESD machine was produced with some changes to the electrical circuit. The transformer stepped up the AC input power to 170V to improve capacitor charging time, a diode bridge rectifier with smoothing capacitor supplied the charging energy for the capacitor bank 10-300μF controlled by an IGBT. Integration of the microcontroller with more control over the electrical parameters allowed for a power supply with a wide range of applications. Figure 73 is a simplified electrical block diagram detailing the major components of the universal ESD power supply.
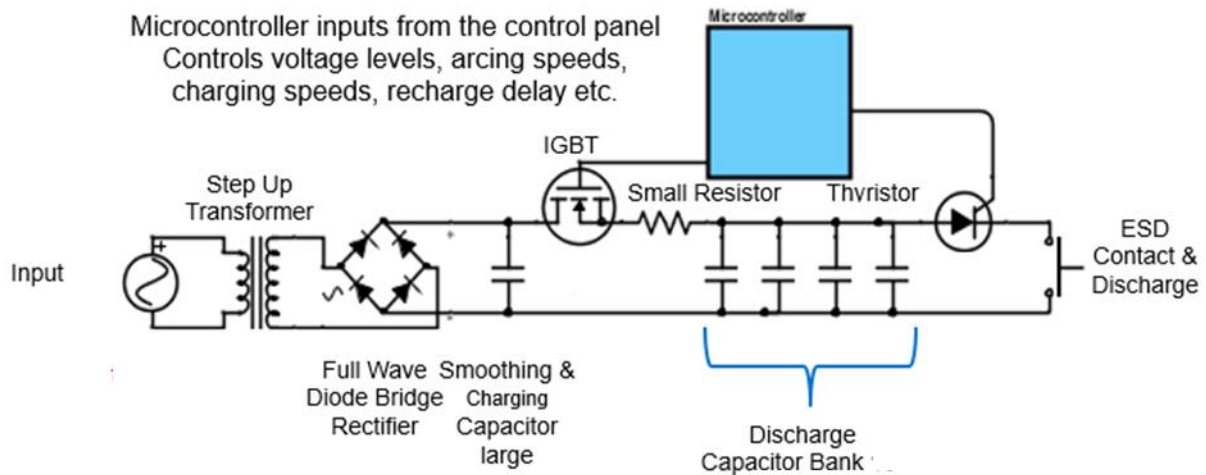
Figure 73: Universal ESD machine simplified electrical diagram

The potential energy output of this power supply related to Equation 2 results in an energy range of 0.0005J to 2.734J. This range can be altered with the addition of further capacitance added to the bank.

The system operates with a rotating applicator, rather than the vibrating applicator used by machines 1 and 2. This increases the contact time and heat generation, but allows more accurate frequency control through the power supply, as opposed to relying on the intermittent contact of the electrode through vibrations. The interface with the ESD parameters have been simplified to setting the control mode, the capacitance, one voltage setting and depending on the control mode a maximum frequency setting. See Figure 43 in experimental setup section for an image of the Universal ESD machine user interface.

4.3.1 Universal ESD machine frequency control

The Universal ESD machine uses two control modes to define the frequency output from the power supply. The charging speed control mode works in the same manner as the machine #2, where a numerical value relates to the slope of the rising voltage, and the frequency is related to the capacitance, voltage set value, charging speed, discharge and recharge delay. The final frequency is dependent then on the constancy of the spinning electrode contact. Figure 74 is a chart of the electrical signals from the power supply, demonstrating the charging speed control. The parameters are set at 135V, 100μF, and 25 charging speed, the resulting pulses will discharge as soon as contact is made, as fast as the capacitors can charge.
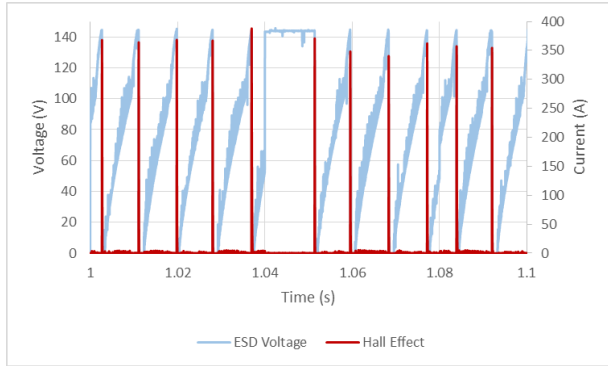
Figure 74: Universal ESD machine charging speed control mode; 25 charging speed; 135V; 100μF
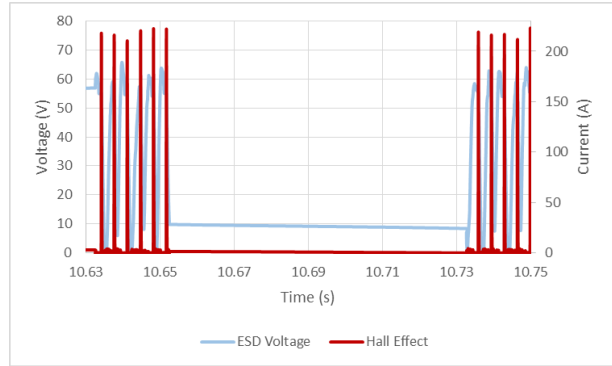
Figure 75: Universal ESD machine frequency control mode; 95 charging speed; 300Hz Max; 50V; 150μF

The frequency control setting considers both the set charging speed as the maximum slope for the voltage of the charging capacitor as well as a maximum frequency value. This maximum value limits the total number of discharges under a certain duty cycle, and thus if the electrode contact is constant the power supply will pause until the next cycle period. Figure 75 is an example of the electrical signals from an experiment with the frequency control mode, where the voltage is set at 120V, capacitance is 150μF, the charging speed is 95 and the maximum frequency is set at 100Hz. Thus the system performs at the 95 charging speed until the 100Hz setting has been met for the 0.1 duty cycle time. Tuning of these two parameters can be used to alter the heat buildup during the process, and is similar to the groups of pulses and pauses proposed in section 0.

Depending on the interaction between the set frequency and charging speed, the frequency control mode can be used to use lower ESD energy parameters, voltage and capacitance, to generate similar heat levels and mass transfer rates.

4.4 Power Supply Performance

To quantify the effects of the electrical parameters an experiment was performed with a range of voltages and frequencies depositing TiC/Ni coatings on a Cu substrate. Depositions were made manually in approximately 30 seconds covering a 3x3 mm area. See Table 11 for the electrical parameters used in the test, and Figure 76 for an image of the copper coupon and coated substrate.

Table 11: TiC/Ni on Cu Universal ESD machine experiment parameters; NB: Frequency refers to the charging speed level

Test #	1	2	3	4	5	6	7	8	9
Voltage	50	50	50	100	100	100	135	135	135
Frequency	25	55	90	25	55	90	25	55	90
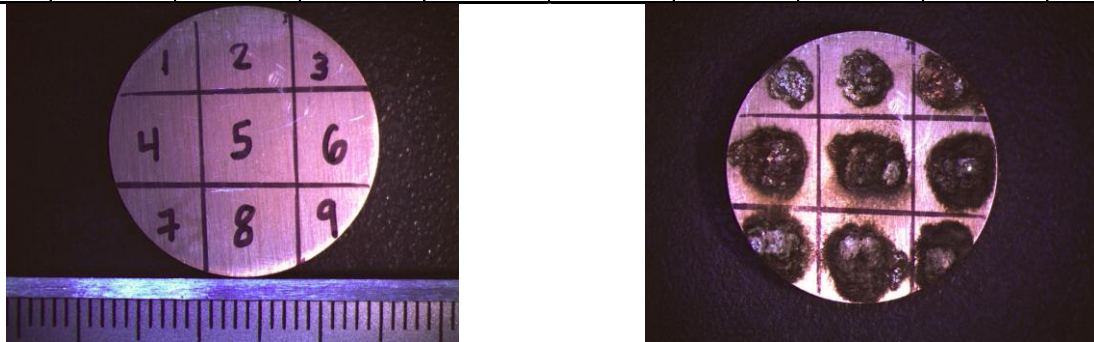
Figure 76: TiC/Ni on Cu coupon coated substrate; before and after respectively

Figure 77 and Figure 78 are a sample of the electrical signals demonstrating the difference in frequency, output current and voltage for the two test parameters.
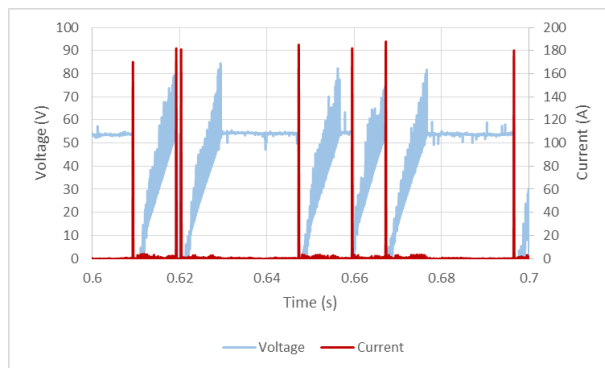
Figure 77: TiC/Ni on Cu experiment test 1 electrical signals
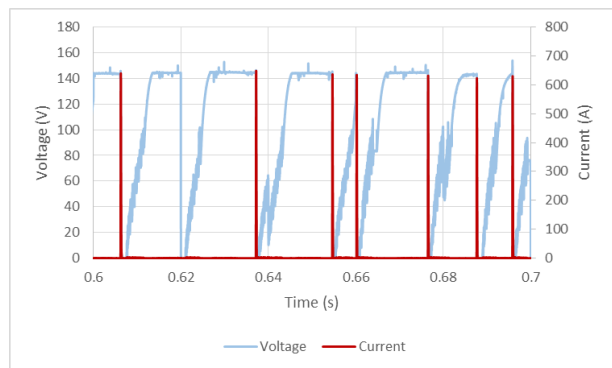
Figure 78: TiC/Ni on Cu experiment test 9 electrical signals

Qualitative analysis of the coating cross sections reveals some signs of oxidation and significant thermal stress cracks due to the thicker coatings deposited at higher voltages and frequencies. Figure 79 shows images of a sample of the experiment parameters from a lower, medium and high power levels. Even at the high energy levels of test 9 there is little evidence of heat effects in the substrate microstructure.

| Test 1: 50V; 25% charging speed | Test 6: 100V; 90% charging speed | Test 9: 135V; 90% charging speed |
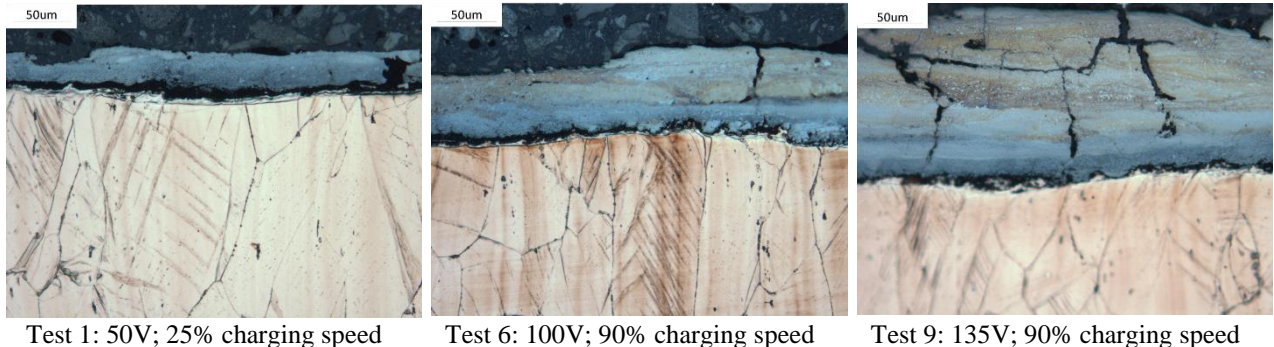
Figure 79: Optical images at 10x magnification for low medium and high parameter TiC/Ni coatings

The optical cross sectional images were evaluated to determine the effect of the frequency and voltage levels on the coating thickness. Figure 80 summarizes the increase in the coating thickness related to the ESD voltage. As the ESD voltage increases there is a nonlinear increase in the coating thickness. As Equation 2 summarizes the voltage has an exponential factor on the ESD energy output, furthermore increasing the voltage increases the possible arc gap during discharge, where the longer plasma arc would produce more heat. It is logical and supported by prior research that increasing the ESD voltage would correspond to increasing coating thickness, without taking into consideration the negative increase in thermal cracking, oxidation and other defects due to excessive heat input. Figure 80 at the 25 charging speed setting exhibits a minor decrease in the coating thickness with increasing ESD voltage, contrary to the results from the other charging speeds. This is attributed to the variability in coating thickness in local areas, and disparity in movement speed and application force when manually applying the ESD process. At all frequency levels the very large range in ESD voltages should correspond to significant increases in the coating thickness, with a potential limit for the ceramic electrode material as proposed in section 2.3.
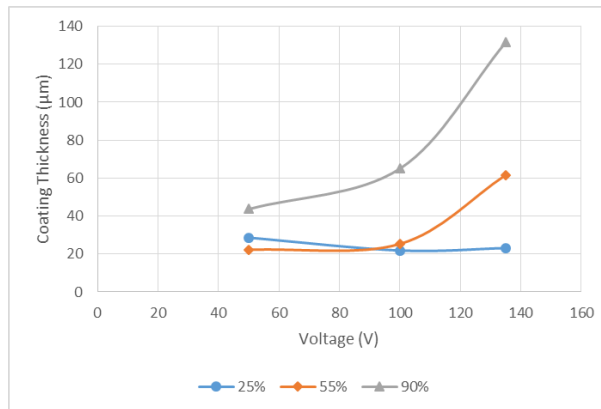
Figure 80: TiC/Ni on Cu coating thickness versus ESD voltage for varying charging speeds

Figure 81 summarizes the same coating thickness data, instead relating the recorded ESD frequency. Since the experiment parameters employed the charging speed control mode with varying voltages,

51

specific frequencies were not tested, rather the resulting frequencies of the confluence of parameters was recorded. The results show that a pairing of the frequency and voltage output from the ESD power supply can have a drastic effect on the coating thickness of the depositions. Again the results are skewed by the manual operation of the experiment, notably at the lower voltage level, increasing the ESD frequency should result in an increase in the coating thickness.
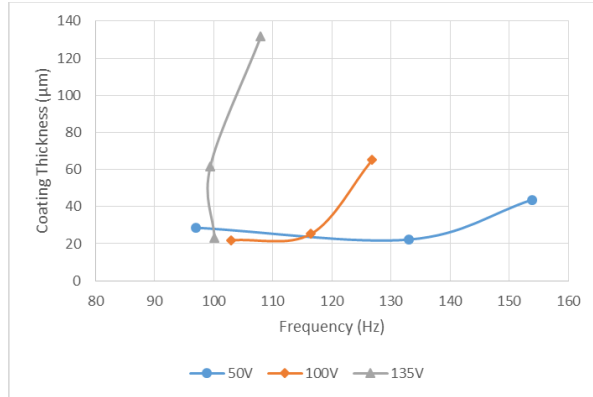
Figure 81: Tic/Ni on Cu coating thickness versus ESD pulse frequency
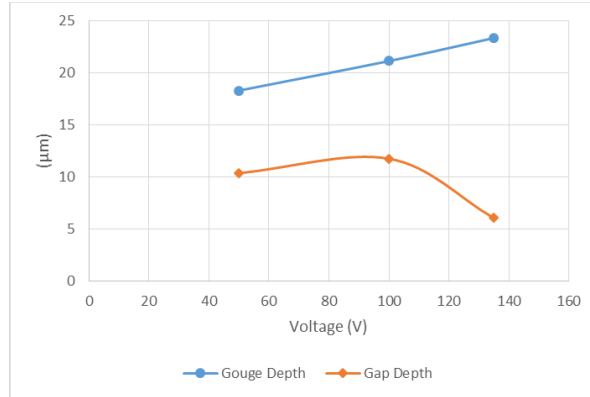
Figure 82: TiC/Ni on Cu gouge depth and gap distance (interfacial crack width) versus ESD voltage

Some coating defects were also quantified to be evaluated against the voltage and frequency parameters. Through evaluation of the optical cross section images the erosion of the initial substrate surface was evaluated as a gouge depth level relative to the un-treated surface, and the average thickness of the interfacial crack between the TiC/Ni coating and Cu substrate was measured. Increases in the power level of the ESD input through increases in the voltage and frequency will increase the heat generated by the process. Increases in coating thickness and thermal input exacerbate the effect of thermal expansion mismatch between the cermet coating and metallic substrate. Figure 82 summarizes the voltage effect on the substrate gouge depth, or substrate erosion and the gap distance, or interfacial crack width averaged across all frequencies for the different voltages. Increasing the voltage, and potentially the arc gap significantly increases the arc forces, heat generation and electrical energy produced by the ESD spark. The experiment showed a corollary increase in the erosion damage to the substrate. The interfacial crack width showed less of a definitive correlation to the ESD voltage.

Analysis of the effect of the ESD pulse frequency on the substrate erosion and the interfacial crack width is summarized by Figure 83 and Figure 84. The graphs show that the experiment did not detect a relationship between these defects and the pulse frequency. It is possible that the erratic relationship of these defects to the pulse frequency is skewed by the variance in the manual operation process. However

it is logical that the pulse frequency would have a lesser effect on these defects when compared to the ESD voltage. Notably for the gouge depth, once the sparks have eroded the substrate and deposited an initial layer of TiC/Ni the subsequent sparks serve to erode the previously deposited coating. Effects on the interfacial crack width would relate the frequency to the total heat generated by the process which may contribute to the negative effects of thermal cracking due to thermal mismatch.
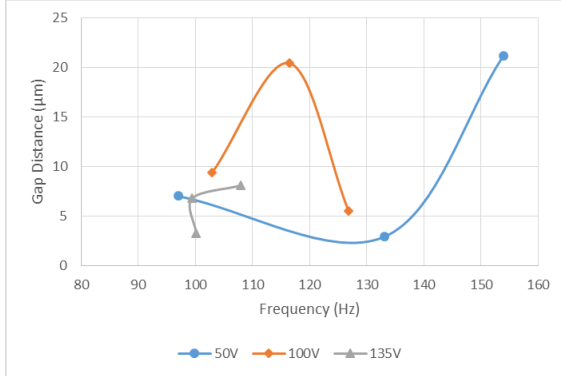
Figure 83: TiC/Ni on Cu gap distance (interfacial crack width) versus ESD pulse frequency
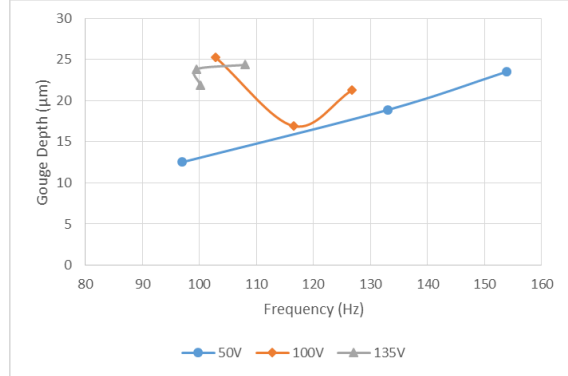
Figure 84: TiC/Ni on Cu gouge depth versus ESD pulse frequency

SEM analysis was used to evaluate the material composition of the coatings and the elemental diffusion of electrode elements into the substrate using EDX analysis. Figure 85 shows SEM images highlighting the EDX analysis points used to quantify the elemental composition and diffusion.

Test 1: 50V; 25% Charging speed   Test 6: 100V; 90% Charging speed   Test 9: 135V; 90% Charging speed
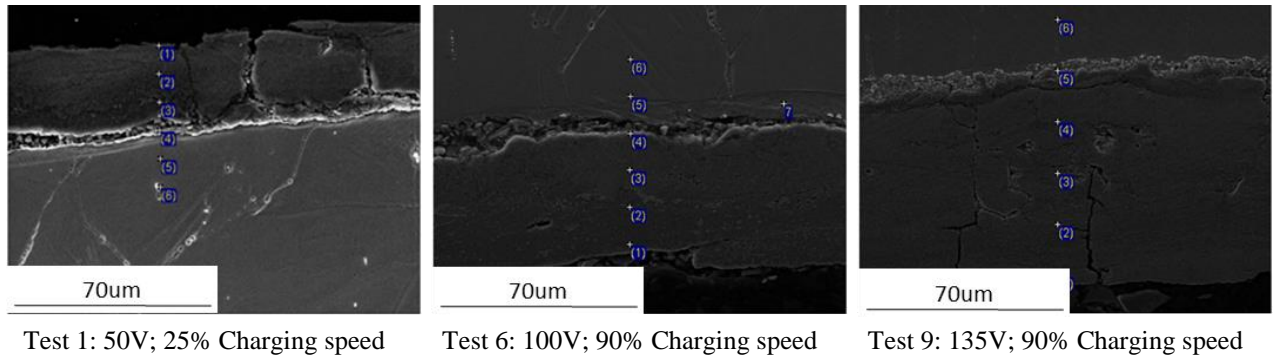
Figure 85: SEM images for low medium and high parameters

The SEM analysis of Tests 1, 6 and 9 were used to evaluate the effect of the parameters on the quantitative EDX analysis. Figure 86, Figure 87 and Figure 88 show the graphs of the Ti, Cu and Ni elemental composition at points relative to the coating, substrate interface, denoted as point 0 of the μm offset surface scale. The diffusion related to the ESD parameters is important for a diverse range of applications. The TiC/Ni coatings on Cu-Cr-Zr are used as protective coatings for the RSW process. The Cu diffusion is important as one of the coatings functions is to prevent brass formation when welding zinc

coated steel sheets. Cu diffusion to the surface of the coatings and Ni alloying with the Cu can affect the coating performance. As the power of the ESD process was increased for Test 1 to Test 9 the copper content at the surface of the TiC/Ni coating is reduced, likely due to the increase in the coating thickness. The Ti and Ni content increases with the same correlation into the substrate, as the ESD power increases.
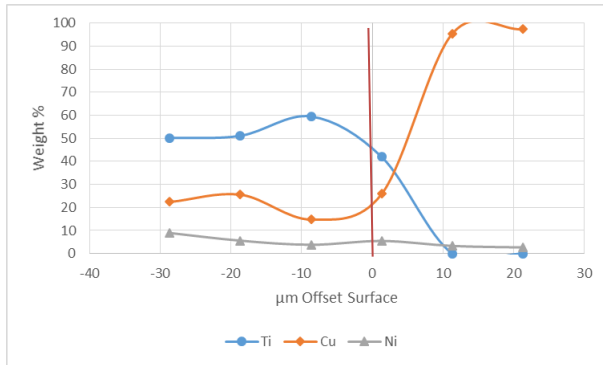
Figure 86: TiC/Ni experiment test 1 EDX data; surface denoted by vertical line
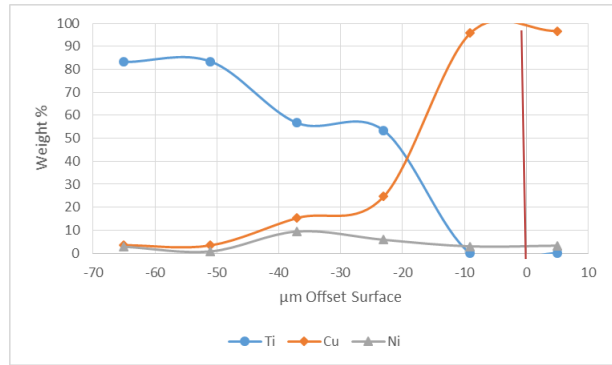
Figure 87: TiC/Ni experiment test 6 EDX data; surface denoted by vertical line
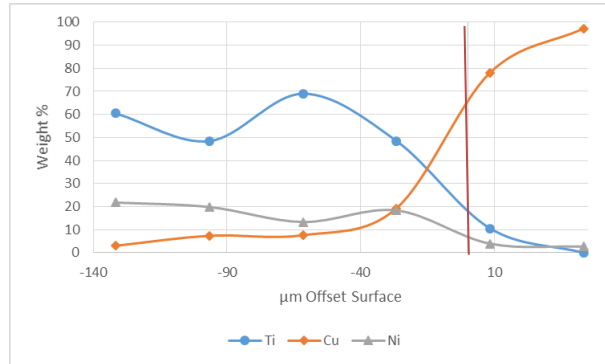
Figure 88: TiC/Ni experiment test 9 EDX data; surface denoted by vertical line

The effect of the electrical parameters can be displayed quantitatively as a function of the movement of the two main elements in the substrate and electrode, titanium and copper. Figure 89 and Figure 90 demonstrate the difference in elemental diffusion and the blocking effect the coating related to the deposited coating thickness on Cu diffusion. Test 9 demonstrates a lower copper content in the ESD coating versus the thinner Test 1 coating. Test 9 also exhibits a significantly lower titanium penetration into the substrate, where Test 1 has titanium content near 0%wt at the coating interface Test 9 penetrates near 35μm before reaching a 0%wt titanium content.
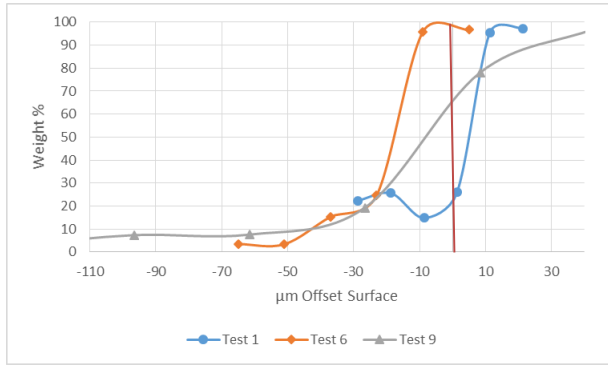
Figure 89: TiC/Ni on Cu experiment EDX results copper diffusion; surface denoted by vertical line
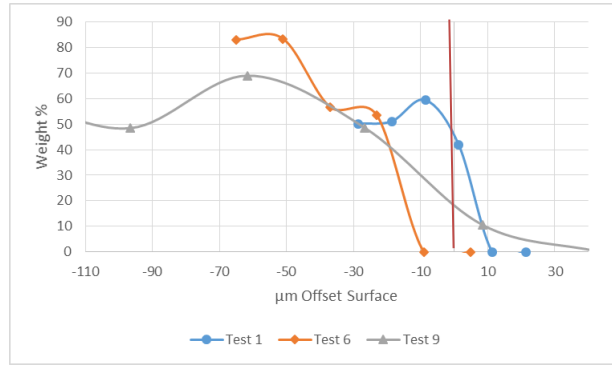
Figure 90: TiC/Ni on Cu experiment EDX results titanium diffusion; surface denoted by vertical line

4.5 Mass Transfer High Speed Images

Using a high speed camera, images were taken of the arc discharge in order to better characterize the mass transfer methods, and the close up visual effects of different electrical parameters. Images were taken at 10,000 frames per second with an aperture setting of 16 and no filters. Experiments were done with a stainless steel electrode, un-pointed with a diameter of 3mm, depositing onto carbon steel. Figure 91 shows the high speed images over a 0.4ms time frame. Clearly observed is the arc formation from the electrode to substrate contact, followed by the ejection of solid and molten electrode material. As the electrode continues to spin the physical molten metal transfer is observed. The medium high electrical parameters used for this experiment resulted in overheating, seen as the glow of the electrode. From Equation 2 these parameters result in an electrical energy output of 0.28J per pulse.
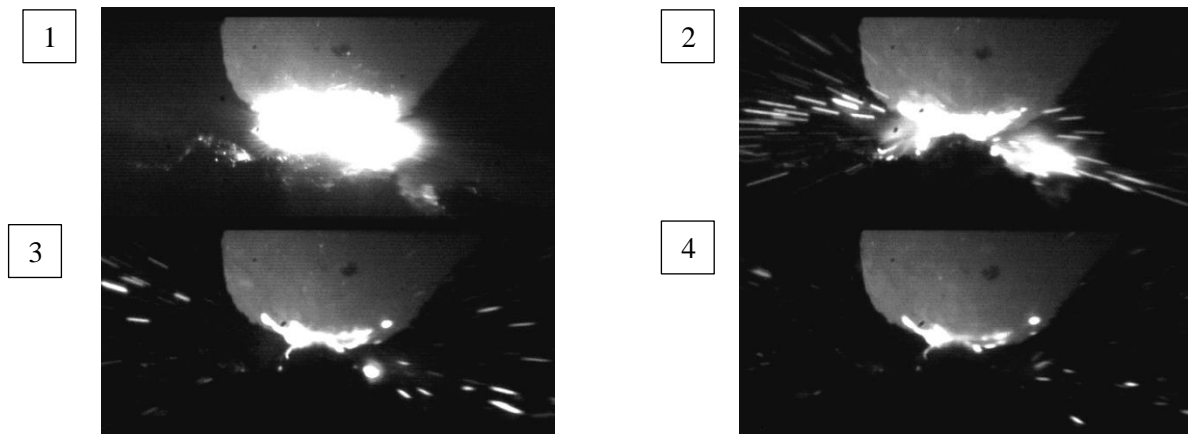
Figure 91: Test 1 75V, 100µF, and charging speed 95; 0.1ms per frame

High speed images were taken with the maximum electrical parameters from the universal ESD power supply. The electrical output per pulse is calculated as 2.73J, 9.72 times greater than the previous test

without considering the effect of pulse frequency on thermal buildup. At these parameters the electrode rapidly overheats seen in Figure 92 as the overexposure of the electrode material. The images highlight a larger quantity of ejected material from the electrode in solid and molten form, corresponding to lower transfer efficiency as this material will not form an effective coating.
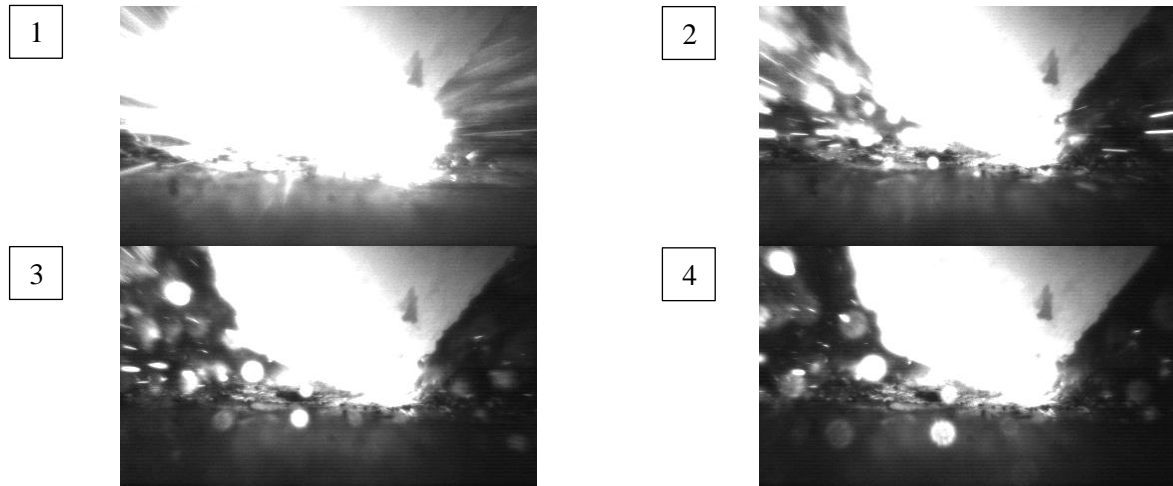
Figure 92: Test 2 135V, 300μF and charging speed 95; 0.1ms per frame overheating

Figure 93 highlights a significant issue with using these high ESD electrical parameters. The images show that there is a molten metal interaction from the electrode surface to the deposited material on the surface. In the background of the image it is clear that there is significant deposits, however they appear rough and un-uniform. The long duration molten metal interactions promote the formation of defects in the coating including porosities, thermal stress cracks and oxidation. If there is significant conductivity between the electrode and the substrate through the molten metal bridge the electrode will not spark, rather the pulse current will be passed through the liquid material, preventing the effective transfer of material through ESD. While previous experiments demonstrated that the coating thickness can be increased with increasing the ESD electrical parameters defects were often the compromise of the faster material transfer. These images relate to the negative effects of overheating the ESD electrode through increasing the electrical energy.
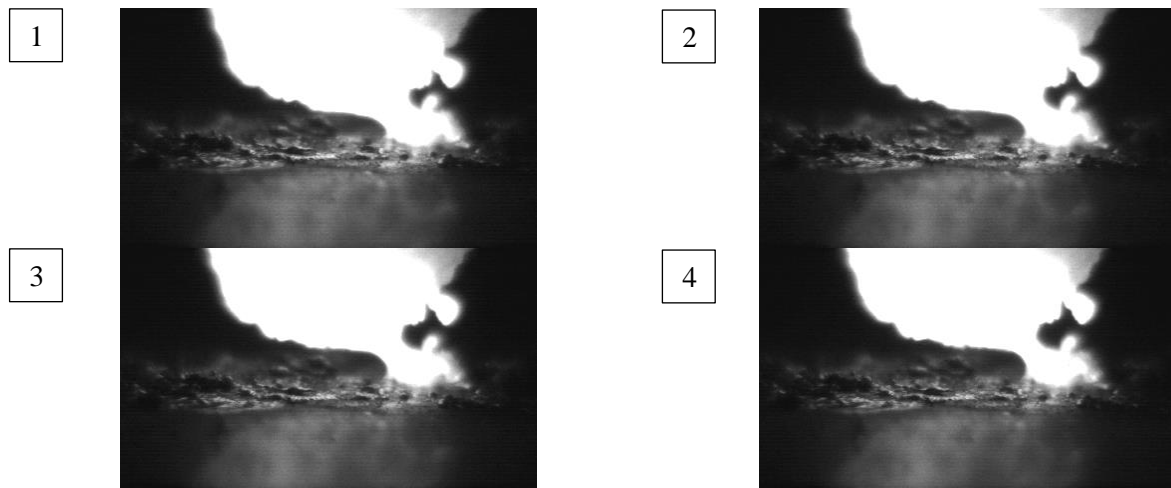
Figure 93: Test 2 135V, 300µF and charging speed 95; 0.1ms per frame molten metal

Further experiments were performed using a local shielding nozzle to flow argon shielding gas at 30CFH during the ESD process. Figure 94 images demonstrate the significant improvement to the arc behavior as well as a lack of overheating in the electrode as only the arc is overexposed. It is concluded that the cooling effects, in addition to preventing reactions with the atmospheric elements, can significantly convectively cool the ESD process when the electrical parameters are high.

Figure 94 Test 3 135V, 300µF and charging speed 95; 0.1ms per frame using a localized nozzle of 30CFH argon shielding gas

4.6 Experiment Summary

Results from the TiC/Ni on Cu experiment and the high speed video tests resulted in data which matches typical ESD performance. However the quantitative analysis of the effect of ESD electrical parameters is skewed by the effects of manual operation of the applicators. Variance in the number of passes over an area, the movement speed and applicator force have a significant effect on the thickness, quality and uniformity of the coatings and is a major cause of the error in the quantitative results from the experiments.

Increasing the voltage and frequency supports the findings from previous studies and the machine #2 tests as the most significant parameters affecting coating thickness and heat generation. Effective selection of parameters and potential use of shielding gas can result in effective coatings even with manual ESD application.

Chapter 5.0: ESD Physical Controls

5.1 CNC motion control

ESD is historically a hand operated coating method, where the considerations for the physical process parameters are constantly adapted to by a skilled operator. The control and understanding of the electrical parameters has resulted in repeatable results with consistent pairings of materials and physical deposition styles. The limitations of a human operated ESD process is evident in the difference between coatings produced by different operators. Constantly changing deposition angle, movement speed, application force and other considerations between coatings made by different operators or coatings made at different times establishes the need for automated production with ESD as well as controlled experiments to determine the effects of parameters when both the electrical and physical considerations are constrained.

In order to meet the requirements for physical control of the ESD machine during these experiments a 3 axis CNC machine was custom built to meet the unique requirements of the ESD process.

5.1.1 CNC machine

The CNC machine employed commercially available stepper motors to control the motion of the x, y and z axis. The rotating applicator integrated with the Universal ESD Machine was mounted on the suspension platform on the z-axis. Figure 95 shows an image of the ESD process integrated with the CNC machine. The system is operated with the use of the Arduino Uno microcontroller and G-Shield motor controller as presented in the Experimental Setup section 3.5. The system is interfaced with the use of the Universal G-Code sender program. G-Code is the positioning and movement code RS-274 protocol for interface with numerical control systems.
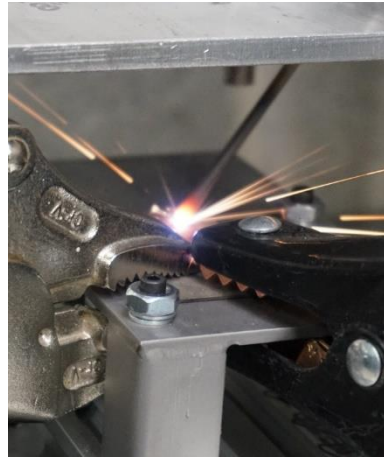
Figure 95: Image of ESD application using CNC control

The CNC equipment allowed for controlled deposition patterns, movement speeds and electrode step-down. A spring loaded suspension system allowed for some rough force control paired with the z-axis step-down.

5.1.2 Controlled mass transfer experiment

With the use of the x, y, z control system the high speed images can be better focused on the deposition area. Further mass transfer images were recorded to examine the arc formation from the universal ESD machine without a rotating electrode. The electrodes were plunged down 0.1mm from the zeroed surface and then retracted to examine if the electrode will still spark under higher application forces, and if the electrode will continue to spark once contact to the substrate surface is broken.

The initial sparking from the ESD process occurs when local contacts between points on the electrode reach the substrate. Joule heating and potentially very small gaps cause the formation of the spark. After the initial contact, if the electrode continues to move forward, and there is still point contact additional sparks may occur. Figure 96 shows images of a 6ms period at initial contact. Arcing continues for another four frames, for a total of 10ms.
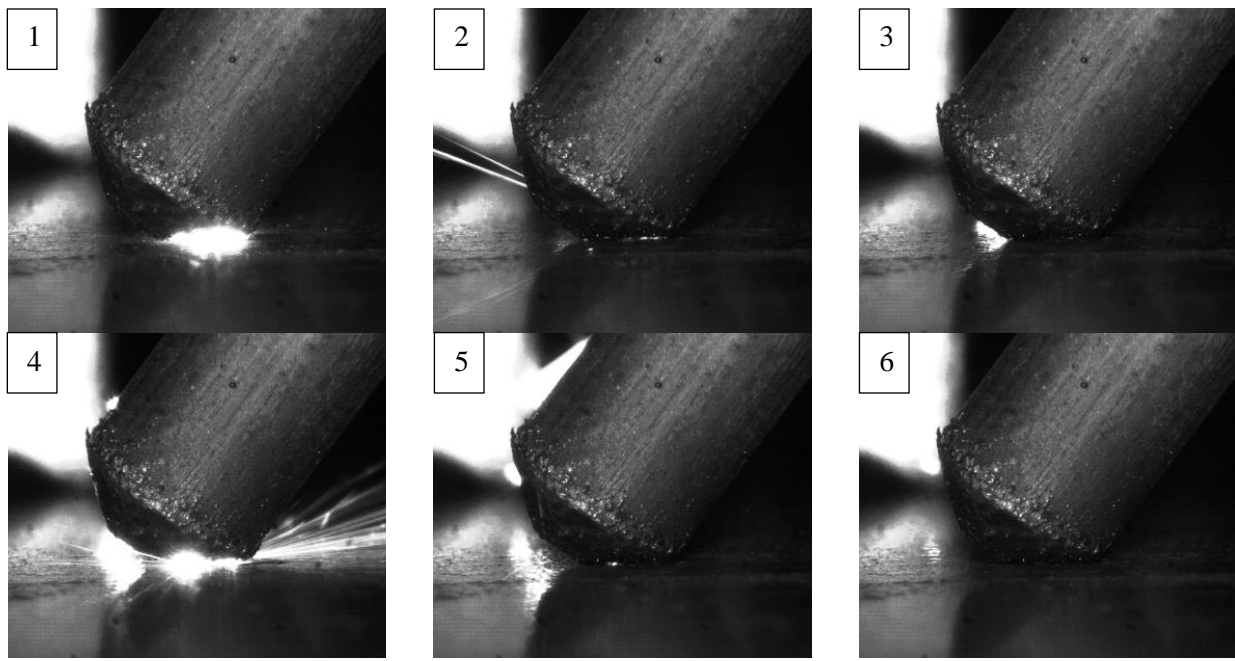
Figure 96: Plunging ESD test high speed images 1000fps initial contact: 100V, 300μF, 400Hz, 95 charging speed

After the arcing from the initial contact as the electrode continues to descend, the normal force reduces the resistance between the electrode and the substrate, and closes potential arcing gaps. As the electrode in this experiment is not perpendicular to the substrate surface the additional force may allow the electrode to slide on the surface as the electrode bends along its length. Smaller low intensity arcs may occur as demonstrated in Figure 97.
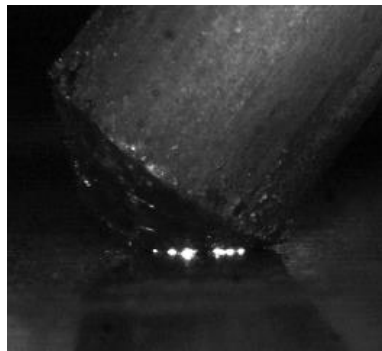
Figure 97: Plunging ESD test high speed images 1000fps excessive force: 75V, 300μF, 400Hz, 95 charging speed

The experiment had the electrode plunge down 0.1mm from the detected initial contact, then the electrode would retract to a 1mm safe position. As the normal force between the electrode and the substrate was reduced and the unloading of the system cause small lateral movements from the electrode bending another set of sparks were produced. A series of arcs proceed as the electrode is retracted, there is a

possibility that the sparks are produced when there are small gaps between the electrode and the surface, the distance of which would be determined by the ESD voltage. A gap cannot be detected in these images. Figure 98 shows image of the retracting electrode sparking for a set of electrical parameters. These images represent the entire sparking time during the electrode retraction, 6ms.
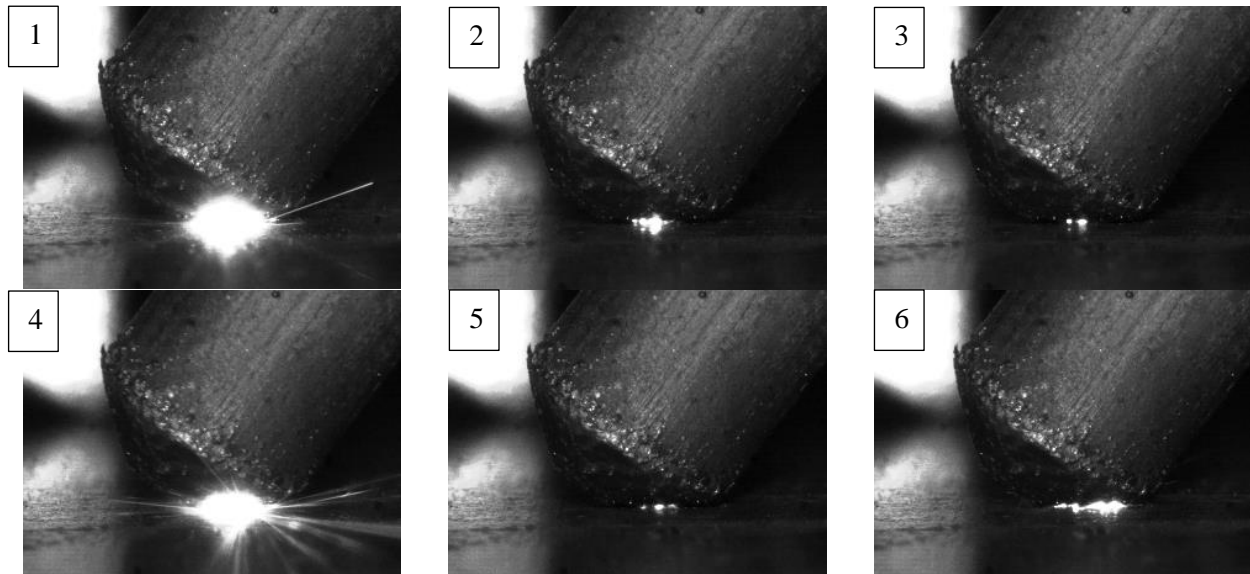
Figure 98: Plunging ESD test high speed images 1000fps final contact: 100V, 300μF, 400Hz, 95 charging speed

A range of parameters were tested to observe the arc intensity and ejected material. Figure 99 demonstrates the increasing intensity and ejected material from the spark as the ESD voltage is increased from 50V, 75V, 100V and 135V (a, b, c and d respectively). The final image (f) shows the effect of Ar shielding gas on a single spark at 135V, when compared to the violent arc and overexposure of the previous image (e) at 135V in atmosphere.
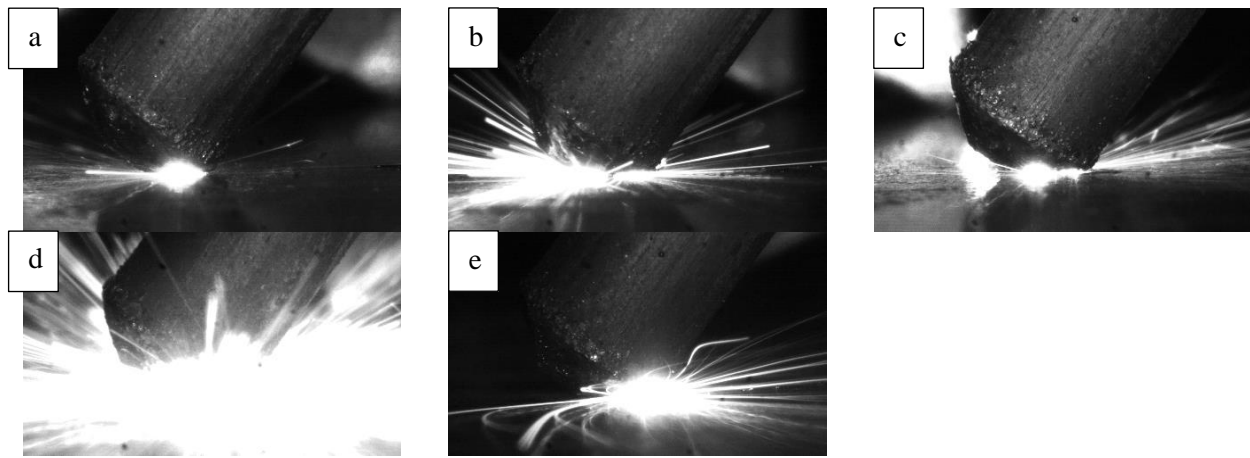
Figure 99: Plunging ESD test high speed images 1000fps; ESD parameters 300μF, 400Hz, 95 charging speed; a) 50V, b) 75V, c) 100V, d) 135V, e) 135V + Ar

5.1.3   Movement Speed

The movement speed of the electrode across the substrate surface affects several important effects during ESD. Notably, depending on the design of the ESD applicator the lateral motion of the electrode could serve as the detachment force required for the ESD electrode to not permanently stick to the substrate surface. Many ESD applications use rotary, eccentric or vibrational motions of the electrode to prevent sticking and promote the detachment of the molten electrode material onto the surface. However without any additional motion the relative motion of the electrode can serve to prevent the electrode from sticking during the ESD process.

The relative motion will affect the deposition quality of the process. In relation to the electrical parameters, high travel speeds can promote smooth coatings, or gaps with no depositions. Low travel speeds can promote excessive coating in localized areas, leaving bare substrate areas with no coating. Depending on the severity this buildup can be a severe defect preventing future coating layers from bonding with the substrate and requiring grinding of the area to allow for subsequent recoating.

Heat transfer during the heat transfer process can be heavily affected by the process movement speed. In order to achieve effective coatings there needs to be a reduction in the heat input into the substrate to prevent the negative effects of the heat affected zone, as well as other precipitation effects. Higher movement speeds reduce the heat input into the substrate with the same ESD electrical parameters. Higher movement speeds will increase the possible covered area in the same amount of time. Reducing the total deposition time is a major factor to reducing the negative effects of overheating the ESD electrode.

5.1.4 Movement Pattern

The movement pattern and step over of the electrode becomes relevant once a computerized control system is employed. Depending on the electrode to substrate material pairing as well as the electrode diameter and the interaction of the other physical and electrical parameters will affect how the deposition pattern influences the quality of the coatings. Considerations need to be made for the limitations of the CNC machine and potential undesired effects of different patterns.

The different patterns used were various scanning lateral motion patterns and spiral patterns. Initial issues with the scanning patterns revealed the effects of the CNC in the form of acceleration rates, maximum movement speeds and complete changes in directions. Beginning from the first point the CNC would accelerate to its top speed, only to need to decelerate, make a small step over and re-accelerate in the other direction. While this deposition pattern is intuitive the time spent for acceleration and deceleration resulted in lower movement speeds at the edges of the scanned area. As a result there were thicker depositions at the edge of the desired level coating area. Subsequent coating layers had significant issues with the varying heights of the deposition and further material was localized to the edge of the coatings. Changes to the scanning patterns to reduce the number of direction changes and acceleration and deceleration events would improve the uniformity of the coatings.

With this issue in mind consideration needed to be given to ensuring the coatings covered the entirety of the deposition area. Different step overs as well as changing the deposition pattern was explored.
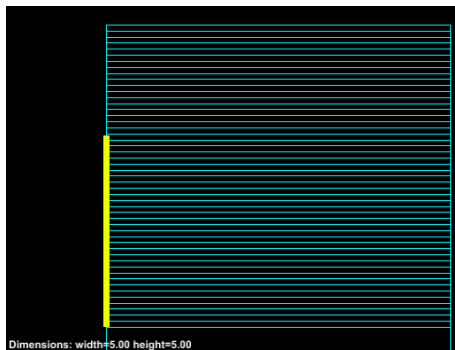
Figure 100: Standard scanning pattern with a square step-over
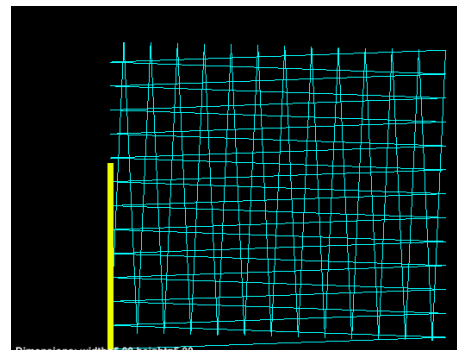
Figure 101: Zig zag pattern in x & y direction to increase area coverage

5.1.4.1 Square Scanning Pattern Steel on Steel Deposition Test

To test the effects of the CNC control on the ESD coatings a test was done with the square step over of 0.2mm see

Figure 100 for reference. The coating was deposited over a 5x5mm area with a constant linear step-down in the z-axis of 0.001mm per line of code. This resulted in a total step-down of 0.25mm per directional scan and 0.5mm for the total coating an initial step-down of 0.1mm was added to initially start the deposition. A pass was made scanning in the x-direction followed by a 5 second pause, then a scan in the y direction.

Table 12 states the parameters used for the different tests, with the aim of determining the effect of the electrical parameters when paired with the CNC control.

Table 12: Scanning ESD CNC Test

Test Number	Voltage (V)	Capacitance (μF)	Charging Speed %	Frequency (Hz)
1	65	100	40	192
2	65	100	65	300
3	65	100	90	457
4	100	100	40	156
5	100	100	65	240
6	100	100	90	313

The cross sectioned images in Figure 102 demonstrate the buildup effect on the edge of the coatings when using this deposition pattern. The increase deposition time at the edge is due to the small step-over movement between each pass compounded by the need for deceleration and acceleration.
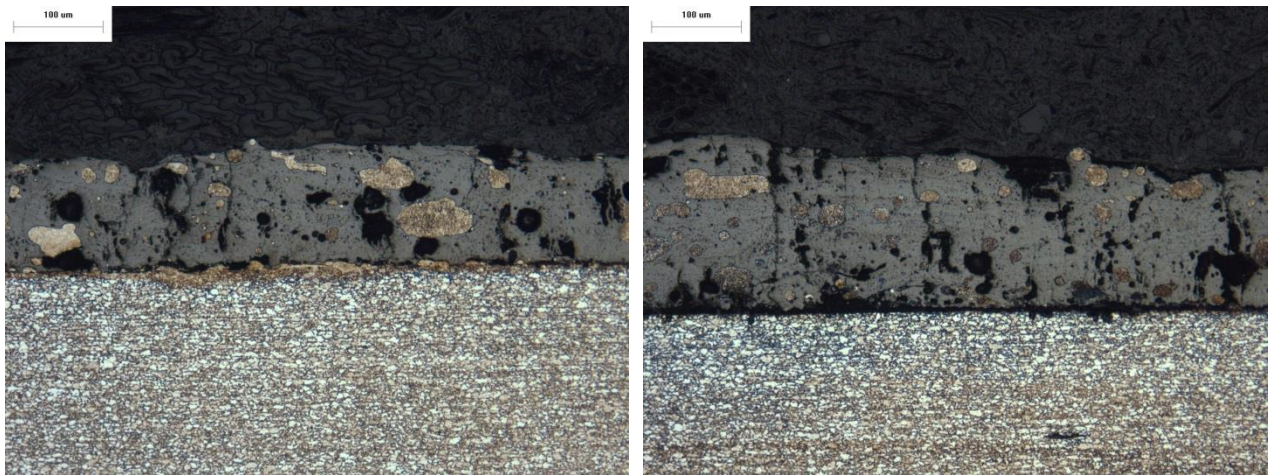
Figure 102: ESD Scanning Pattern Test number 5: a) Center of the deposition; b) Edge of the deposition

The difference between the center and the edge of the coatings is increased when the deposition rate rises due to higher electrical power output. Figure 103 demonstrates the difference in the average coating thickness between the edge and the center of the coating, as well as the 65V and 100V parameter tests.
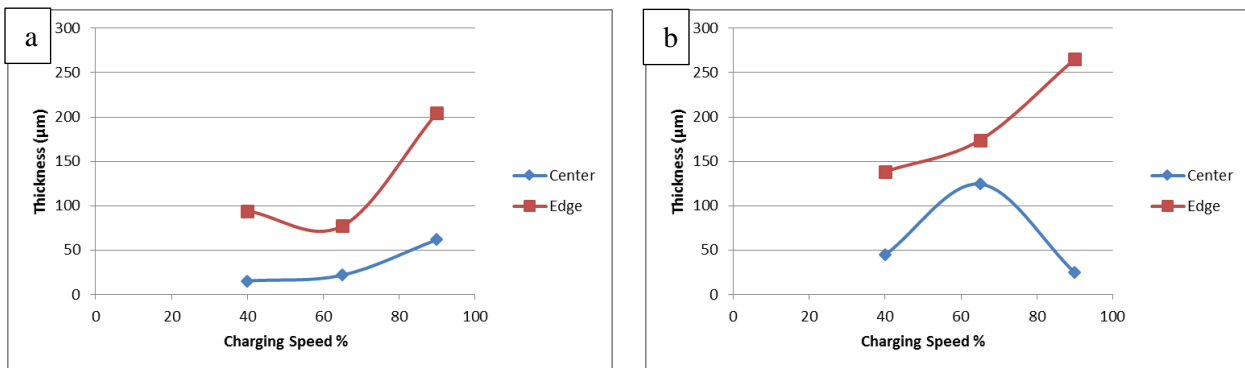
Figure 103: Center and Edge of coating disparity a) 65V 100µF; b) 100V 100µF

5.1.4.2 *Zig-Zag Pattern Steel on Steel Deposition Test*

The deposition pattern illustrated in

Figure 101 results in half the acceleration and deceleration motions as the square pattern and covers the same area in less time. Here the step-over remained at 0.2mm between each pass. The step-down was initially 0.1mm and each scan had a step-down of 0.15mm, the total step-down for the x & y direction scans and initial step-down was thus 0.4mm. The test was done with a range of parameters to compare the effect of the electrical parameters with the CNC control to those tests done by hand. See Table 13 for the tabulated electrical parameters and coating thickness measurements.

Table 13: Zig Zag steel on steel deposition test parameters, average coating thickness and standard deviation of coating thickness

Test #	Voltage (V)	Charging Speed	Max Frequency (Hz)	Average Frequency (Hz)	Coating Thickness (µm)	StDev (µm)
1	45	40	275	240	18.1	1.4
2	45	65	426	359	50.2	11.3
3	45	90	492	285	101.3	36.8
4	75	40	178	159	154.8	23.2
5	75	65	307	278	201.3	6.3
6	75	90	405	340	207.2	75.2
7	105	40	151	136	274.0	26.1

Comparing the Zig Zag pattern to the Square pattern, showed that reducing the number of direction changes helped to mitigate the buildup effect at the edge of the coatings. Figure 104 illustrates a cross section image of a coating with the zig-zag pattern; the image shows that there is limited deviation of the coating thickness across the width of the image, ~1.2mm of the total 5mm coating.
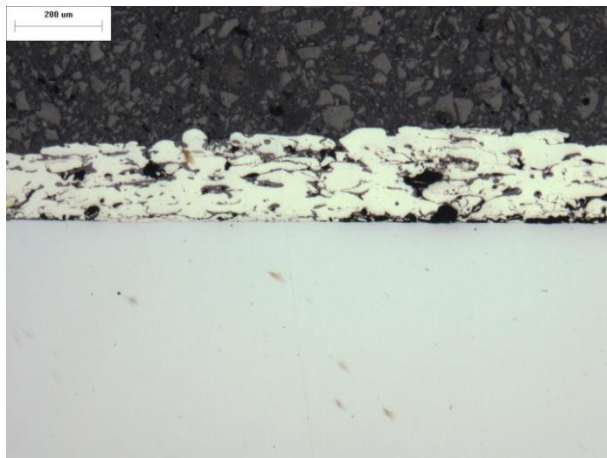
Figure 104: Test number 4 image ~1.2mm of a 5mm coating

Analysis of the coating thickness with different electrical parameters resulted in more predictable results than those tests performed by hand. This supports the use of the CNC to maintain consistent coating thicknesses and quality. Figure 105 relates the effects of the voltage and the frequency versus the deposition rate, as the coating thickness during ESD. The frequencies were not constant for these experiments as the ESD power supply had yet to be upgraded to the Hz based frequency control.
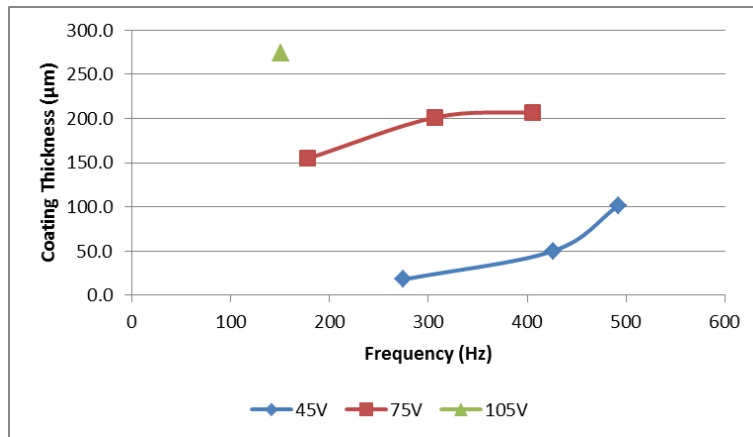
Figure 105: Voltage and frequency effect on coating thickness

5.1.4.3 Spiral Pattern

The spiral deposition patterns mitigate some of the acceleration issues by maintaining a relatively constant angular velocity with direction changes dispersed evenly within the circular arc. Initial spiral pattern used an octagon spiral pattern with 8 direction changes per revolution see Figure 106. This pattern removed the localized area for acceleration and deceleration as was present in the previous two patterns.
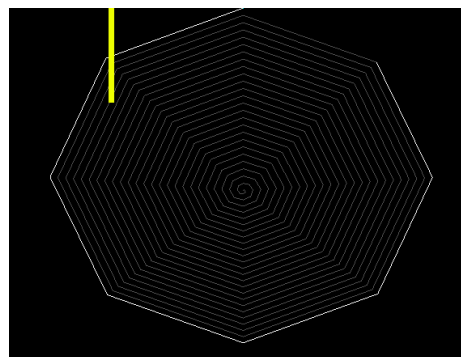
Figure 106: Octagon spiral pattern

A range of electrical parameters were used to test the effect of voltage and frequency and the performance of the new pattern. Table 14 states the electrical parameters used and the results of the coating measurements from the cross sectioned samples.

Table 14: Octagon spiral ESD Test electrical parameters and coating measurements

Test Number	Voltage (V)	Set Frequency (Hz)	Capacitance (µF)	Average Coating Thickness (µm)	Standard Deviation (µm)
1	35	150	100	8.71	1.70
2	70	150	100	25.57	2.61
3	90	150	100	113.39	18.59
4	35	250	100	12.71	1.00
5	70	250	100	73.27	21.85
6	90	250	100	181.08	30.37

Figure 107 demonstrates predictable results with a different trend to the zig-zag pattern. As the deposition patterns produce increasingly stable results and predictable coatings the coating thickness measurements will better reflect the effect of the voltage and frequency.
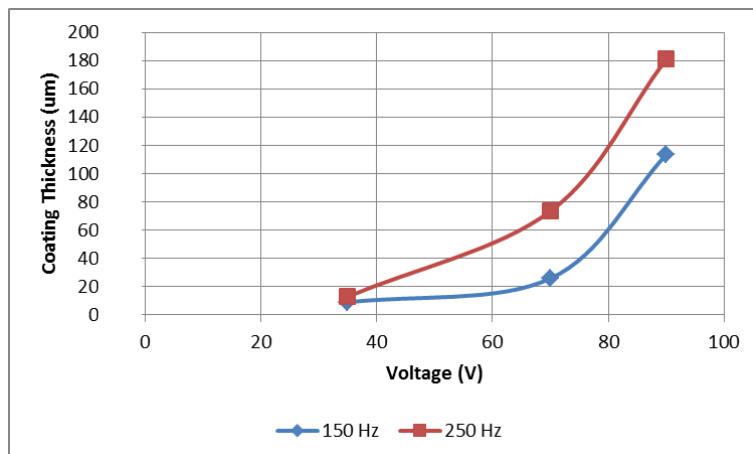
Figure 107: Octagon spiral pattern coating average coating thickness results versus the electrical ESD parameters

5.1.5 Bending test

Applications for ESD of metallic coatings often apply to buildup and repair applications. In order to test the performance of the ESD coating with different electrical parameters on the mechanical properties of a repaired object an experiment was performed with a bending test. The bending test served to test if the coatings would delaminate while subjected to extreme, tension, compression and shear stresses. This experiment also highlighted the difficulties in applying larger area coatings with a constant step-down pattern. In order to maintain a consistent coating pre-experiments were performed to ensure that the step-down would be sufficient to maintain contact for the duration of the experiment, coating a 20cm diameter

area with the spiral pattern. Table 15 reports the ESD parameters used, the differences in the step-down per line, the total step-down and the measured material loss from the electrode. Material loss often exceeded the total step-down, as long duration coatings, approximately 12.35 minutes, and excessive overheating exacerbates electrode erosion.

Table 15: Bending test experiment ESD parameters

Test Number	Voltage (V)	Maximum Frequency (Hz)	Capacitance (µF)	Step-down (mm/line)	Total Step-down (mm)	Material Loss (mm)
1	75	100	300	0.001	0.4	0.657
2	75	400	300	0.002	0.8	1.229
3	75	400	300	0.0035	1.4	1.115
4	100	100	300	0.004	1.6	2.548
5	100	100	300	0.008	3.2	4.292

The bending test was performed with an Instron tester with a three point bending apparatus, maximum displacement of 20mm. Figure 108 graphs the displacement and load data from the compressive bending test. The uniform loading profile, the lack of physical damage and the qualitative lack of cracking noises during testing supports the effective metallic bond forming the ESD coating. Considering the excessive overheating due to the high electrical parameters and high rates of electrode erosion the coatings should contain the defects exhibited in previous sections. With this considered all of the coatings slightly improved the loading performance versus the uncoated substrate, test 0, and did not present evidence of shear failure or delamination.
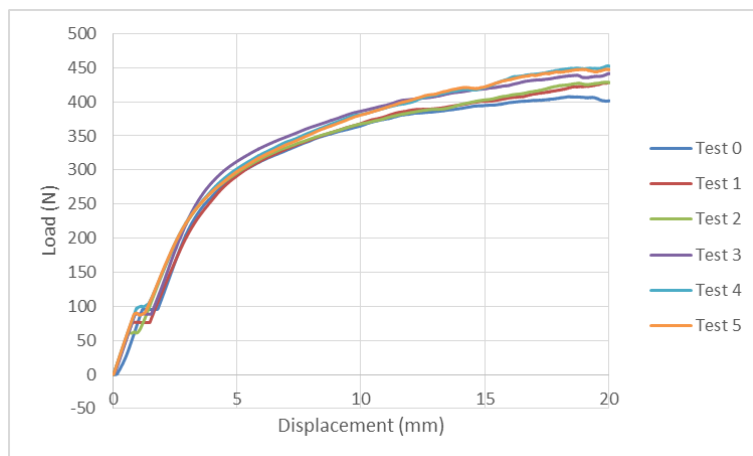
Figure 108: Bending test compressive load data

Table 16 reports the increase in maximum load as with the increasing ESD electrical power output. This relates that the ESD coatings did not weaken the performance of the initial steel sheet substrate; rather the ESD coating provided mechanical reinforcement. These findings support the use of ESD as a repair method for high value mechanical components, as it has been reportedly used.

Table 16: Bending test maximum load values

Test Number	0	1	2	3	4	5
Maximum Load (N)	407.66	427.79	429	441.62	452.89	447.92

5.2   Force Feedback

5.2.1   ESD application normal force

Application force during ESD is a major concern during both automated and manual operations. Some small applied force is required to maintain intermittent and localized contact of the ESD electrode, while excessive force will result in the short circuiting of the electrode and the cessation of the arcing process. With the CNC patterns different methods of increasing the force as the ESD electrode is consumed are considered. Initially depositions were made with a linear increase in the z-step-down. This resulted in coatings that contacted near the beginning of the patter, but as the electrode warmed, the deposition rate increased the linear z-step-down rate proved ineffective.

When used with the spiral and octagon patterns the linear step-down rate was ineffective when the radius of the spiral increase, as the step-down rate between G-Code commands remained the same, whereas the linear distance between points increased.

In order to mitigate this issue an initial step-down rate was determined, and then a further exponential increase in the step-down rate relative to the line number in the G-Code was applied. This attempted to mimic the increase in deposition rate from electrode warming, as well as account for the increases in linear distance in the spiral patterns. Small coatings worked well with this method; however larger coatings had greater disparities between the material deposition rates and linear distances between points and exact increases in step-down rate were difficult to determine.

The step-down rates were also affected by the electrode size, materials for the electrode and substrate, as well as the electrical parameters. The most effective z-step-down rate was determined to be one that looked at the arc length of the spiral and accordingly applied a certain z-step-down rate per mm of arc length. This method required a higher force at the beginning of the coating to account for the increase in

71

deposition rate later in the coating pattern. See Figure 109 for an illustration of how the different z-axis step-down rates affect the z-position over time, with the same actual final step-down.
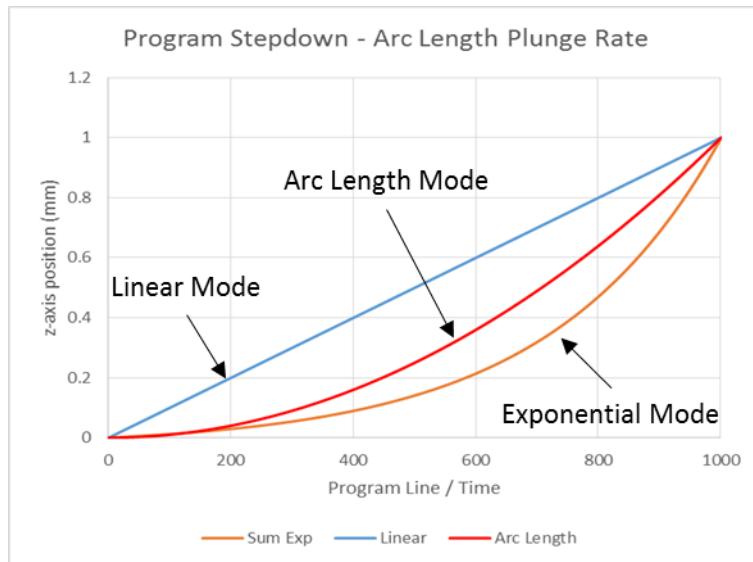
Figure 109: Different z-step-down rates

Over large areas issues with high heat input to the substrate or un-level substrates compound so large areas of the deposition area have no coatings.

5.2.2   Force sensing

Force feedback was proposed using the ESD CNC system integrated with a capacitive force sensor, detailed in the experimental setup section. Data collection from the capacitive force sensor was facilitated via the NI-DAQ 6003 USB device, which detected the voltages 0.5V to 1.5V which can be interpreted as corresponding force measurements in Newtons. Due to the use of the NI-DAQ device the data collection and initial processing was done via a LabView graphic user interface. Several considerations were added to mitigate the effects noise detected by the sensor to achieve a more realistic force reading. See Figure 110 and Figure 111 for the developed GUI and block diagram program respectively for force sensor data collection.
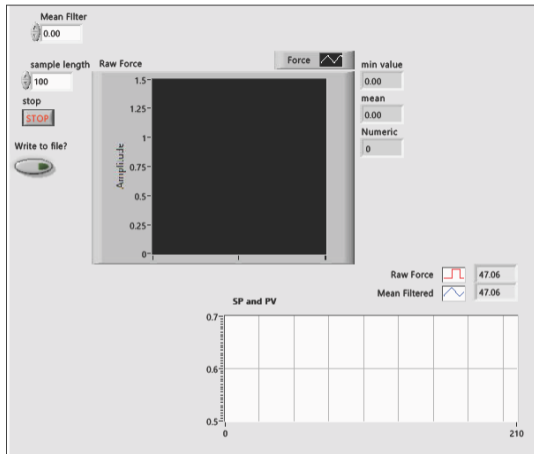
Figure 110: LabView GUI for capacitive force sensor data collection
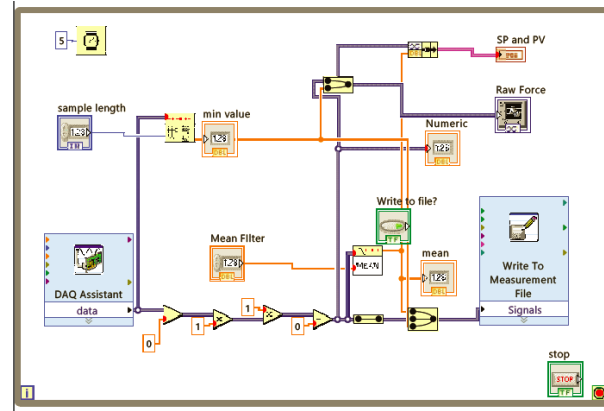
Figure 111: LabView block diagram for capacitive force sensor data collection

5.2.2.1 Sensor Noise

Despite the validity of the capacitive sensor setup several issues arise with the ESD and CNC system which prevent accurate force measurements. Mechanical noise adds vibrations from the ESD applicator electric motor and electrode rotation, oscillations in the z-axis suspension system, lack of rigidity in the x-y stage, and reaction forces from the ESD sparks. Significant levels of electrical noise are produced by the high current pulses produced by the ESD process as well as interference from electrical components which comprise the ESD and CNC power supplies.

The high sensitivity of the capacitive sensor and potential damage to the system has resulted in constant oscillations of the force data. Depending on the sample frequency the oscillations have a different period. See Figure 112 and Figure 113, the high frequency noise from the low frequency force readings have a standard deviation of 0.0157V which corresponds to 0.7N. This level of noise is acceptable for the control of the ESD system, considering all of the other noise sources.

73
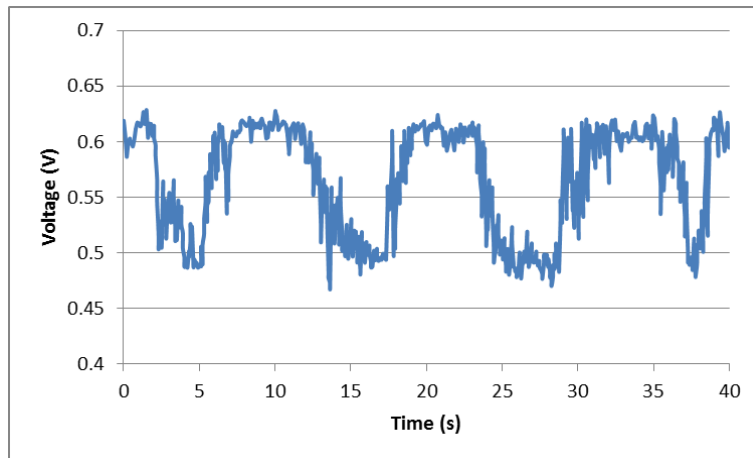
Figure 112: Force Sensor Measurements No Lab Noise 5Hz

In order to mitigate the effects of the force sensor oscillations a moving minimum can be used to filter the data from the high frequency force sampling. Figure 113 illustrates how increasing the sample size of the moving minimum begins to accurately represent the force under no load, where 0.5V is 0N. With this filter the high frequency noise has a standard deviation of 0.0195V which represents 0.88N an acceptable noise level.
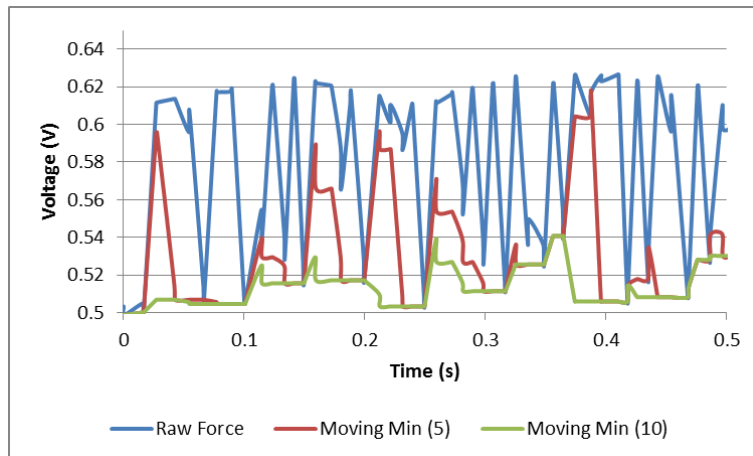
Figure 113: Force Sensor Measurements No Lab Noise 200Hz

The relatively lower frequency oscillations appear to have maxima of 0.62V under a no load condition. This level of noise represents approximately 28N an unacceptable level of uncertainty for the effective control of the ESD process.

74

5.2.3 Open loop response

Positioning the force sensor below the substrate gets good results when the force is being applied straight down, see Figure 114. This position allows for the force sensor to detect the normal force between the electrode and the substrate without noise effects from the suspension system or bearings in the z-axis affecting the readings.
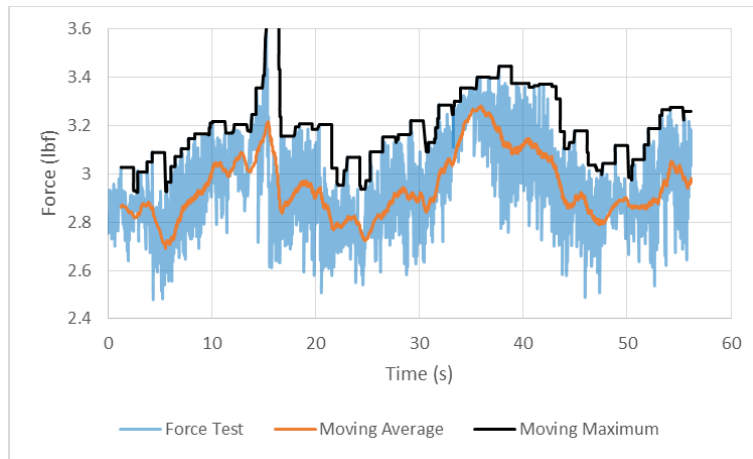
Figure 114: 1mm step-down force; sensor below the substrate

This position proves to be a negative when the singular position detects oscillations in the force measurements due to actual ESD patterns. Figure 115 shows the force readings during ESD with a spiral pattern. As the electrode completes the arcs of the spiral the force measurement fluctuates.
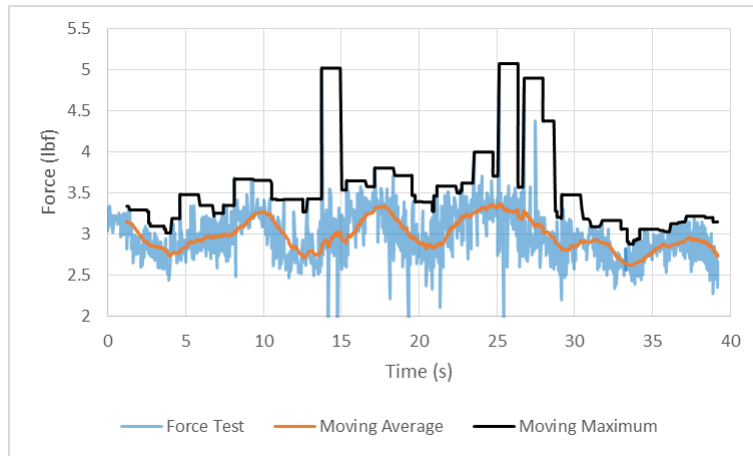
Figure 115: Force measurements with sensor below the substrate during a spiral deposition

In order to mitigate these effects the force sensor was mounted on the suspension system for the ESD applicator. In this position there is an increase in the mechanical instability as the effects of the spring,

bearing movement and bending of the electrode are more severely present. However the following force measurements show that this position removes the artificial oscillating effect of the ESD patterns.

5.3 PID Controller

LabVIEW is used for recording of the force, voltage and current measurements in real time from the ESD CNC system. The LabVIEW VI was altered to parse the G-Code saved as sequential commands to be sent through the LabVIEW NI DAQ interface.

5.3.1 PID Feedback control

A proportional-integral-derivative or PID controller was used to generate the rate of z-axis change responses from the force data. The PID system functions by feeding back the error from the last recorded operation to alter the future response.

Relating to the plant system illustrated in Figure 33 with CNC force feedback system the desired force is set as the input r, the current force is fed into the PID controller from the data queue as y, and the control signal is the position change from the current z-axis position. The control signal is added to the parsed G-Code commands and sent to the GRBL controller via the Virtual Instrument Software Architecture (VISA) serial connection.

5.3.2 LabVIEW Control

The pre-packaged VISA was used to communicate through the USB serial connection to the GRBL software loaded on the Arduino Uno. This built in interface allows for the LabVIEW program to mimic all of the functions of the Universal G-Code Sender software and while running background operations with the force sensor, see experimental setup Figure 55. The LabVIEW VISA function allows for the reading and writing functions to the GRBL serial port.

The command structure was based off the open source visual interface titled GRBL-GUI developed to connect to the GRBL Arduino software via a USB serial port. This LabView program intended to mimic the basic functions of the Universal G-Code sender in order to form a connection and send the GRBL syntax G- Code commands. This software lacked the significant functions characterizing the Universal G-Code Sender software. See Figure 116 for the LabView block diagram for the simplified GRBL communicator.
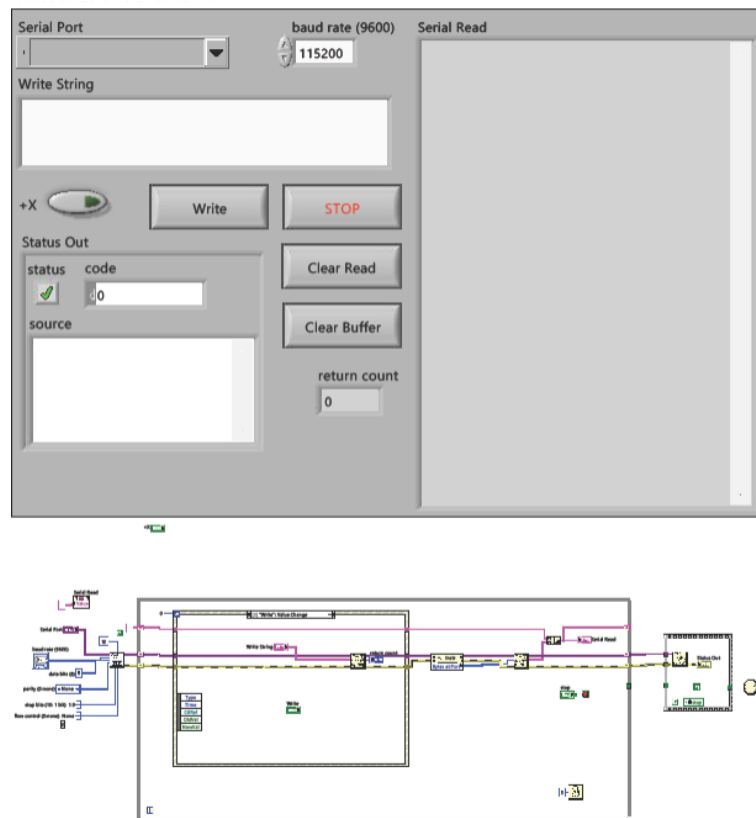
Figure 116: GRBL-GUI LabView program

The LabView VI was designed to parse a pre-made G-Code program, and cut in z-axis commands generated from the force sensor feedback loop.

Appendix D: LabView force feedback program details the development of the LabView VI with two different attempted loop structures.

5.3.3 Gain Tuning

In order to determine the PID gains the CNC was set up with a compression spring to simulate the normal force exerted by the ESD electrode onto the substrate surface. With this setup the parsing software could be run for extended periods of time and allow for an auto-tuning process to determine the appropriate PID gains for the effective output response of the controller.

The LabVIEW Auto tuning PID sub VI was used for the PID force control system. This sub VI uses the Ziegler-Nichols heuristic tuning method in order to determine the gain values for the PID controller. With this method initial PID gains are estimated or guessed and the system is run over a long period of time. Once the system is stable oscillating about the set force the noise from the sensor is estimated by the system. Upper and lower limits on the simulation are chosen along with a general response speed. The program then proceeds to change the set force to the upper and lower limits to test the system response and tune the gains. [38] Figure 117 illustrates the tuning process over a long period of time, as the PID gains are altered the z-position becomes more stable, and the force is able to maintain a stable oscillation about 0.8V.
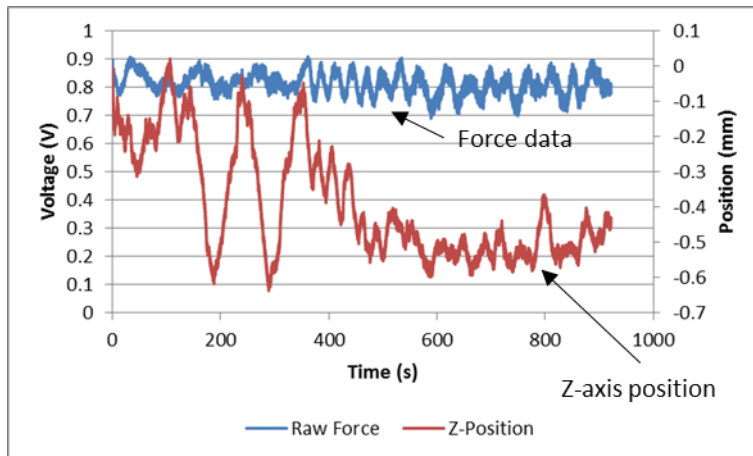
Figure 117: Tuning PID Gains at 0.8V

The proportional gain is tuned to achieve the desired response time between the upper and lower force limits. Once the system has settled and is oscillating about the new set point the derivative and integrative gains are changed in order to reduce the overshoot and steady state error.

Using the auto tuning method controllers were evaluated to determine whether the added control of the integral and derivative gain values improved the response from the system. Each controller type was iterated for at least three cycles of a 0.1V amplitude about a set point of 1V.

The response time of the PID controller was noted to be slower than desired when the controller was applied to the real world CNC controlled ESD application. In order to determine whether the proportional, integrative, derivative, or any combination of the controllers would be more effective the auto tuning process was repeated for different types of controllers.

The auto tuning function returned the PID gains for the different types to improve the settling time and reduce steady state error. For this experiment the different controllers were evaluated by the amplitude of the steady state error, as well as the time required from 0.75V, approximately no load at the time of the test, to 1V force.

Figure 118 illustrates the force response, and z-axis position for the tuned PID controller. With the force preset to approximately 0.75V from the force sensor the controller required near 500 seconds in order to achieve the set point of 1V. The steady state error with this controller proved to be erratic with large random amplitude oscillations. Even after allowing the controller to settle for 1000 seconds, well beyond the deposition time for most of the ESD tests there remained significant error.
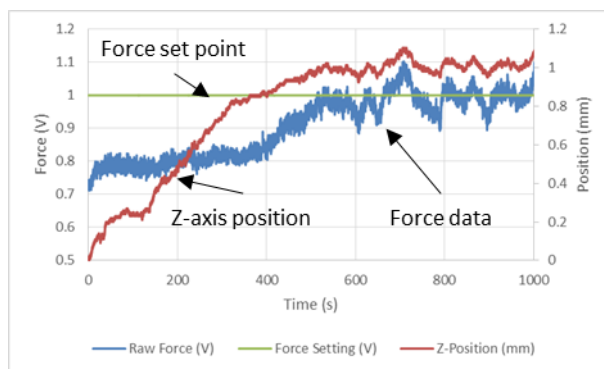
Figure 118: PID Controlled Force Test

Figure 119 illustrates the controller test for the auto-tuned PI gains. This controller demonstrated significantly faster settling time, near 35 seconds. The response from the raw force values and the z-axis

position show that the response from the controller reduces the rate of step-down well before the set point of 1V. The PI controller reduces the effect of overshoot and resulted in a much lower steady state error than the PID controller response.
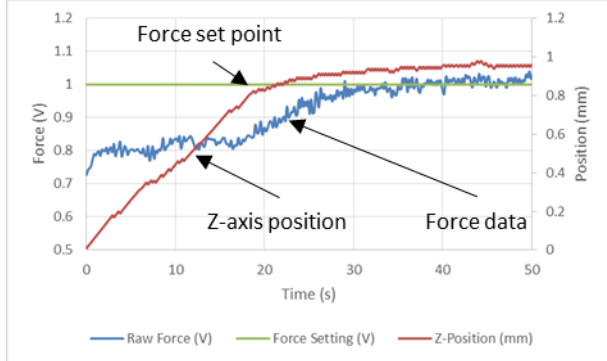
Figure 119: PI Controlled Force Test
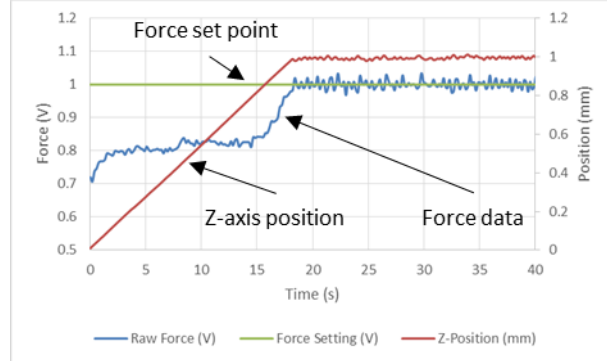
Figure 120: P Controlled Force Test

Figure 120 illustrates the controller output for the P controlled system. Clearly seen by the reaction of the z-axis position the output rapidly reacts to the negative error input, resulting in the maximum output for each step. This results in the fastest settling time near 18 seconds. The steady state error appears to be constant oscillations about the set point, with little issues with overshoot.

Table 17 reports the results of the different controllers evaluating the settling time to 1V from 0.75V, the steady state noise about 1V and the deviation between data points during the steady state. The comparison of the values clearly shows that the P controller is the most effective in controlling force feedback system, the quick response time, and low steady state error will be critical when the ESD process is added to the control system.

Table 17: PID Controller Gain Experimental Results

	Time to Reach (s)	Maximum Steady State Noise	Minimum Steady State Noise	Average Error	Standard Deviation
PID	515.03	1.124	0.885	0.258%	0.0389
PI	35.52	1.041	0.949	0.173%	0.0172
P	18.41	1.035	0.967	0.061%	0.0137

With the proportional controller gains determined the force feedback system can be used to control the CNC machine for ESD coatings.

5.4 Closed loop response

The PID control system tuned with the auto-tuning process can now respond to limited changes in the ESD force during operation. The initial closed loop response of the control system resulted in promising results for the force control versus the open loop response where just the force sensor had difficulties in reading stable results.

5.5 Parameter Study with Preliminary Force Control

Employing the force feedback system, and CNC controlled spiral patterns the physical considerations for the ESD electrical parameters can be kept constant. An experiment was done with steel electrodes, depositing on DP980 steel. A range of electrical parameters were tested as well as the effects of the argon shielding gas. See

Table 18 for the range of tested electrical parameters, the set of experiments were repeated for Tests 10-18 with 30CFH local argon shielding gas. The universal ESD power supply was operating in frequency control mode, with a charging speed of 95, and varying maximum frequency settings. The depositions were applied to a 5mm diameter circular area with a stopover of 0.1mm per spiral pass, and a CNC federate of 800mm/min. The force feedback was maintained at 0.65V with an unloaded reading of 0.55V, resulting in a constant force approximately 4.4N.

Table 18: CNC and force feedback controlled ESD experiment; electrical parameters

Test #	1	2	3	4	5	6	7	8	9
Voltage (V)	50	75	100	50	75	100	50	75	100
Capacitance (µF)	200	200	200	200	200	200	200	200	200
Max Frequency (Hz)	100	100	100	200	200	200	300	300	300

Cross sections were processed and examined with optical microscopy. The 10x magnification images which presented a 1385mm width sample of the coatings were measured to relate the effects of the electrical parameters to the ESD voltage and frequency settings. 13 equally spaced coating thickness measurements were taken from the coating substrate interface to the surface of the coatings. The results were averaged and reported in Table 19 with accompanying standard deviations, comparing the argon shielded and non-shielded experiments.

Table 19: CNC and force feedback controlled ESD experiment; coating thickness measurements

Frequency (Hz)	100	200	300		Voltage (V)	50	75	100
Average No Ar (µm)	120.51	87.28	91.30		Average No Ar (µm)	53.30	90.65	155.13
Average Ar (µm)	92.09	160.65	185.13		Average Ar (µm)	92.15	185.49	160.23
StDev No Ar (µm)	36.07	29.13	20.19		StDev No Ar (µm)	16.98	26.67	41.74

StDev Ar (µm)	18.46	39.95	35.10	StDev Ar (µm)	29.91	42.55	21.06

The average coating thicknesses and standard deviations are summarized in the charts in Figure 121 and Figure 122. The coating thickness curves for the experiments done in atmosphere show a decrease in the average coating thickness with the increase in the ESD frequency. The argon shielded experiments show the opposite with a significant increase in coating thickness with the increase in frequency, and the resulting total ESD power output.
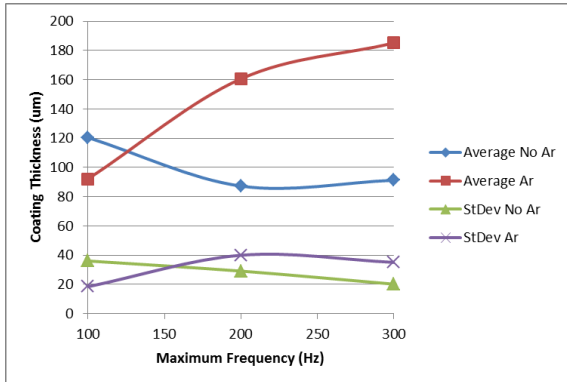
Figure 121: Maximum ESD frequency parameter related to coating thickness with Ar shielding gas
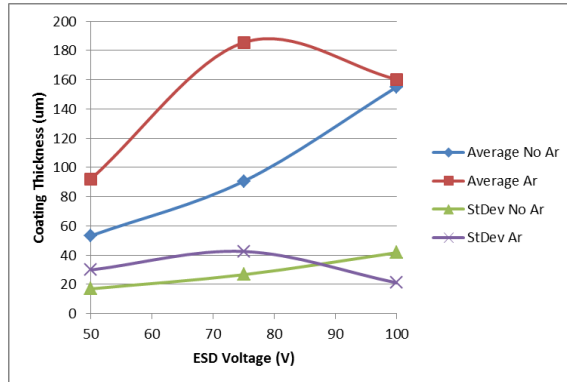
Figure 122: ESD voltage parameter related to coating thickness with Ar shielding gas

The coating thickness curve related to the ESD voltage shows a steady increase in coating thickness, with increasing voltage, and ESD energy output. The argon shielded experiments show an initial increase, followed by a drop in coating thickness.

Uncharacteristic behavior of the electrical parameter experiment can be attributed to a small sample size, or the need for further improvements to the CNC force feedback system. The experiment was done using the data queue force feedback CNC integration LabVIEW program. During depositions lags in the command predictions, typically characteristic of the GRBL program were observed. Implementation of the newer feedback control system and, or optimization of the CNC pattern to facilitate force feedback could rectify the coating thickness results with the hypothesized conventions.

5.5.1 Coating defects

The cross section images were evaluated qualitatively for the frequency and voltage effects on coating defects. The typical defects include transverse and interfacial cracking, pores, and oxidation.

The optical cross section images at 20x magnification are detailed in Figure 123, with increasing frequency in with increasing row reference and increasing voltage with increasing column reference. The

experiment done in atmosphere revealed that the low power parameters, test 1 and 2 at 50V and 75V and 100Hz resulted in coatings with little or no oxidation. Test 3 which had an ESD voltage of 100V with a frequency of 100Hz and Test 4, with a voltage of 50V and frequency of 200Hz both exhibited oxidized coatings due to overheating during the ESD process. Notably Test 3 has a thick layer, near equal to the thickness exhibited in Test 1, covered by oxidized material. This relates to the low step-over distance of 0.01mm per spiral pass, meaning that the coatings overlap significantly. The increase in voltage at low frequency of 100Hz resulted in a very significant increase in the coating thickness, but at the cost of oxidizing the deposited materials.

Experiments in the first column, with the ESD voltage of 50V and increasing pulse frequency exhibit the most consistent surface conditions with a smaller standard deviation in the coating thickness. Increasing the Test number, and primarily increasing the ESD voltage increased the defect density, mainly pores and decreased the surface uniformity.
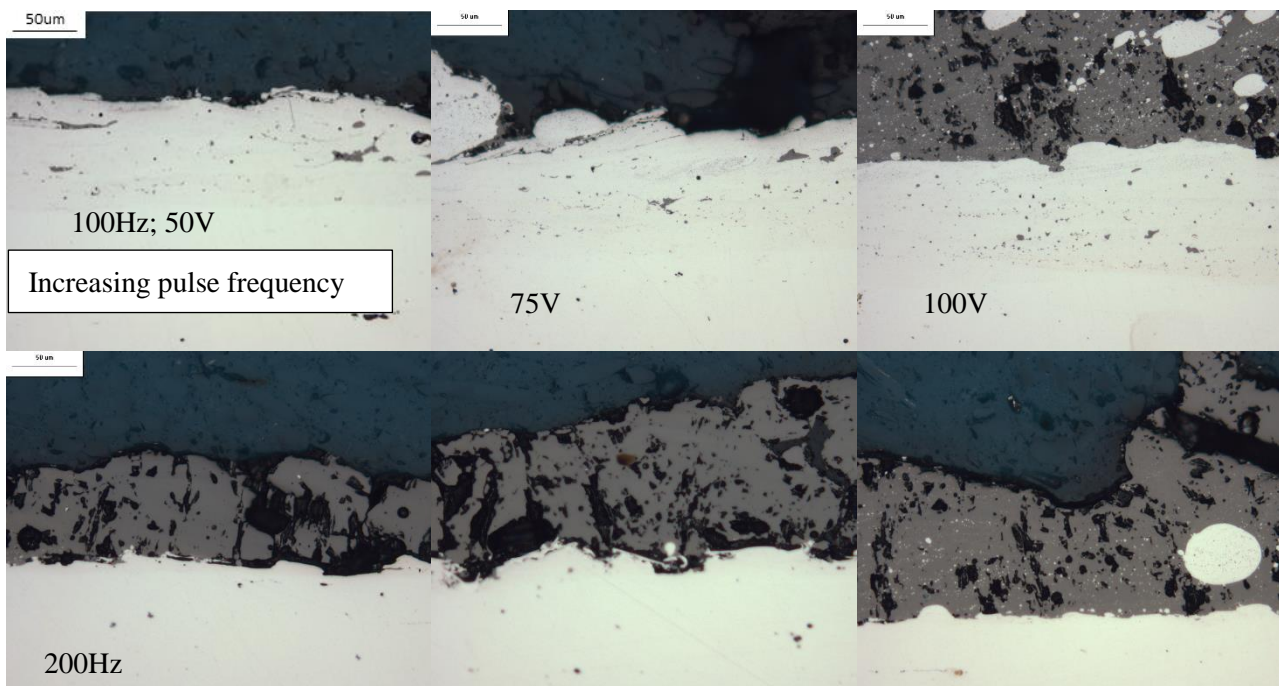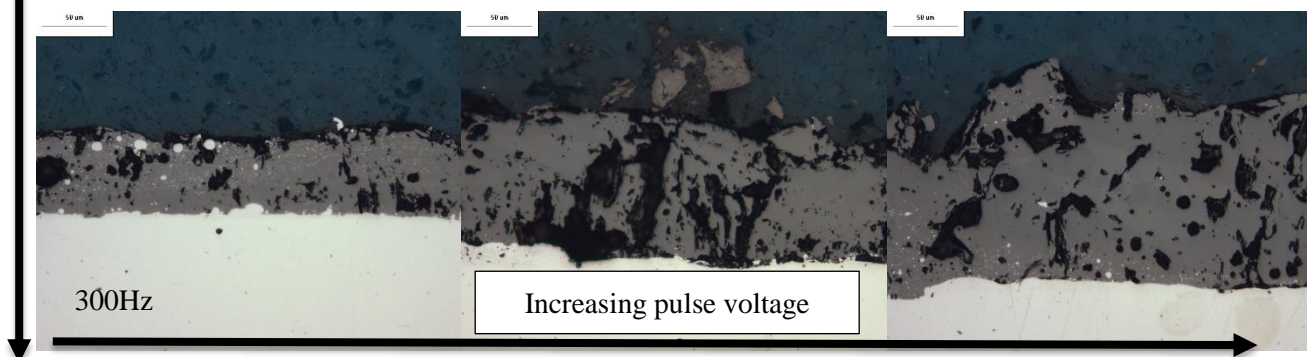
Figure 123: Tests 1-9; no argon 20x magnification optical images

The argon shielded experiments are in Figure 124, reporting the optical cross section images at 20x magnification, with an exception for Tests 14 and 17 which coatings were too thick to be captured in the 20x magnification image. Test 1 revealed a coating which is near imperceptible to the base metal, increasing the voltage from Test 10 to Test 12, resulted in an increase in the coating thickness and an increase in the defect density. Increasing the frequency from down column one, Test 10, Test 13 and Test 16 demonstrate the effect of increasing frequency, and heat generation on the oxidation of the deposited coating, even with the added cooling and shielding effects of the argon gas.

Test 14 and Test 17 at 75V and 200Hz and 300Hz respectively are the highest powered parameters which demonstrate un-oxidized coatings. The average coating thicknesses for these parameters were 267µm and 303µm respectively. Further increase in the ESD pulse energy in Test 15 and 18 resulted in overheating, causing excessive oxidation of the coating and large defect densities.
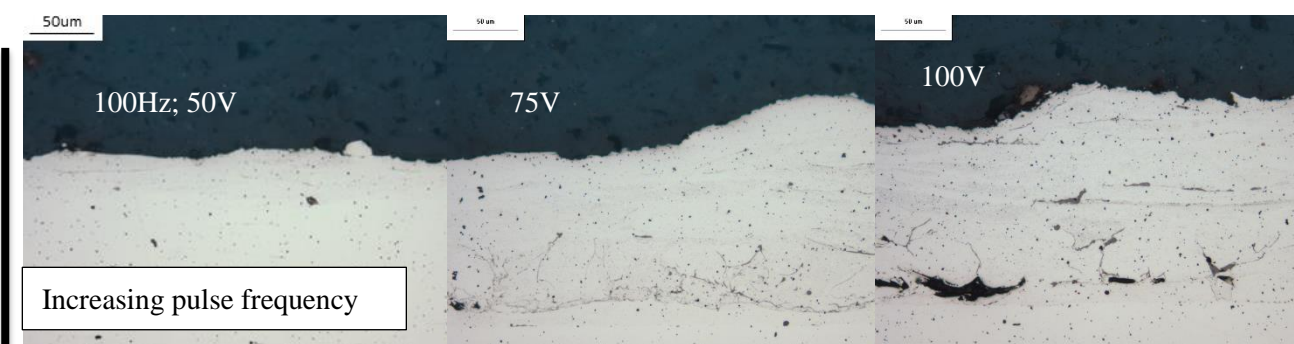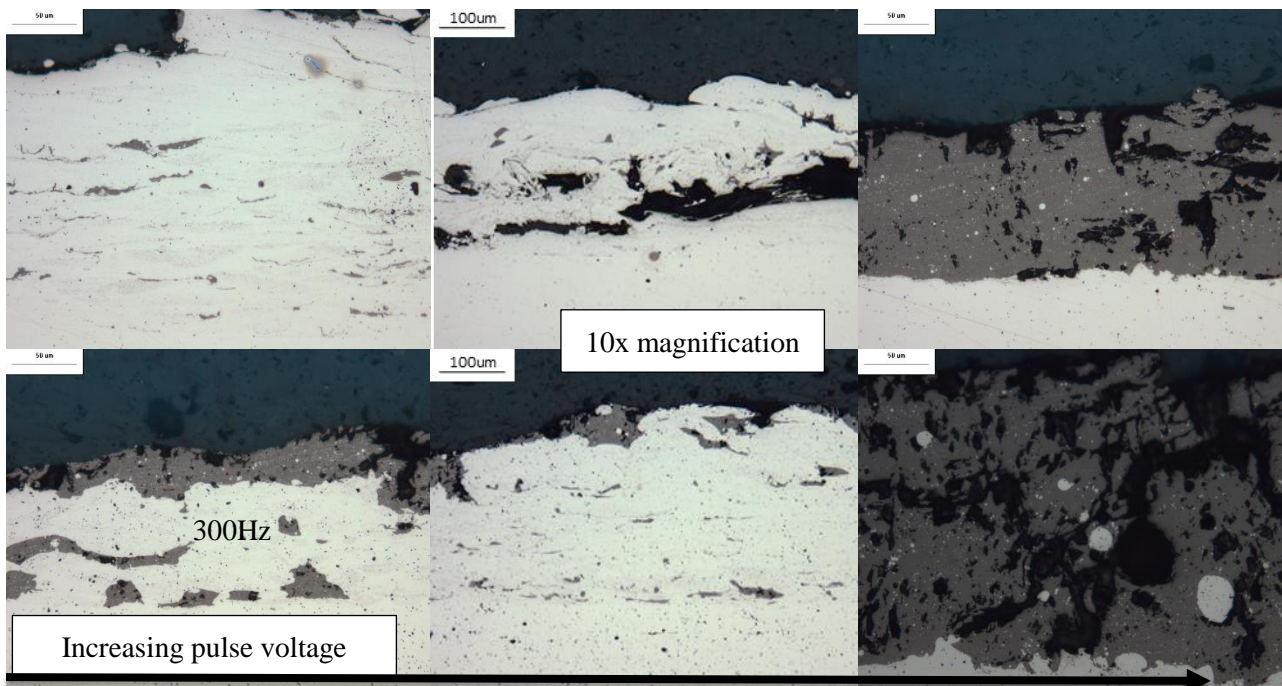
Figure 124: Tests 10-18; 30CFH argon shielding gas; 20x magnification optical images; NB: Test 14 and 17 10x magnification

This experiment concludes that there is a significant relationship between the coating quality, related to the material pairing, and the ESD pulse voltage and frequency. The use of argon shielding gas can be employed to convectively cool the ESD process, allowing for the use of higher ESD parameters and corresponding to higher effective mass transfer rates. The shielding effect of the argon gas improved oxidation prevention during the ESD process. The use of low voltage and frequency parameters can also produce low oxidation coatings without the use of shielding gas.

Chapter 6.0: Conclusions and Recommendations

6.1   ESD power supply design

The development of advanced ESD power supplies were evaluated versus the typical simplified ESD circuit design in Machine #1.

6.1.1   ESD Machine #2

1. A power supply was developed and evaluated with the addition of a microcontroller and solid-state switching devices so that the capacitor discharge can be controlled.
2. The implementation of a logic based interface allowed for the development of high and low voltage pulses, sequences of groups of pulses, pauses between pulses, a secondary parallel circuit which discharged simultaneously and charging speed control.
3. The advanced electrical parameters allows for the fine tuning of electrical power, relating to heat generation for potential new applications.

6.1.2   ESD Machine #3: Universal power supply

1. To meet the needs of a wider variety of material pairings a capacitor bank was implemented with a greater range of voltage settings.
2. The use of a rotating applicator increased the frequency of electrode to substrate contact, reducing the effect of the previously used vibrating electrode on the pulse frequency.
3. A constant charging speed control mode and a frequency control mode were implemented which allowed for the variation of heat generation through the grouping of discharge pulses followed by pauses. Previous studies and deposition experiments showed that lower electrical energy parameters can be used when higher heat is generated through the grouping of pulses.
4. Voltage and frequency were determined to have the most significant effect on the coating thickness and quality.

6.2 Mass transfer effects

1. A high speed camera was used to observe the spark behavior during the ESD process.

2. The high electrical parameter experiments demonstrated molten metal interactions at the surface, relating to the prevalence of defects and oxidation in the deposited coatings. The images proved that overheating of the electrode significantly reduces the quality of the coatings.

3. Argon shielding gas when locally applied reduces the overheating of the ESD process when using the same electrical parameters. Convective cooling paired with preventing atmospheric interactions with the molten metal are attributed to the benefits.

6.3 Physical controls

1. Variations in the movement speed, pattern and application force during manual application of the ESD process have been shown to affect the uniformity of coatings. In order to determine the isolated effect of the electrical parameters a CNC machine and force feedback system were developed.

2. Experiments revealed issues with the deposition patterns executed by the CNC machine were noted, where the coating thickness increased near the edge of depositions where changes in direction were made. Optimized patterns were developed to reduce the effects of direction changes.

3. The physical controls system was used in an experiment comparing the effect of the electrical parameters and shielding gas, when the physical parameters are more consistent.

   a. Management of the voltage and frequency revealed a range of parameters where oxidation, pores and cracks were kept to a minimum, while the coating thickness was substantial. Increases beyond this range resulted in rapid increases in coating thickness, with an accompanying increase in oxidation and defect density.

   b. The use of shielding gas to convectively cool the process, as well as shield from atmospheric interactions served to increase the range of effective voltage and frequency settings.

6.4   Recommendations

The experiments, procedures and developed equipment used in this study can be used to determine the effective parameter range for new applications and material pairings. Notably the effect of the ESD parameter on the electro-spark alloying process and elemental diffusion is possible.

The beneficial effect of controlling the physical parameters shown in this study can be improved with the use of more accurate, and faster reacting robotic systems. A major deficiency in the force feedback system presented in this study is the slow interaction between the force controller and the CNC machine. The implementation of purpose built and optimized robotic solutions would improve the physical controls and expand the potential experiment conditions and industrial applications.

The advanced ESD power supplies evaluated present further possible combinations of pulse sequences, with electrical and physical parameters to improve the ESD coating performance as is presented in some of the studies examined in the background section. A combination of the improved power supply circuits, control logic, and a transducer managed pulse generator can present even more improvements in ESD power supply performance.

References

[1] J. L. Reynolds, R. L. Holdren and L. E. Brown, "Electro-spark deposition," *Advanced Materials & Processes,* pp. 35-37, 2003.

[2] TWI Ltd, "What is electrospark deposition (ESD)? Frequently asked quations," TWI Ltd, 2016. [Online]. Available: http://www.twi-global.com/technical-knowledge/faqs/process-faqs/faq-what-is-electrospark-deposition-esd/. [Accessed 20 October 2016].

[3] Huys Industries Ltd, "Electro-spark deposition (ESD)," Huys Industries Ltd, 2016. [Online]. Available: http://huysindustries.com/processes/electro-spark-deposition/. [Accessed 20 October 2016].

[4] G. Ken-Hicken, "Gas-tungsten arc welding, welding brazing, and soldering," *ASM Handbook,* vol. 6, pp. 190-194, 1993.

[5] Cold Weld, "How it works," Cold Weld , 2016. [Online]. Available: http://www.coldweldusa.com/how-it-works.php. [Accessed 31 October 2016].

[6] A. Lesnjak and J. Tusek, "Process and properties of deposits in electrospark deposition," *Science and Technology of Welding and Joining,* vol. 7, no. 6, pp. 391-396, 2002.

[7] S. Tang, T. Nguyen and Y. Zhou, "Materials transfer in electro-spark deposition of TiCp/Ni metal-matrix composite coating on Cu substrate," *Welding Research,* vol. 89, pp. 172-180, 2010.

[8] P. Wang, G. Pan, Y. Zhou, J. Qu and H. Shao, "Acceleratd Electrospark Deposition and the wear behavior of coatings," *Journal of Materials Engineering and Performance,* vol. 6, no. 6, pp. 780-784, 1997.

[9] The Editors of Encyclopedia Britannica, "Transformer - electronics," Encyclopedia Britannica, 2016. [Online]. Available: https://www.britannica.com/technology/transformer-electronics. [Accessed 21 October 2016].

[10] Electronics Tutrials, "Power diodes and rectifiers," Aspencore Network, 2015. [Online]. Available: http://www.electronics-tutorials.ws/diode/diode_5.html. [Accessed 20 October 2015].

[11] Electronics Tutorials, "Full wave rectifier," Aspencore Network, 2015. [Online]. Available: http://www.electronics-tutorials.ws/diode/diode_6.html. [Accessed 20 October 2016].

[12] W. L. Hosch, "Capacitance - electronics," Encyclopedia Britannica, 22 September 2006. [Online]. Available: https://www.britannica.com/science/capacitance#ref27559. [Accessed 21 October 2016].

[13] F. N. H. Robinson, E. E. Suckling, S. B. McGrayne and E. Kashy, "Electricity - physics," Encyclopedia Britannica, 22 September 2006. [Online]. Available: https://www.britannica.com/science/electricity/Deriving-electric-field-from-potential#toc71559. [Accessed 21 October 2016].

[14] R. I. Scace, "The science of electronics," Encyclopedia Britannica, 15 February 2016. [Online]. Available: https://www.britannica.com/technology/electronics/The-science-of-electronics#ref194777. [Accessed 20 October 2016].

[15] The editors of Encyclopedia Britannica, "Thyristor - electronics," Encyclopedia Britannica, 2016. [Online]. Available: https://www.britannica.com/technology/thyristor. [Accessed 20 October 2016].

[16] I. Galinov and R. Luban, "Mass transfer trends during electrospark alloying," *Surface and Coatings Technology,* vol. 79, pp. 9-18, 1996.

[17] J. Reynolds, R. Holdren and L. Brown, "Electro-spark deposition," *Advanced materials and processes,* vol. 161, no. 3, pp. 35-37, 2003.

[18] J. Liu, R. Wang and Y. Qian, "The formation of a single-puls electrospark deposition spot," *Surface and coatings technology,* vol. 200, pp. 2433-2437, 2005.

[19] R. Johnson, "Electrospark deposition: Principles and applications," *Society of Vacuum Coaters 45th Annual Technical Conference,* pp. 87-92, 2002.

[20] A. V. Ribalko, K. Korkmaz and O. Sahin, "Intensifiction of the anodic erosion in electrospark

alloying by the employment of pulse group," *Surface and coatings technology,* vol. 202, pp. 3591-3599, 2008.

[21] A. Ribalko and O. Sahin, "The use of bipolar current pulses in electrospark alloying of metal surfaces," *Surfaces and Coatings Technology,* vol. 168, pp. 129-135, 2003.

[22] A. Ribalko, O. Sahin and K. Korkmaz, "A modified electrospark alloying method for low surface roughness," *Surface and coatings technology,* vol. 203, pp. 3509-3515, 2009.

[23] MatLab, "Introduction: PID Controller Design," March 2012. [Online].

[24] National Instruments, "PID theory explained," National Instruments, 29 March 2011. [Online]. Available: http://www.ni.com/white-paper/3782/en/. [Accessed 20 October 2016].

[25] V. Belik, R. Litvin and M. Kovalchenko, "Effect of substrate temperature on the electrospark deposition, structure, and mechanical properties of coatings. I. Kinetics of substrate heating during electrospark deposition," *Powder Metallurgy and Metal Ceramics,* vol. 50, pp. 698-703, 2012.

[26] S. Frangini and A. Masci, "A study on the effect of a dynamic contact force control for improving electrospark coating properties," *Surface and coatings technology,* vol. 204, pp. 2613-2623, 2010.

[27] National Instruments, "USB-6003," National Instruments, 2016. [Online]. Available: http://sine.ni.com/nips/cds/view/p/lang/en/nid/212385. [Accessed 20 October 2016].

[28] M. Fassler, C. Hurzeler and J. Nikolic, "Force Sensing Technologies," Autonomous Systems Lab, Zurich, 2010.

[29] R. Russel, Robot Tactile Sensing, Sydney: Prentise Hall, 1990.

[30] Single Tact, "Single Tact User Manual," 2016. [Online]. Available: http://www.singletact.com/SingleTact_Manual.pdf. [Accessed 28 September 2016].

[31] Photron, "FASTCAM Mini UX50," Photoron USA Inc., 2016. [Online]. Available: http://photron.com/high-speed/cameras/fastcam-mini-ux50/. [Accessed 20 October 2016].

[32] Arduino, "Arduino Uno," Arduino, 2016. [Online]. Available: https://www.arduino.cc/en/Main/ArduinoBoardUno. [Accessed 20 October 2016].

[33] Synthetos, "grblShield," Synthetos.com, 2015. [Online]. Available: https://www.synthetos.com/project/grblshield/. [Accessed 30 October 2016].

[34] S. Jeon, "GRBL home," GRBL Github, 17 August 2015. [Online]. Available: https://github.com/grbl/grbl/wiki. [Accessed 20 October 2016].

[35] UGS, "Universal Gcode sender version 1.0.6," Universal Gcode sender, 2015. [Online]. Available: http://winder.github.io/ugs_website/. [Accessed 21 October 2016].

[36] D. Leung, "ESD Power supplies - The past andthe future," Huys Industries, North York, 2015.

[37] D. Leung, "The Huys ESD power supply #2 - Operation manual," Huys Industries, North York, 2015.

[38] National Instruments Co, "PID Autotuning VI and Limitations," National Instruments, 2014. [Online]. Available: http://digital.ni.com/public.nsf/allkb/D2E364AAF4D74EE6862575840049BC6E. [Accessed 29 September 2016].

[39] Department of Commerce United States of America, "Electric current information for all countries," International Trade Administration, [Online]. Available: http://www.trade.gov/mas/ian/ECW/all.html. [Accessed 21 October 2016].

[40] S. Sze and W. C. Holton, "Semiconductor device - Electronics," Encyclopedia Britannica, 28 January 2009. [Online]. Available: https://www.britannica.com/technology/semiconductor-device. [Accessed 20 October 2016].

[41] T. E. o. E. Britannica and A. Tikkanen, "Rectifier - Electronics," Encyclopedia Britannica, 11 September 2012. [Online]. Available: https://www.britannica.com/technology/rectifier. [Accessed 20 October 2016].

[42] Electronics Tutorial, "Thyristor Tutorial," Aspencore Network, 2015. [Online]. Available: http://www.electronics-tutorials.ws/power/thyristor.html. [Accessed 20 October 2016].

[43] A. Sattar, "Application note for insulated gate bipolar transistro (IGBT) basics," IXYS Corporation.

[44] Electronics Tutorials, "Insulated gate bipolar transistor," Aspencore Network, 2015. [Online]. Available: http://www.electronics-tutorials.ws/power/insulated-gate-bipolar-transistor.html. [Accessed 20 October 2016].

[45] The Editors of Encyclopedia Britannica, "Hall Effect - physics," Encyclopedia Britannica, 2016. [Online]. Available: https://www.britannica.com/science/Hall-effect. [Accessed 20 October 2016].

[46] Electronics Tutorial, "Hall Effect sensor," Aspencore Network, 2015. [Online]. Available: http://www.electronics-tutorials.ws/electromagnetism/hall-effect.html. [Accessed 20 October 2016].

[47] Honeywell Inc, Hall Effect sensing and application, Freeport: Honeywell Inc Micro Switch Sensing and Control.

Appendices

Appendix A: Electrical component descriptions Transformer

Transformers are common electrical devices used to step up or down incoming voltage to meet the requirements of the application. The voltage is altered through the process of electromagnetic induction where the initial voltage passes through a set of coils, and the output voltage is received by a different set of coils. The ratio between the coils determines the factor by which the voltage was altered; see Figure 125 for an illustration of a typical transformer. [9] For ESD a transformer is used to modify the municipal power, often 110-120V 10-15A 60Hz alternating current (AC) to the levels suitable to power or charge the capacitors for the ESD process. [39]
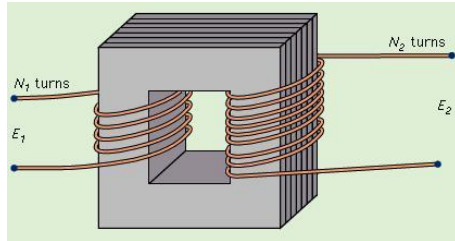
Figure 125: Iron core transformer [9]

Rectifiers

Rectifiers are electrical devices used to convert the AC power from the transformer to DC power. This is required for the charging of the capacitors for the use in ESD power supplies. ESD is a direct current electrode positive (DCEP) process and thus requires a biased polarity to function. Furthermore switching the polarity of the charging current for the capacitors will result in negating the stored charge and potentially damaging the component. Typical and efficient rectifiers are comprised of varying configurations of diodes. Diodes are two terminal semiconductor devices which function off varying impurities, geometries and the polarity biasing conditions to provide positive and negative junctions. The diodes are used in rectifiers to control the flow of current, biasing the polarities by presenting a high or low resistance. [40] Depending on the number and orientation of diodes the rectifier will either convert one, or both polarities of the AC power. Figure 126 illustrates the electrical components and output from a half wave rectifier, which represents the simplest rectifier circuit. This setup is used to convert only the positive or negative polarities of the AC power into half period pulses of DC power. [41]
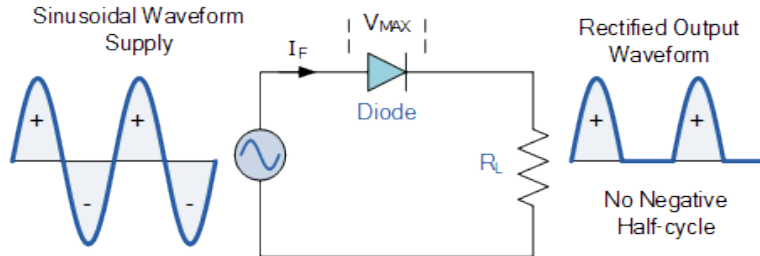
Figure 126: Half wave single diode rectifier [10]

Figure 127 illustrates the full wave double diode rectifier, this more complicated circuit employs two diodes which take turns in supplying power to the resistive load. This configurations has the benefits of retrieving more of the electrical power from the AC input, and creating more consistent DC output. [11]
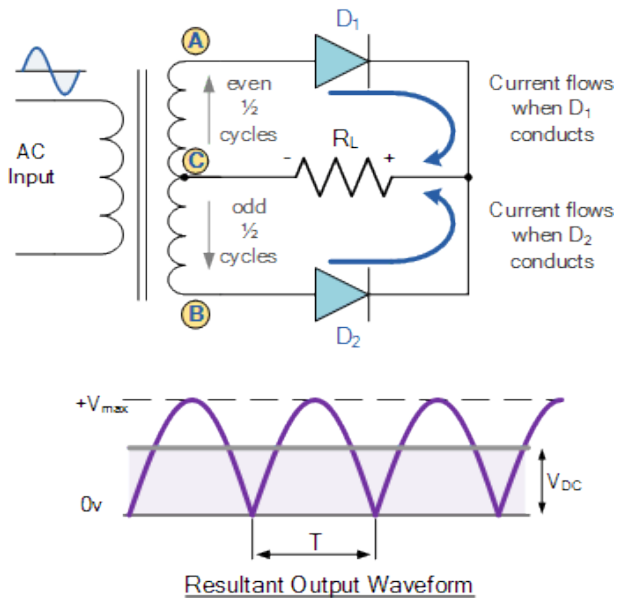

Figure 127: Full wave double diode rectifier [11]

A more efficient rectifier circuit is the diode bridge rectifier, which employs a loop of diodes to produce full wave DC power from the AC input. Figure 128 illustrates the diode orientation to produce a full wave positive DC output from AC input. [41] [11]
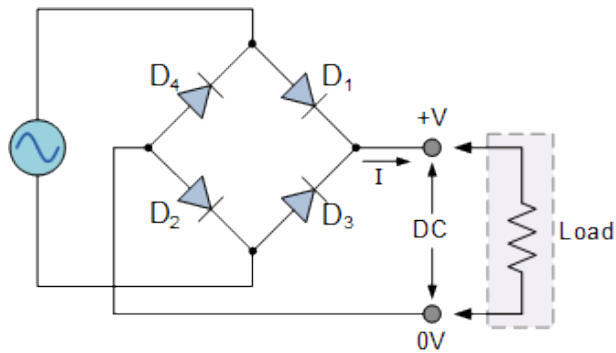
Figure 128: Diode bridge rectifier [11]

The current flow illustrated in Figure 129 and Figure 130 demonstrates how the diodes act as high and low resistance gates to produce a full wave DC output from an AC input. The advantage of the diode bridge rectifier is the lower cost and footprint of the additional diodes versus the transformer required for the two diode design of the full wave rectifier. [11]
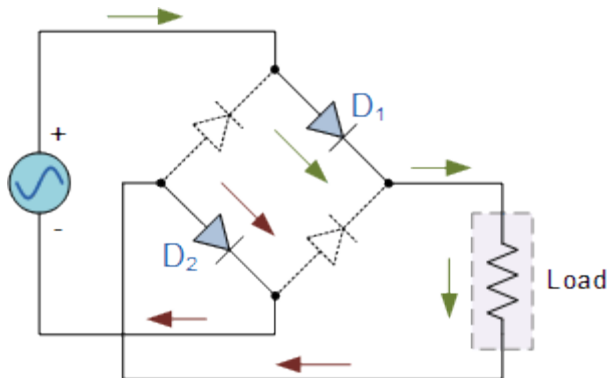

**Figure 129: Diode bridge rectifier positive half cycle [11]**
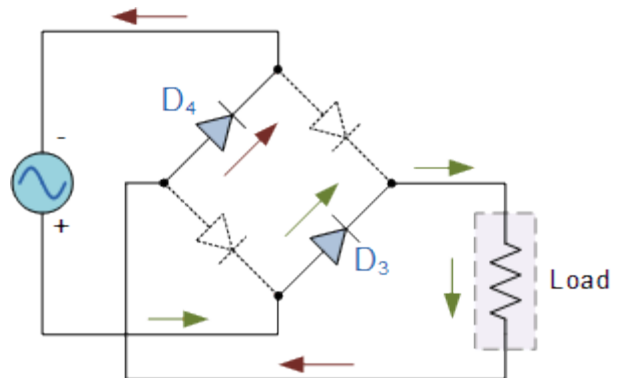
Figure 130: Diode bridge rectifier negative half cycle [11]

Smoothing capacitors

Once the AC current has a single polarity, regardless of the use of a half wave or full wave rectifier there are periodic pulses of DC current with the same shape as the AC amplitudes. Smoothing capacitors employed after the rectifiers serves to maintain the DC current, with smaller fluctuations, near the amplitude maximum of the pulses. Figure 131 illustrates the effect of a smoothing capacitor on the DC output of a diode bridge rectifier. [11]
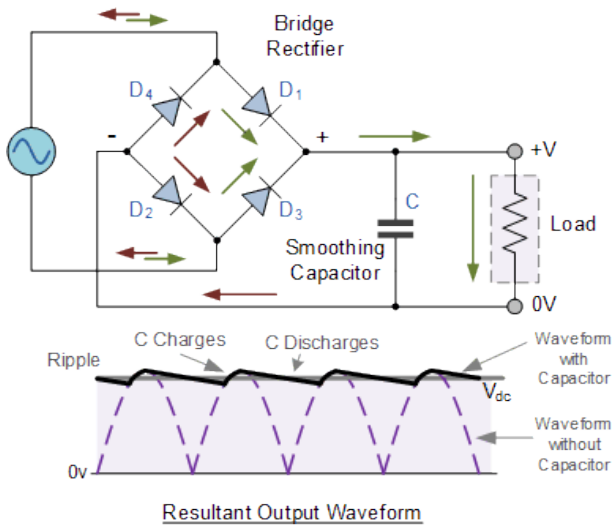
Figure 131: Full wave diode bridge rectifier with smoothing capacitor [11]

Thyristors

Thyristors are devices similar to transistors, but comprising four layers of semi-conductors, resulting in three sets of P-N junctions. The resulting component is like a unidirectional controllable diode which has three interfaces, the anode, cathode and gate. Figure 132 illustrates the symbol and interfaces used for wiring thyristors, it is represented as a unidirectional diode controlled by the gate input. The gate interface controls the state of the thyristor between a high resistance with low current or off state, and a low resistance high current or on state. In this way the thyristor can be used as an electronically activated switch. [14] [15]
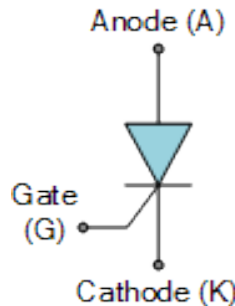
Figure 132: Thyristor diagram [42]

Insulated gate bipolar transistor

The IGBT is an effective semiconductor switching device, notably combining the high current carrying capability of bipolar junction transistors and the high state switching speeds of field effect transistors (MOSFETs). This device is voltage controlled via the gate input to act as a bipolar transistor and switch current and resistance states. Figure 133 illustrates the electrical symbol for an IGBT, represented as a bipolar voltage controlled MOSFET. [43] [44]
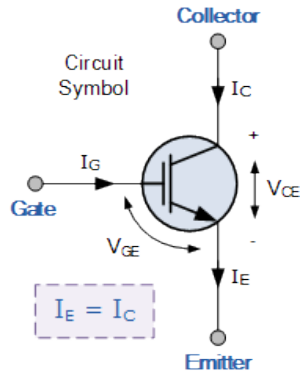

Figure 133: IGBT electrical diagram [44]

Hall Effect Sensor

Hall Effect sensors measure the electromagnetic effects caused by a current passing through a perpendicularly oriented conductor. Figure 134 illustrates a Hall Effect sensor disturbed by an external magnetic field representing the electromagnetic force of moving electrons. The Hall Effect dictates that the magnitude of the detected magnetic force is directly related to the magnitude of the passing current. The sensor is then designed to amplify an output signal in volts which represents the current magnitude. [45] [46] [47]
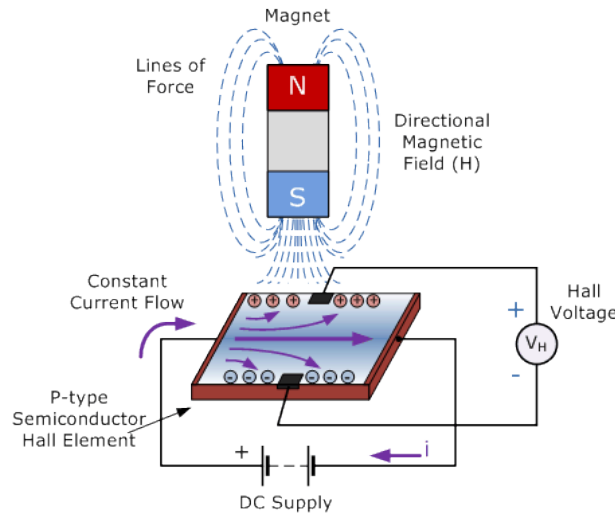
Figure 134: Hall Effect sensor interaction with magnetic fields [46]

Appendix B: Arduino Uno Schematic
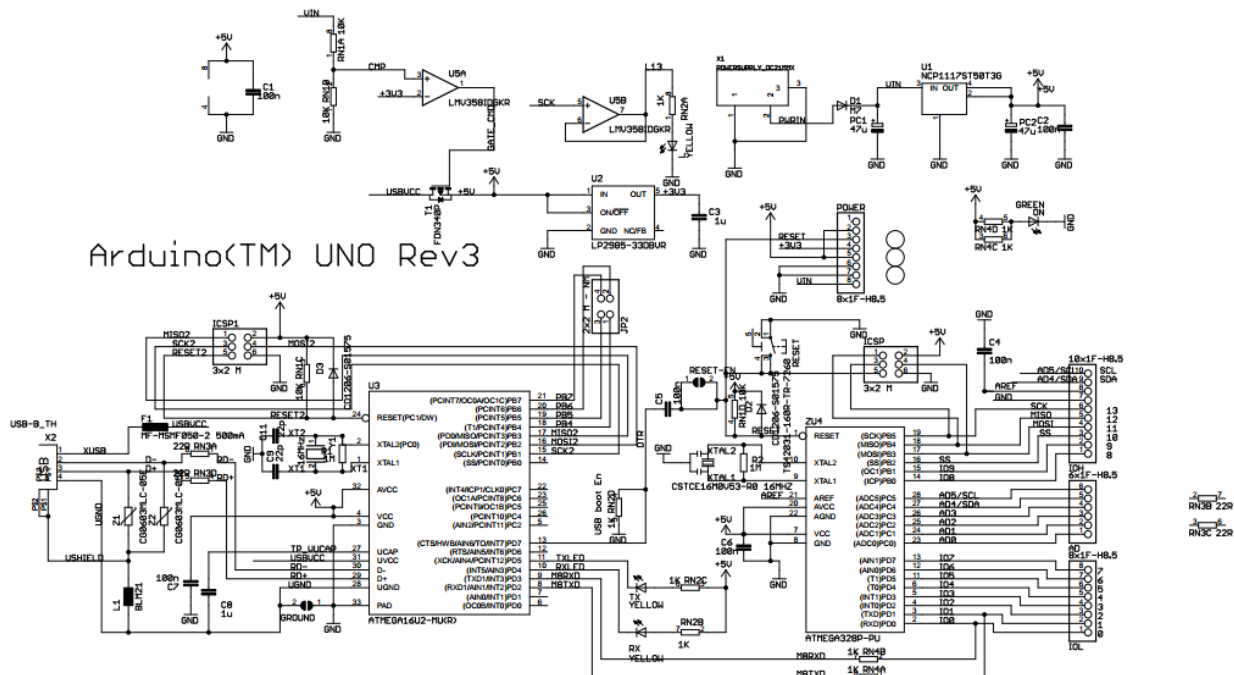
Figure 135: Arduino Uno schematic

Appendix C: ESD Machine #2 Control Modes Experiment

Table 20: ESD Machine #2 control mode experiment parameters

| ESD 1 (V)	ESD 2 (V)	ARC (V)	ESD Frequency (%)	ARC Frequency (%)	High Pulses	Low Pulses	Sample Rate
35	20	13	40	20	2	2	33000
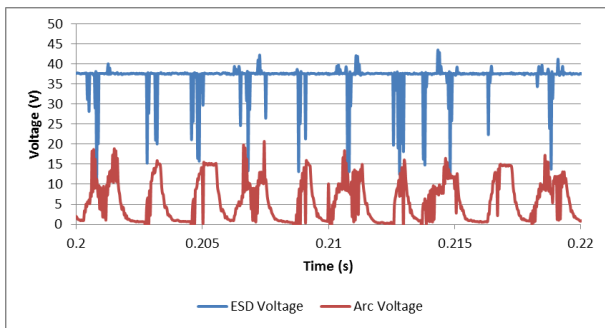
Figure 136: ESD Machine #2 Control Mode 0
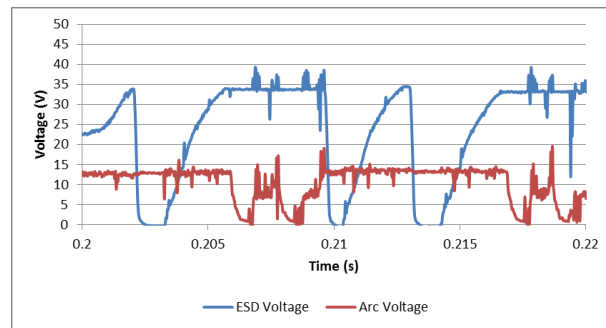
Figure 137: ESD Machine #2 Control Mode 1
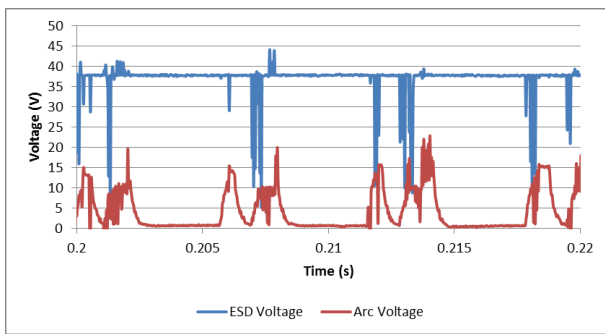
Figure 138: ESD Machine #2 Control Mode 2
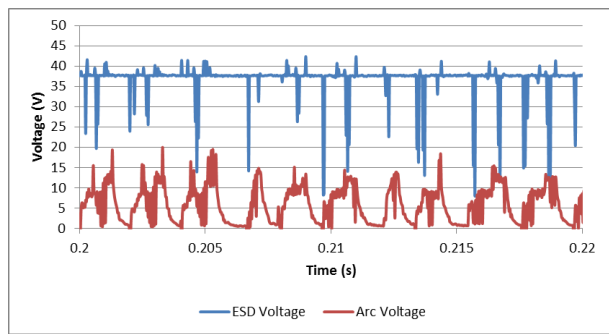
Figure 139: ESD Machine #2 Control Mode 3
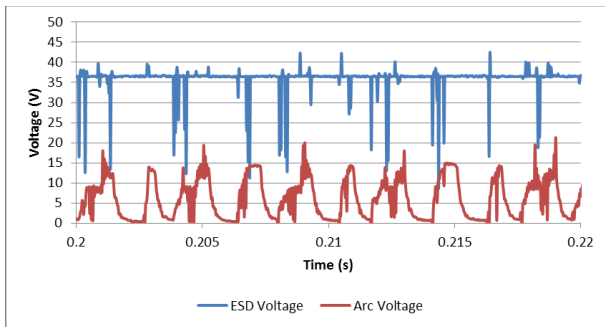
**Figure 140: ESD Machine #2 Control Mode 4**
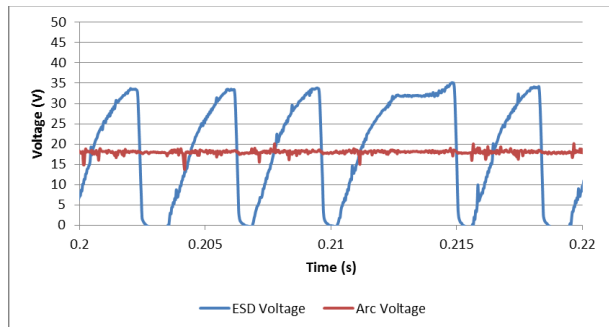
**Figure 141: ESD Machine #2 Control Mode 5**
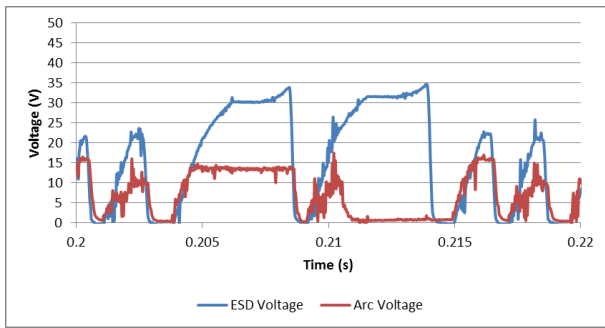
**Figure 142: ESD Machine #2 Control Mode 6**
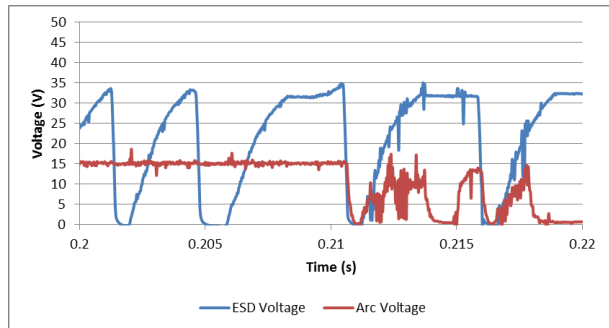
**Figure 143: ESD Machine #2 Control Mode 7**
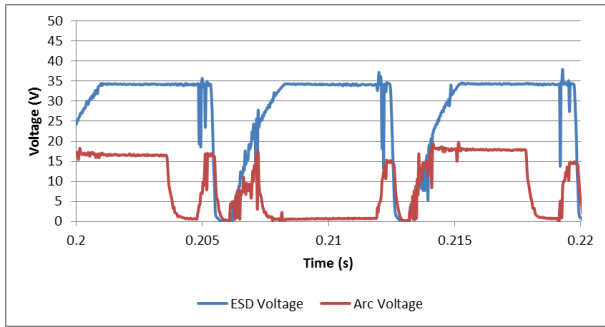

Figure 144: ESD Machine #2 Control Mode 8
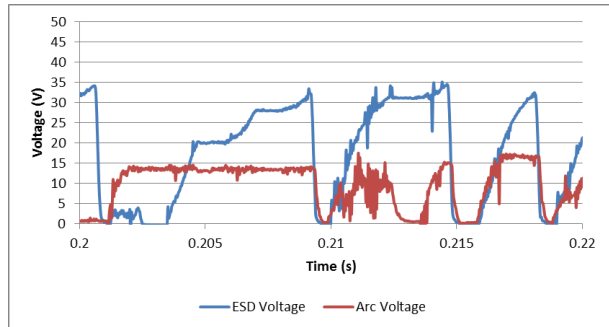

Figure 145: ESD Machine #2 Control Mode 9
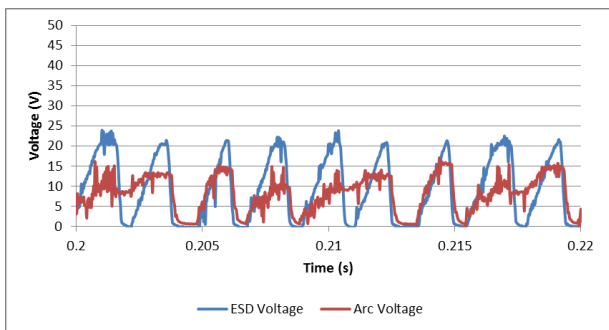
Figure 146: ESD Machine #2 Control Mode 10

Appendix D: LabView force feedback program

With the GRBL-GUI program as initial design a LabView program was developed with additional functions to facilitate the force feedback and automated G-Code sending. The program initially reads in the G-Code sequence from the specified .txt file. The length of the file sets the number of iterations in the for-loop. This loop parses the G-Code commands and splices in real time commands containing the change in the current z-axis position. A parallel while-loop records the current force data and queues it for transfer into the for-loop.

Two different force sensing hierarchies were tested. Initially in order to allow the force sensor to operate near the sampling speed of 200Hz it was nested in its own parallel loop structure to facilitate the different cycling speeds. The force sensor loop operated on a waiting timer to operate the force sensor at a real time rate. This was very effective to record the real time force data from the CNC ESD operations.

This programming hierarchy functioned on the principle of data queues which rapidly send data between parallel running loops in an ordered sequence. In this data setup the loops act as producer and consumer functions, where the while loop with the Force data produces data on demand to be sent to the for-loop to operate the PID Control function and generate a change in z-position to send to the GRBL controller. Without the buffer from the data queue each loop would need to complete its operations in order to pass data in another loop. This function allows for the parallel operation of the loops and subsequently the feasibility of the force control of the ESD process. See Figure 147 for the LabVIEW VI diagram and user interface used for the data collection and G-Code transfer.
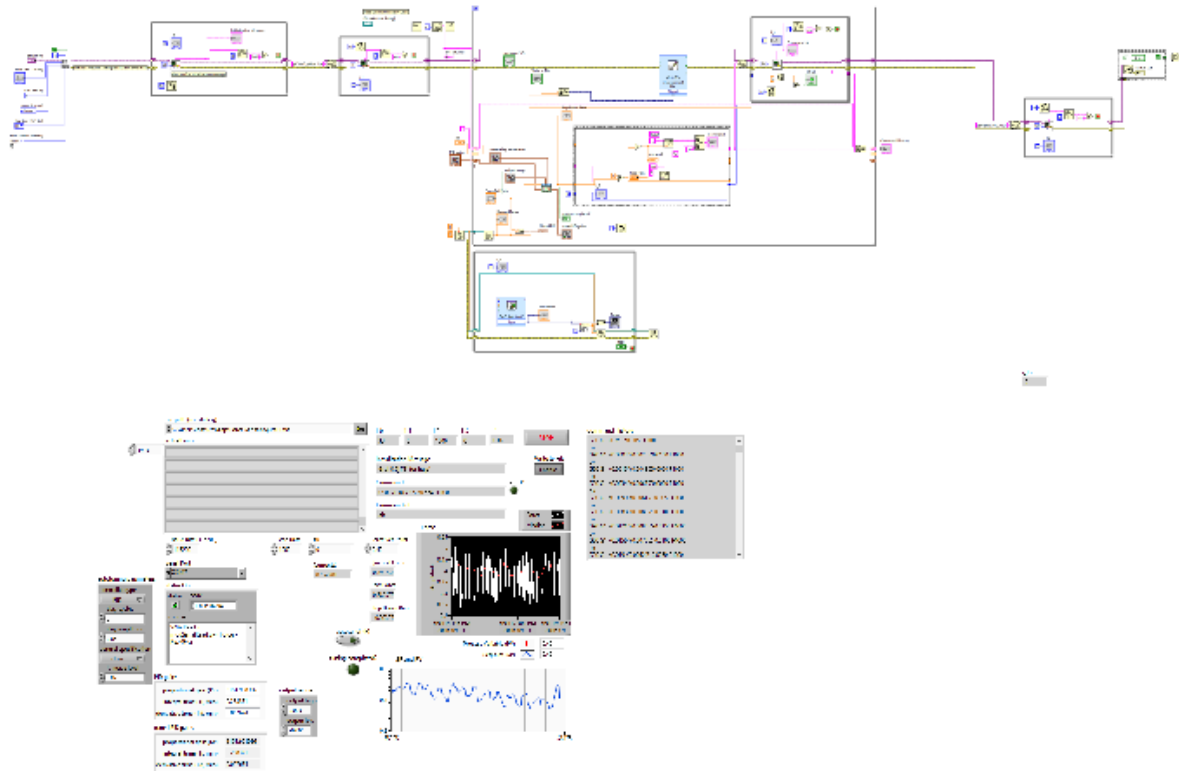
Figure 147: LabVIEW VI and User Interface

Due to the consumer or slave loop being the force sensing loop, data was only requested on demand from the parsing loop. This resulted in the force sensing loop only operating at the frequency of the code parsing sequence, which operates at the computing speed of the GRBL program on the Arduino program. This sequence only loops once the ok command is received that the previous G-Code command has been understood and completed by the CNC machine. This low cycling frequency resulted in a large delay in the force feedback system and resultantly delayed responses from the controller.

In order to improve the response time of the force feedback controller a different loop hierarchy was explored. Operating the slave loop at a higher frequency than the master command loop would result in a buildup of force data and the feedback would be reacting to force data from the previous G-Code command. It was deemed possible to nest the force feedback loop within the cycling structure of the command loop. The new structure did away with the queue structures, and functioned off the principle of a moving minimum in order to manage the high frequency noise from the capacitive force sensor. The difference in operation speed of the two loops allows for 20 data points to be filtered as the first action of the processing loop, this action operated at the maximum speed of the force sensor, the loop then

104

proceeded with the rest of the parsing and communication actions. This proved to provide a more real time force data monitoring for use in the PID feedback. Figure 148, Figure 149, Figure 150, demonstrating the design changes to the program versus Figure 147 detailing the GUI, block diagram part 1, block diagram part 2 and the program hierarchy respectively.
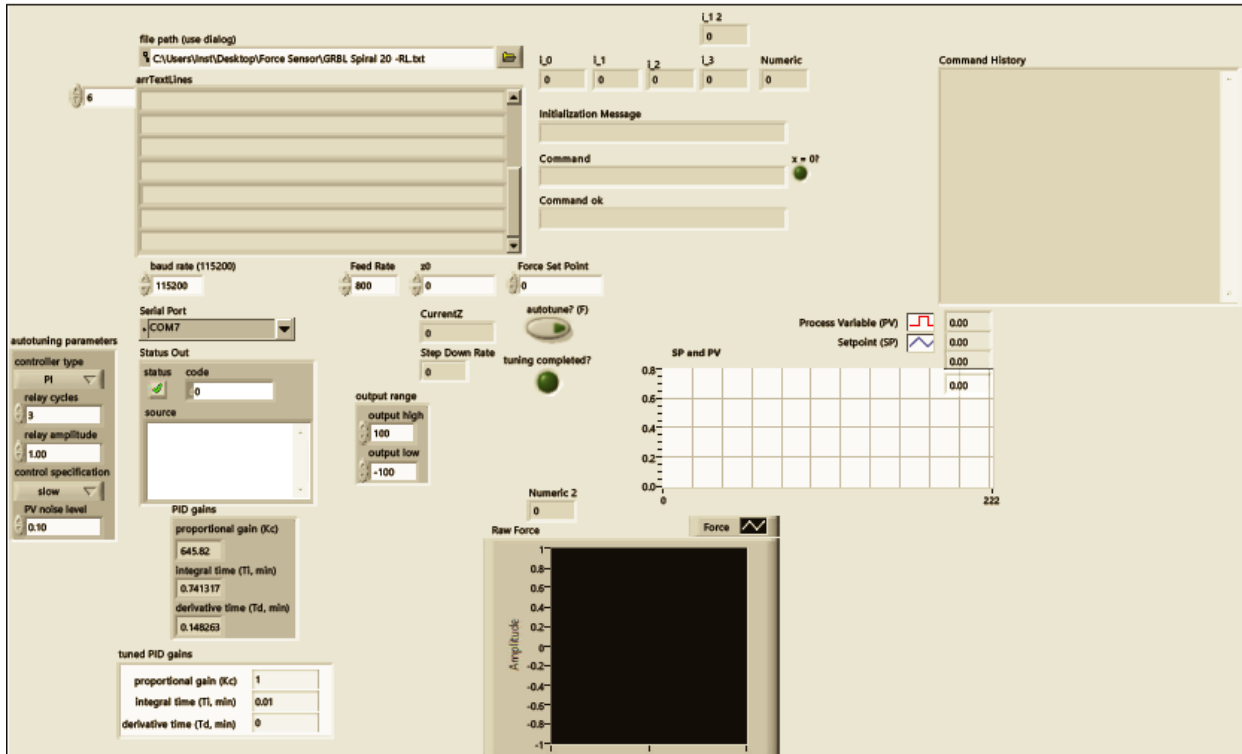

Figure 148: Force feedback VI GUI
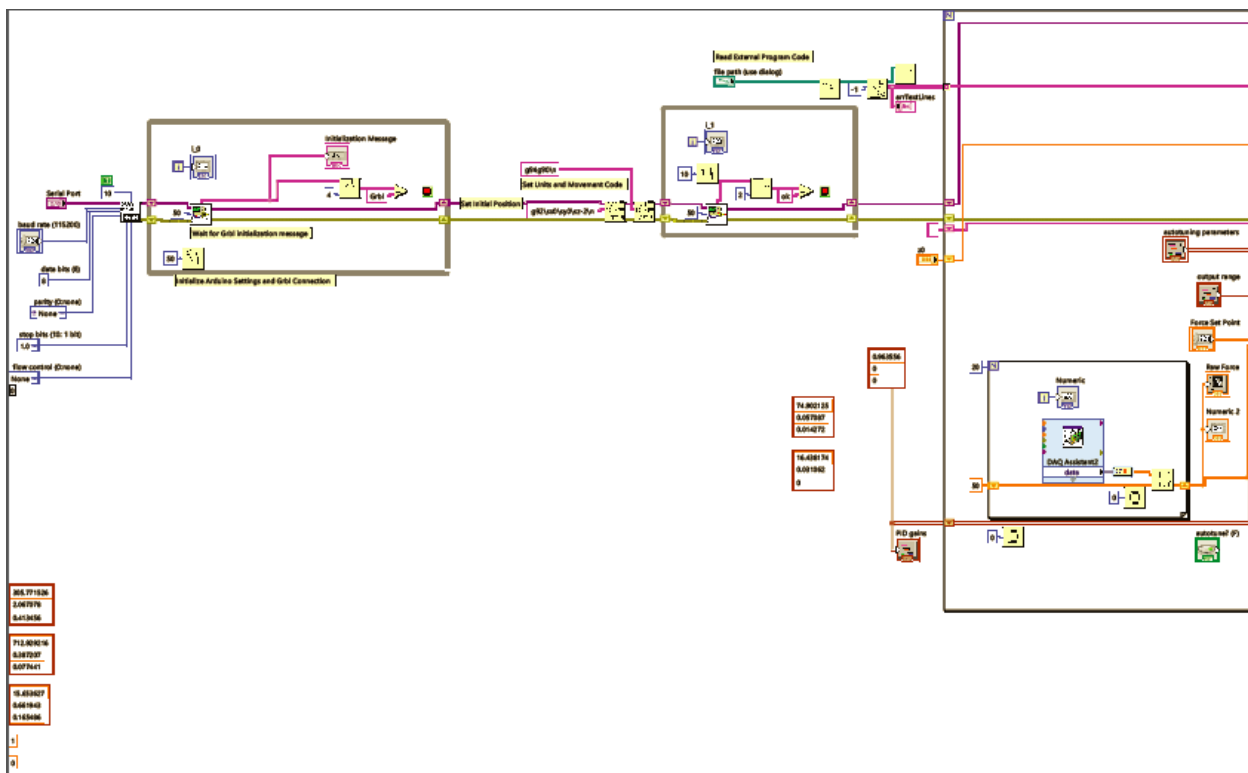
Figure 149: Force feedback VI block diagram part 1
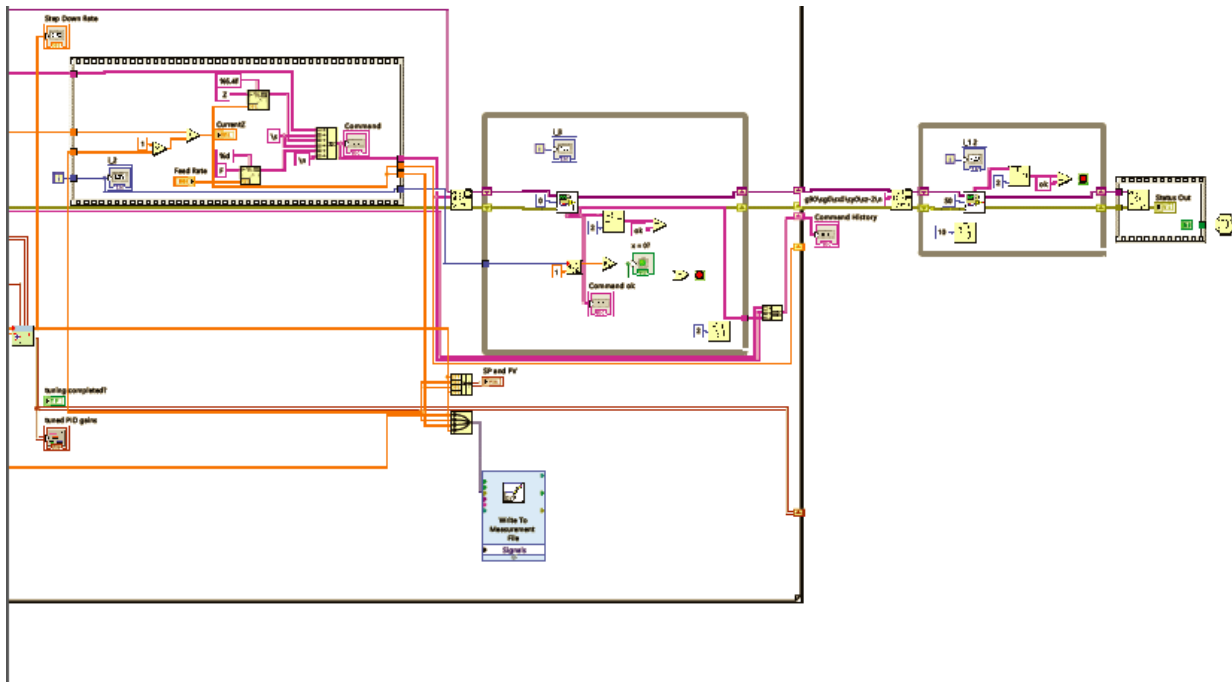
Figure 150: Force feedback VI block diagram part 2

106

Appendix E: Force feedback circle experiment

In order to demonstrate the effect of the force control an ESD experiment was designed to create continuous concentric circles of 5mm diameter. Each circle was defined by a single line of code, as a result the system only recalculates and sends new force data every one revolution of the CNC machine. With the set parameters the force was recalculated approximately once every second. With this slow refresh rate and high deposition rate the effectiveness of the force feedback system can be appropriately tested. Each circle command requires approximately 1 second to send back an ok response to the system. At this rate the force system cannot respond to sudden changes in force which appear at different areas of the circle.
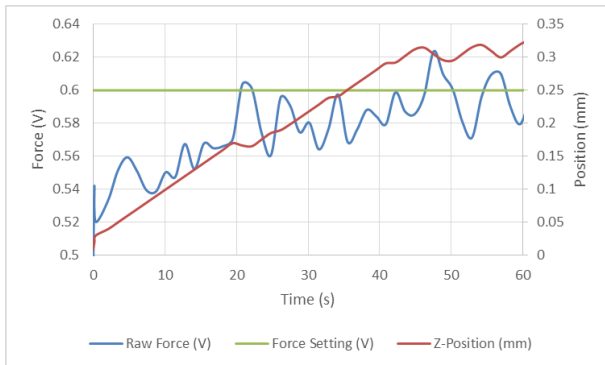

Figure 151: Force Controlled CNC test No ESD
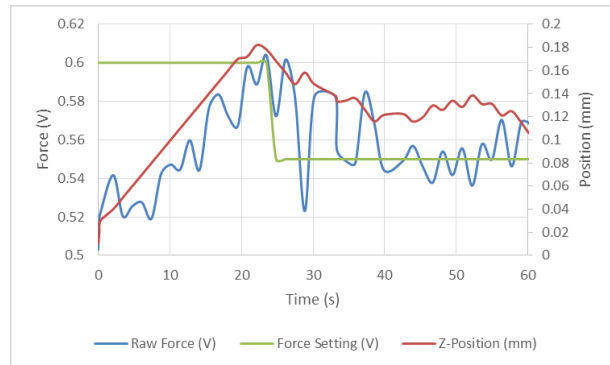
Figure 152: Force Controlled ESD Test; 100V, 200Hz, 200µF, 50 passes of 5mm diameter circle; no argon
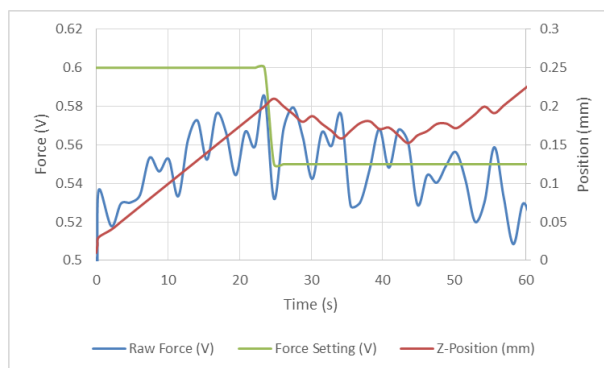

Figure 153: Force Controlled ESD Test; 100V, 200Hz, 200µF, 50 passes of 5mm diameter circle; 30 CFH argon
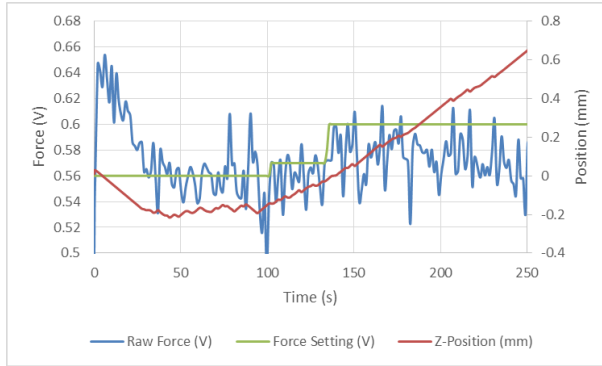
Figure 154: Force Controlled ESD Test; 100V, 200Hz, 200µF, 200 passes of 5mm diameter circle; 30 CFH argon

Changes in the relative level of the stage as well as aberrations in the smoothness of the substrate can have drastic effects on the applied force. The normal force changes along a single movement serve to create a large disparity in the standard deviation of the force sensor readings. The slow reaction time of the force sensor with the CNC commands also results in a compounding effect on the noise levels in the system. Increasing the number of G-Code commands for a certain action will result in an increase in the complexity of the G-Code, but may serve to allow for faster convergence, and reaction of the force controller.
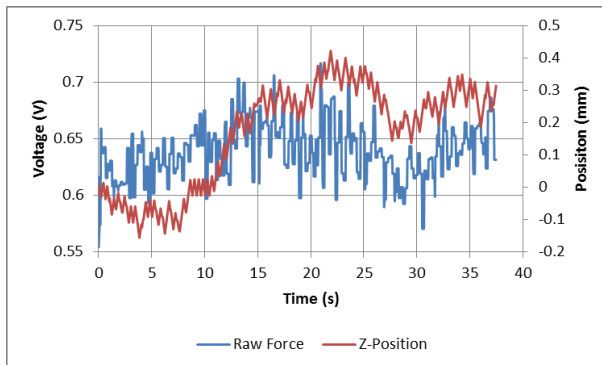

Figure 155: PID Control System during ESD Force set at 0.65V

A significant limitation of the feedback system is that the force may change rapidly due to CNC moves, however the parsing control system only allows for force measurements and adjustments at the end of every line of code. Thus the system cannot react to sudden drastic changes in the application force.